AEDC-TR-68-164

THE FEASIBILITY OF A CLOSED LOOP MULTIPLE COMPONENT ROCKET THRUST STAND

Aerojet-General Corporation
Test Systems Engineering Department—Test Operations
Sacremento, California

October 1968

ARNOLD ENGINEERING DEVELOPMENT CENTER
AIR FORCE SYSTEMS COMMAND
ARNOLD AIR FORCE STATION, TENNESSEE

NOTICES

When U. S. Government drawings specifications, or other data are used for any purpose other than a definitely related Government procurement operation, the Government thereby incurs no responsibility nor any obligation whatsoever, and the fact that the Government may have formulated, furnished, or in any way supplied the said drawings, specifications, or other data, is not to be regarded by implication or otherwise, or in any manner licensing the holder or any other person or corporation, or conveying any rights or permission to manufacture, use, or sell any patented invention that may in any way be related thereto.

Qualified users may obtain copies of this report from the Defense Documentation Center.

References to named commercial products in this report are not to be considered in any sense as an endorsement of the product by the United States Air Force or the Government.

THE FEASIBILITY OF A CLOSED LOOP MULTIPLE COMPONENT ROCKET THRUST STAND

Aerojet-General Corporation
Test Systems Engineering Department - Test Operations
Sacremento, California

AF – AEDC
Arnold AFS Tenn

FOREWORD

The work presented herein was sponsored by Arnold Engineering Development Center (AEDC), Air Force Systems Command (AFSC), Arnold Air Force Station, Tennessee, under Contract F40600-67-C-0015, Program Elements 6240518F and 6540215F, Projects 5730 (Task 573004) and 4344.

The work was accomplished by the Aerojet-General Corporation, Test Systems Engineering Department - Test Operations, Sacramento, California. The work was performed from June 1967 through May 1968. The manuscript was submitted for publication on September 3, 1968.

The reproducibles used to reproduce this report were provided by the author.

This technical report has been reviewed and is approved.

Forrest B. Smith, Jr.
Research Division
Directorate of Plans
and Technology

Edward R. Feicht
Colonel, USAF
Director of Plans
and Technology

ABSTRACT

This report considers the extension of rocket engine thrust stand and jet engine thrust stand dynamics by the use of an "active strut" hydraulic compensator unit installed as an integral member of the force measurement system. A mathematical model was constructed to approximate the dynamic characteristics of a typical rocket engine thrust stand and active strut servo system; the model was mechanized for analog computer simulation. Based upon results of the computer analysis, a physical test stand model was constructed in the Aerojet-General Corporation Sacramento Controls Laboratory. A hydraulic force generator was mechanized to introduce a step-like forcing function to the physical test model. After preliminary testing of the "uncompensated" thrust stand, the active strut compensator was inserted into the thrust stand force measurement system. Controls Laboratory developmental testing of this compensated system suggested that significant improvements could be achieved in the force measurement system dynamic response characteristics. Frequency response data indicated that the compensated force measurement system bandwidth could be increased by a factor of four with a significant increase in damping. The Controls Laboratory physical test model was reassembled in the Aerojet Sacramento Test Area. Three solid rocket motors were statically test fired on the uncompensated thrust stand to form a reference base. The active strut compensator was then installed, and three solid rocket motors were statically test fired on the compensated stand. A comparison of the two sets of data illustrate that the active strut is indeed capable of significantly improving transient rocket thrust stand data.

CONTENTS

APPENDIXES

I. ILLUSTRATIONS

Figure Number

Figure Number

Figure Number

NOMENCLATURE

a_{CP}	=	Compensator piston area - $in.^2$
a_{DAMP}	=	Damping servo effective area - $in.^2$
a_e	=	Mechanical servo effective area - $in.^2$
a_S	=	Compensator piston shaft area - $in.^2$
B_{CP}	=	Compensator piston damping factor - lbs/in per sec
B_{Fx}	=	Flexure damping factor - lb/in per sec
B_{HW}	=	Headwall damping factor - lb/in per sec
B_{LC}	=	Load cell damping factor - lb/in per sec
B_M	=	Motor damping factor - lbs/in per sec
B_T	=	Tripod damping factor - lbs/in per sec
F_A	=	Applied force - lbs
F_C	=	Measured force level - lbs
J_{HW}	=	Headwall moment of inertia - in-lb-sec^2
K_{Fx}	=	Flexure spring constant - lb/in
K_{HW}	=	Headwall spring constant - lbs/in
K_{LC}	=	Load cell spring constant - lbs/in
K_T	=	Tripod spring constant - lbs/in
L	=	Load cell string height - in.
L/ga	=	Ratio of pipe length to the product of pipe inner area and gravitational constant
M_{CASE}	=	Case mass - lb-sec^2/in
M_{CP}	=	Compensator piston mass - lb-sec^2/in
M_{Fx}	=	Flexure mass - lb-sec^2/in
M_{LC}	=	Load cell mass - lb-sec^2/in
M_M	=	Motor mass - lb-sec^2/in
M_T	=	Tripod mass - lb-sec^2/in
P_1	=	Actuator opening side pressure - psia
P_2	=	Actuator closing side pressure - psia

P_a = Atmospheric pressure - psia

P_{ACC} = Accumulator pressure - psia

P_{CL} = Mechanical servo closing line pressure - psia

P_{OP} = Mechanical servo opening line pressure - psia

P_R = Return line pressure - psia

P_S = Mechanical servo valve line inlet pressure - psia

V_1 = Actuator opening side volume - ft^3

V_2 = Actuator closing side volume - ft^3

V_{FLEX} = Mechanical servo line volume - ft^3

V_{IN} = Inlet pipe volume - ft^3

$\dot{w}_1$ = Hydraulic flow from the mechanical servo to the opening actuator line - lbs/sec

$\dot{w}_2$ = Hydraulic flow from the mechanical servo closing side to the return line - lbs/sec

$\dot{w}_{1_D}$ = Damping servo opening side flow rate - lbs/sec

$\dot{w}_{2_D}$ = Damping servo closing side flow rate - lbs/sec

$\dot{w}_{CL}$ = Flow from the actuator into the mechanical servo line - lbs/sec

$\dot{w}_{IN}$ = Hydraulic fluid flow rate into the mechanical servo inlet line - lbs/sec

$\dot{w}_{OP}$ = Flow from the mechanical servo into the actuator - lbs/sec

$\dot{w}_{OUT}$ = Mechanical servo return flow rate - lbs/sec

$\dot{w}_R$ = Mechanical servo flow rate into the discharge line - lbs/sec

$\dot{w}_{SV}$ = Hydraulic flow from the accumulator line to the mechanical servo - lbs/sec

x_{CASE} = Case deflection - inches

x_{CP} = Compensator piston deflection - inches

x_{Fx} = Flexure deflection - inches

x_{HW} = Headwall deflection - inches

x_{LC} = Load cell deflection - inches

x_M = Motor deflection - inches

x_T = Tripod deflection - inches

β = Hydraulic fluid compressibility - psi

ρ = Hydraulic fluid density - lbs/ft^3

θ_{HW} = Headwall rotation - radians

τ = Time constant - seconds


High-Gain Operational Amplifier

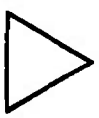
Summing Amplifier

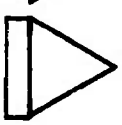
Integrating Amplifier

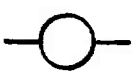
Potentiometer


Linear Spring

Square-Root Device

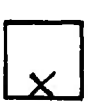

Multiplier

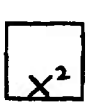

Squaring Device

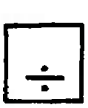

Divider

Electronic Comparator

SECTION I
INTRODUCTION

1.1 THRUST MEASUREMENTS IN ROCKET ENGINE TESTING

In the captive testing of both liquid and solid rocket engines, engine-generated thrust data are acquired in order to verify engine design and to permit the calculation of specific and total impulse parameters. In order to accommodate the measurement of force, rocket engines are installed within the framework of mechanical thrust stands and isolated from ground reference through load cell and flexure struts. For ballistic data, the thrust stand takes the approximate form of a single degree-of-freedom mechanical system, exhibiting a lightly damped primary resonance in the axial or longitudinal mode.

For long-duration rocket tests (on the order of ten seconds or longer), accurate steady-state thrust data can normally be acquired by the standard application of conventional measurement techniques. Following engine ignition, the thrust data are observed to oscillate about the true thrust level, due to the lightly-damped thrust stand resonance. However, once the mechanical system is permitted to "ring out", the subsequent force measurement accuracy can be as high as ± 0.1%, with a high degree of reliability. Errors in the force measurement system caused by redundancy, interaction due to deflection under load, the unstable pendulum effect, etc., can often be anticipated by means of pre-test static calibrations, and appropriate steady state corrections applied during data reduction.

Dynamic data reconstruction is not so readily accomplished. During and immediately following the engine start and shutdown transients, thrust stand oscillations that are reflected in the acquired thrust data do not easily submit to analytical correction. Various attempts have been made to analytically eliminate thrust-data distortion caused by the thrust stand dynamics - these include the on-line or off-line reconstruction of thrust by means of both analog

and digital computer processing. Although these approaches have increased the force measurement system bandwidth, certain assumptions must be made regarding systems linearity, while the computer program invariably involves the noise-amplifying process of differentiation.

In dealing with short-duration rocket engine static test firings, dynamic data distortion produced by the limited thrust stand bandwidth can cause severe problems in data interpretation. It is for this type of test environment that the feasibility of hydraulically operated active strut compensators has been evaluated.

1.2 THE ACTIVE STRUT COMPENSATION CONCEPT

Short-duration high-acceleration rocket motors, when statically test fired on conventional ballistic thrust fixtures, yield thrust data that exhibit a high degree of oscillation produced by the inertial contribution to the total system force balance. Rather than attempting to eliminate this data distortion analytically, an approach has been suggested whereby a hydraulic compensator assembly is installed in the normal force measurement strut. The "active strut" compensator is programmed to automatically maintain the rocket engine fixed in space so that the inertial force exhibited by the rocket engine remains minimal. Under these conditions, the reaction force transmitted through the measurement strut (and hence the measurement load cell) is at all times approximately equal to the engine-generated rocket thrust. This concept represents active compensation whereas the computerized approach represents passive compensation. With active compensation, no assumptions are made regarding systems linearity, while inner-loop stabilizing feedback can be substituted for the implicit or explicit computer differentiation process.

The active strut concept described in this report consists of a hydraulic actuator that is inserted into the conventional force measurement strut. The actuator piston is driven, with respect to the cylinder case, so as to maintain the rocket motor fixed in reference space. To accomplish this effect, a closed-loop null-seeking servo system is employed, consisting of a feedback

potentiometer, signal conditioning electronics, and an electro-hydraulic servo valve assembly. Any motion of the rocket engine with respect to the reference null produces a feedback position signal which, after amplification and conditioning, is impressed across the coils of the electro-hydraulic servo valve. Hydraulic oil is thus directed to the active strut compensation actuator in order to return the engine to reference null. An inner-loop accelerometer signal is employed, through a redundant servo valve system, to produce the required electronic stabilization.

The Aerojet-General Corporation approach to establishing the feasibility of this active strut concept consisted of a three-part program that is documented in this report: (1) a thorough analog computer simulation study was conducted in order to provide a preliminary design of the active strut compensation system, (2) a physical thrust stand model was constructed and a series of developmental tests were conducted to demonstrate the feasibility of active strut compensation under "laboratory" conditions, and (3) the system that had been developed in the laboratory was transported to the Aerojet Test Division for a series of solid rocket motor static test firings to demonstrate the feasibility of active strut compensation under "field" test conditions.

SECTION II
ANALYTICAL STUDY OF THE ACTIVE STRUT

2.1 INTRODUCTION

A preliminary analytical study was conducted through the use of an electronic analog computer to determine the feasibility of employing a hydraulic compensation cylinder (active strut) in series with the standard thrust stand force measurement system to improve the thrust stand force measurement response characteristics. A number of distinct compensation techniques were investigated, including the direct mechanical position feedback mode with lead-lag mechanical compensation, and the mechanical feedback mode with electronic acceleration stabilization. The most desirable active strut configuration, based upon computer-derived data analysis, involved the application of an electrical accelerometer inner feedback loop, with a mechanical position feedback outer loop. Preliminary values of loop gains were defined in accordance with optimum response predicted by the computer model.

This section describes in detail the generation of the system mathematical model (with the appropriate system equations tabulated in Appendix II), the mechanization of the mathematical model for analog computer simulation, and the results of the analog computer study.

2.2 SYTEM MATHEMATICAL MODELING

The active thrust strut mathematical model was derived by considering the system illustrated in Figure 1. In addition to suggesting the placement of the electro-hydraulic equipment assumed for the active strut computer implementation, Figure 1 also describes the pressure and flow rate variables that were considered of sufficient importance to be generated explicitly in the computer program. The true distributed-parameter mechanical system was

decomposed into a seven-node lumped-parameter analogy, as illustrated in Figure 2, for computer simulation. Each of the major mechanical thrust stand components were considered as individual masses, coupled to adjacent components by means of mechanical springs together with minimal damping "dashpots" not illustrated in Figure 2. The motor-tripod-compensator piston assembly was coupled to the compensator case-load cell-flexure-headwall system by force equations derived from dynamic hydraulic considerations.

Referring to Figure 1, the hydraulic pump was assumed de-coupled from the active strut system through the application of an appropriate hydraulic accumulator. The accumulator is initially filled with high-pressure inert gas; the hydraulic pump is then activated, and the accumulator is charged to the desired pressure level (3000 psi). Any sudden flow demands are accommodated by a discharge from the accumulator, while the 3000 psi hydraulic pump acts simply to replenish the accumulator supply. For this reason, it was considered in all analyses that the accumulator pressure (P_{ACC}) was constant, equal in magnitude to 3000 psi. It was further assumed that the accumulator would be physically placed in close proximity to the acceleration-feedback servo valve, shown installed directly against the actuator in Figure 1. This placement was required due to the fact that the inner-loop feedback servo valve response was considered of prime importance, in comparison to the response of the outer-loop position feedback servo, i.e. the inner-loop compensator is responsible for improving the force measurement system response speed, while the outer-loop compensator functions only to maintain the steady state motor position fixed in reference space. Thus, the accumulator is located near the inner-loop servo to minimize hydraulic line dynamic distortion, while relatively long lines couple the accumulator to the position-feedback servo stage.

The mechanical position-feedback device assumed in the computer study consisted of a power actuator and can be envisioned as the second stage of a conventional servo valve. The four-way spool is connected mechanically to the motor mass; hence, as the mass moves from equilibrium due to motor-generated

forces, hydraulic oil flow is directed from the mechanical servo stage to the active strut compensator in a direction so as to oppose this motion.

To illustrate the physical operation of the Figure 1 compensation system, consider an excitation force F_A to be imparted to the motor mass system as shown. The action of the external force is that of accelerating the motor mass assembly in a positive direction, i.e. to the left in Figure 1. Assuming an acceleration feedback mode of compensation, an accelerometer mounted upon the motor mass system detects the positive motor acceleration; the accelerometer output voltage is amplified and applied across the coils of the inner-loop feedback servo valve. The second stage servo valve spool shuttles to the right, permitting high-pressure hydraulic oil from the accumulator to flow into the P_1 (opening) side of the active strut actuator. Simultaneously, hydraulic fluid flows from the P_2 or closing side of the actuator to return (characterized as a constant atmospheric pressure P_a). The resulting differential pressure induced across the compensator actuator piston thus attempts to balance the motor-generated input force F_A. The differential pressure force is, however, also exerted upon the compensator case, causing that case to accelerate to the left in inertial space, and hence placing the measurement load cell in compression. In the absence of an outer-loop position feedback, the acceleration-feedback system would function until a force balance were produced across the actuator piston, and until the forces acting upon the case from the differential pressure and from the load cell were balanced. Due to the finite servo system bandwidth, however, the response is not infinite so that some motion of the motor mass system must occur to the left. The outer-loop mechanical feedback mechanism is installed in order to provide motor mass position reference; i.e. as the motor moves to the left under the influence of F_A, the mechanical position feedback stage directs flow into the P_1 side of the active strut actuator in order to return the motor mass to the original equilibrium position. The combination of inner-loop and outer-loop servo compensators thus function to (1) maintain the motor mass acceleration at zero and (2) maintain the motor mass steady state position at some equilibrium reference.

From a purely mechanical point of view, the Figure 1 compensation system can be viewed as a mass transformer. In the basic differential equation that, to a reasonable first approximation, is found to govern the behavior of the rocket engine thrust stand,

$$F_A = M\ddot{x} + B\dot{x} + Kx \qquad (1)$$

where x represents the motor mass deflection from equilibrium and F_A is the external excitation force, the difference between the true motor-generated force (F_A) and the force measured by the load cell (Kx), consists primarily of the inertial force term $M\ddot{x}$. The frictional force term $B\dot{x}$ is small and can therefore be discounted. Thus, the large motor mass M, experiencing an instantaneous acceleration $\ddot{x}$, produces the dynamic distortion normally encountered with uncompensated thrust stand force measurement systems. Employing the compensation system of Figure 1, the active strut actuator attempts to maintain the motor mass fixed in inertial space by maintaining the motor mass acceleration at zero. In an ideal sense, the motor acceleration is held at zero, while the actuator case accelerates into the load cell; thus the motor $M\ddot{x}$ dynamic term is replaced by the $m\ddot{x}$ term contributed by the actuator case. Due to the fact that the case mass is only a small fraction of the motor mass, a transformation takes place that greatly reduces the force measurement system dynamic distortion. In the real-world situation, motor mass acceleration is not maintained completely at null, and hence the mass-transformation concept is slightly in error. However, the ability of the active strut compensator to minimize motor mass acceleration is a physical key to understanding the active strut operation.

Note that the mechanical position feedback servo stage is case-referenced to ground. It is also a well-known fact that during a rocket engine test firing, the "ground" reference is somewhat less than ideal, i.e. the ground reference contains both high-frequency and low-frequency distortions. During motor ignition and thrust buildup the entire ground system (normally a steel deck-plate anchored into concrete for sea-level firings, or an altitude chamber

base for simulated altitude firings) is observed to shift forward, i.e. in the direction of the motor-generated thrust vector. This low frequency shift in the ground reference will be detected by the mechanical position feedback servo stage such that the motor mass system will be repositioned in accordance with the ground motion. Note however, that since the entire thrust stand reference moves, including all side force takeout struts involved in multicomponent testing, that the final steady state motor mass position will be in accordance with all other "stationary" members of the force measurement and takeout systems. This situation is considered to be more desirable than the alternate approach of maintaining the motor mass fixed in inertial space.

High frequency perturbations in the ground reference will also be sensed by the mechanical feedback servo stage, together with high frequency vibrations exhibited by the motor. The fact that the mechanical feedback stage is physically located some distance from the active strut actuator, however, will tend to hydraulically damp these high frequency perturbations and, in fact, provide a source of dither for the servo system. The resulting perturbations as monitored in the force transducer output signal should be no more severe than those experienced during the normal uncompensated thrust stand test firing.

The system of nonlinear integro-differential equations illustrated in Appendix II was employed to characterize the active strut system of Figures 1 and 2. The mathematical model contains, as shown in Appendix II, a total of 31 coupled equations with 31 variables, together with a large number of parameters. Due to the complexity of the model, the equations were programmed for analog computer simulation, thus permitting all variables to be solved simultaneously for all combinations of system parameters investigated. Each of the model equations is now considered qualitatively.

Equation II-1 describes the pressure drop existing between the accumulator and the accumulator discharge line (to the mechanical servo stage) as a function of hydraulic oil flow rate and the rate of change of this flow rate (flow acceleration). The differential pressure that exists across this section of the hydraulic delivery system ($P_{ACC} - P_S$) is equated to two flow

contributions, i.e. the static contribution ($c/\rho\ \dot{w}_{IN}^2$) and the dynamic contribution ($L/ga\ W_{IN}$). The static pressure drop is that observed under steady state flow conditions of hydraulic oil with a density of ρ lb/ft^3 and is characterized by the "c" value of Equation II-1; this hydraulic resistance is in turn determined by the length, area and type of piping involved. The dynamic term arises due to the fact that a force is required to accelerate the hydraulic oil from one steady state velocity to any subsequent steady state velocity and is governed by the length-to-area ratio of the delivery piping. The L/ga and c/ρ terms represent parameters that were investigated for physical realizability during computer simulation runs.

Equation II-2 illustrates that, to a reasonable first approximation, the mechanical servo stage inlet line pressure rate of change varies as a linear function of the difference between inlet and outlet hydraulic oil flow rates to and from the line. The constant of proportionality ($\beta/\rho\ V_{IN}$) is determined by considering the physical aspects of the delivery piping, i.e. V_{IN} represents the weighted value of pipe volume required to connect the pressure accumulator to the delivery line. It should be noted that the value of hydraulic oil compressibility normally tabulated in the references implies an air-free environment, while the entrained air normally observed in actual operation reduces the value of compressibility significantly.

Equations II-3 and II-4 define the flow rates existing between the mechanical servo stage and the hydraulic cylinder, near the servo stage. Note that the equations consider the conditions that exist for both positive areas (motor motion in a positive direction with respect to equilibrium) and negative areas (motor motion in a negative direction with respect to equilibrium). As shown in Equation II-21, servo stage area is assumed to be directly proportional to motor deflection, with the constant of proportionality being a direct function of the servo stage orifice area size. The fact that most servo valve power spools are designed with slotted orifices is invoked to define the proportional area versus position relationship. The positive and negative polarities of the hydraulic oil flow rates are in accordance with the sign conventions established in Figure 1.

Equations II-5 and II-6 are similar to Equation II-2 and again indicate that the pressure rates of increase in the lines connecting the mechanical servo stage to the active strut compensation cylinder are directly proportional to the net flow rates entering the lines. Again the polarity conventions established in Figure 1 are maintained.

Equations II-7 and II-8 are similar to Equation II-1 and define the pressure drops that exist in the lines connecting the mechanical servo stage to the active strut cylinder ports. Note that, unlike the case of Equation II-1, however, both positive and negative flow rates can occur during normal operation of the system, and hence the computer model must accommodate this bi-directional criterion.

Equations II-9 and II-10 are similar in structure to Equations II-3 and II-4, and indicate the flow rates to and from the active strut cylinder from the damping (inner-loop feedback) servo valve as a function of motor acceleration. Thus, for a positive motor acceleration, the servo valve area is related as indicated in Equation II-22, while for negative motor acceleration, a negative effective area is obtained.

Equation II-11 is similar to Equations II-2, II-5, and II-6.

Equation II-12 is similar to Equations II-1, II-7, and II-8.

Equation II-13 describes the rate of pressure increase in the P_1 (opening) side of the actuator. As observed, the pressure rate of change is equated to the sum of three individual contributions, i.e. (1) the pressure rise caused by inlet flow from the inner-loop servo valve, (2) the pressure rise caused by inlet flow from the outer-loop mechanical position servo stage and (3) a pressure rise caused by compression of the entrained fluid within the P_1 cavity. The cylinder pressure is observed to increase for positive mechanical and inner-loop servo flow rates, and decrease due to increases in the P_1 cavity volume. The central term of Equation II-13 is the component that provides systems damping, i.e. as the pressure P_1 increases, the volume V_1 is observed to similarly increase, causing the rate of change of P_1 to reduce.

Equations II-14 and II-15 provide expressions for the generation of the two system variables required to implement Equation II-13. It is noted that, due to the low piston deflections required in the typical active strut mechanization, the weight of hydraulic fluid contained within the P_1 cavity can be considered constant.

Equations II-16, II-17, and II-18 are similar to Equations II-13, II-14, and II-15.

Equations II-19 and II-20 state that the volumes contained in the P_1 and P_2 cavities of the compensation actuator are assumed equal to the equilibrium volumes (with the compensation piston and cylinder case at equilibrium) and are further functions of the subsequent relative positions of case and cylinder.

Equations II-21 and II-22 have been considered previously. Note that the servo valve is assumed to be characterized by means of a first-order lag in Equation II-22; the transfer function involves a voltage input and an effective second stage spool area output.

Equation II-23 is obtained by applying Newton's law of translation to the motor mass of Figure 2, and as such is the familiar F = Ma relationship.

Equation II-24 is obtained by applying Newton's law to the tripod mass.

Equation II-25 results from the application of a force balance around the compensator piston, and again equating the net force to the piston mass-acceleration product.

Equation II-26 considers a force balance at the compensator actuator case.

Equations II-27 and II-28 are derived from Newton's law of translation as applied to the load cell and flexure respectively.

Equation II-29 is derived from Newton's law of rotation as applied to the headwall or force takeout structure. The rotational form of Newton's dynamical laws is invoked, due to the fact that an input force tends to rotate the headwall about some stationary pivot.

Equation II-30 is a geometrical identity for small angles.

Equation II-31 is the expression that was employed to determine the thrust as measured in the conventional thrust stand assembly. The "spring constant" involved is comprised of a portion of the flexure constant, together with that of the load cell.

As stated previously, the set of nonlinear integro-differential equations was considered sufficient for the simulation of the proposed active strut concept. Although the problem could be expanded considerably (in theory, to infinite dimensions due to the distributed-parameter nature of the problem) the 31-equation model was judged sufficient to characterize the principal modes of systems dynamics.

2.3 COMPUTER MECHANIZATION

After assigning all parameters involved in the Appendix II mathematical model specific preliminary ranges in value based upon past experience and engineering judgment, the system was mechanized for analog computer simulation. The resulting simulation diagram is illustrated in Figure 3. Note that, using the method of scaling directly from the differential equations as illustrated in Figure 3, it was not necessary to generate the so-called "scaled equations". This permitted each of the system parameters to be expressed as a generalized potentiometer setting; hence it was possible to easily vary parameters by simply varying the associated potentiometer setting to the appropriate value. This method of scaling allowed a large number of physical system variations to be investigated, e.g. various lengths of piping runs between the accumulator and mechanical servo stage were programmed, while a number of compensator piston area and cavity volume parameters were investigated.

As previously illustrated in Figure 1, it was assumed that the inner-loop servo valve would be closely coupled to the compensation actuator, and further that the hydraulic accumulator and return line plumbing would be closely coupled to the servo valve. No acceleration or compressibility effects were thereby included in the model for this servo valve. Conversely, it was considered that the mechanical position feedback stage would be located near the motor assembly; tubing runs of six feet were then assumed between the accumulator and the mechanical servo stage, and between the servo stage and the compensation actuator. The volumes associated with pressure nodes P_S, P_R, P_{CL} and P_{OP}, were thus computed for the equivalent of six linear feet. Further, the pressure drop parameters and L/ga values associated with this geometry were computed and employed in simulating the model. Although in actually conducting computer simulations, these parameters were varied over a considerable range, the data mentioned above were considered representative and were employed in the final design simulations.

In order to compensate a motor generated thrust level of 2000 pounds, a two-inch diameter actuator piston was considered. Further, after preliminary calculations, it was found that a volume equivalent to a one-half inch to a one inch total stroke was acceptable. A shaft area of 0.5 square inches was assumed, although this parameter did not appear to be significant. The accumulator pressure of 3000 psi was employed in all computer simulations, due to the assumption of a gas-charged accumulator as mentioned previously. A return pressure was taken equal to atmospheric. The values of maximum servo stage and servo valve areas were design parameters, as well as the ranging of the motor-mounted accelerometer.

The following mechanical motor and thrust measurement system components were considered as representative:

	COMPONENT	MASS $\left(\frac{\text{lb-sec}^2}{\text{in}}\right)$	SPRING CONSTANT (lb/in)	DAMPING RATIO
1.	Motor	1.0	---	0.04
2.	Tripod	0.1	200,000	0.04
3.	Compensator Piston	0.005	---	---
4.	Case	0.01	---	---
5.	Load Cell	0.05	200,000	0.04
6.	Flexure	0.01	200,000	0.04

The headwall was described as a single degree-of-freedom rotary system with a moment of inertia of 400 in-lb-sec^2, a moment arm (L) of 20 inches, and an equivalent headwall spring constant of 162,000 lb/in. Damping factors were computed such that each uncoupled single degree-of-freedom system would possess a damping ratio of 0.04. Further, the damping factors of the case and compensator piston acceleration equations were considered as variables, the values of which would be analyzed during computer simulation. It was determined during the process of conducting system analysis runs that the damping factors associated with these terms had no effect upon the total system's response characteristics, i.e. an order of magnitude variation in B_{CASE} and B_{CP} had no noticeable effect upon the compensated system response. Thus, the final value of B_{CP} and B_{CASE} was taken such that the corresponding uncoupled systems would exhibit damping ratios of 0.4.

As observed in the computer mechanization of Figure 3, provisions were included in the program for the investigation of: (1) use of the mechanical position feedback stage only, i.e. the removal of the electrical compensation servo valve; (2) use of the mechanical position feedback servo stage with the addition of a mechanical lead compensator located in the motor-to-spool connecting linkage; (3) use of the mechanical compensation servo stage with an effective area versus spool position discontinuity occurring at a variable value of stroke; (4) use of the electrical damping servo valve with motor

velocity feedback; and (5) use of the electrical damping servo valve with motor acceleration feedback. The choice of operational mode was reflected in a series of computer switch and potentiometer settings, i.e. by appropriately selecting a series of switch positions and potentiometer settings, any combination of the above options could be established for analysis.

Prior to actually operating the analog computer, a static voltage check was calculated and verified. In employing a static voltage check, all variables that exist as the outputs of analog integrators are assigned specific numerical values. Based upon these values, all other variables involved in the mathematical model can then be calculated. Once the numerical check has been completed, the integrator output voltages (proportional to the numerical values assigned for these variables) are introduced by means of "static check" potentials. All additional variables of the computer program are then supplied with voltages in accordance with the program wiring. A point-by-point check is made, through the complete analog program; if all voltages agree (after considering the particular scale factors at each point in the program) with the previously calculated static check solution, the analog program is considered verified. In the normal case, however, conditions are encountered in which the actual recorded voltage and the voltage required to satisfy the static check calculation disagree at certain points within the program. This condition implies that (1) the mathematical model has been simulated incorrectly, (2) the analog control board has been wired incorrectly (i.e. not in accordance with the print), or (3) the electronic analog computer components are malfunctioning. Once the program has been "de-bugged" to the extent that all voltages agree with the predetermined static check voltages, the final program is considered operational, and the computer simulation begins. In the subject case, the voltage check was verified prior to initiating any computer runs.

2.4 RESULTS OF COMPUTER STUDY

A series of analog computer simulations were conducted, using the Figure 3 simulation diagram, with the parameters initially as specified previously in this section. Preliminary simulations were directed at determining the system

response obtained with only the mechanical position-feedback servo stage installed. As illustrated in Figure 4, the data predicted by the computer for this compensation mode suggested that the resulting measured thrust profile would be highly oscillatory. In fact, the response of the system was observed to be no better than the uncompensated system. The thrust rise time assumed was approximately 60 milliseconds, from an initial value of zero to a final steady state force level of 1200 lbf. Thrust stand and motor deflection data indicate that the entire mechanical system oscillates with a fundamental frequency of the motor spring-mass system (20 hertz). This effect is invariably that of the motor-mass system while the effects of all auxiliary modes are insignificant. Compensator cylinder flow rates further imply that the oscillatory response of the motor assembly is reflected in the hydraulic fluid response. However, phase lag is involved such that the compensation effects of the hydraulic flows are minimized. Note that although the motor is in fact driven back to an equilibrium position by the action of the mechanical position-feedback compensator, the response is observed to be extremely sluggish due to the low gain of the servo system. Higher gains cause the feedback system to become marginally stable or completely unstable, due to the absence of lead in the all-mechanical compensator mechanization.

Introducing a lead-lag compensator in the mechanical linkage between the motor and the position feedback spool produces the response characteristics illustrated in Figure 5. Here it is noted that the system oscillations die out more rapidly than those predicted in the all-mechanical system response of Figure 4. However, the response of the motor in returning to the zero-deflection equilibrium state is still quite sluggish. Although a slightly higher gain could be employed due to the lead-lag compensator phase lead contribution, the net result is only a minimal improvement over the original Figure 4 system. Removing the lead-lag compensator from the mechanical position-feedback servo stage and providing the inner-loop servo valve with velocity feedback produced a set of response variables that were quite similar to those of Figure 5. Thus, the effect of the lead-lag compensation network and that of velocity feedback through a separate servo valve are comparable with respect to the predicted final response.

The analog computer derived data of Figure 6 were obtained from the system illustrated in Figure 1, i.e. an inner-loop acceleration-feedback servo valve with an outer-loop position-feedback mechanical servo stage. Note that the maximum motor deflection from equilibrium has been reduced slightly; further, the thrust stand oscillations that were clearly observed in Figures 4 and 5 have been eliminated. It was also possible, through employing acceleration feedback, to substantially increase the gain (effective orifice area versus spool position relationship) of the mechanical servo stage. With this acceleration-feedback system, the motor is driven from the maximum deflection back to the equilibrium position in approximately 100 milliseconds. Following termination of the ramp force excitation, the measured thrust variable and the input thrust variable are observed to agree within a time span of 50 milliseconds.

In Figure 7, the acceleration-feedback servo system of Figure 1 is subjected to a series of step-function excitations, following the initial truncated ramp excitation. In particular, the true input thrust level is stepped from an initial value of 1200 lbf to a final value of 1600 lbf. Following systems stabilization at this new force level, the input thrust variable is reduced, in step-function fashion, to 800 lbf. The input thrust level is next returned to the 1600 lbf level by means of a step-function excitation, and ultimately returned to a final steady state value of 400 lbf through the application of a ramp excitation. Although the recorded variable scaling was such that apparent "overscaling" occurred in the Figure 7 data, the computer voltages involved did not overscale; hence the measured force data illustrated in Figure 7 are legitimate. In particular, it is observed that following an initial measured force overshoot (and slight subsequent undershoot in the case of the 800 lbf step functions) the measured force level agrees with the true force level within approximately 70 milliseconds, following the application of the step-function excitation. These data, when compared to actual data derived from testing of the physical model designed to ring at approximately 20 hertz, produced a remarkably good correlation.

In analyzing the Figure 6 and 7 data, it should be emphasized that no electrical compensation networks were employed in the inner-loop feedback path. This was due to the fact that only a generalized mathematical model was employed in the Figure (3) mechanization. The application of electrical shaping networks could markedly improve the response of this system by introducing additional selective phase lead contributions.

SECTION III
PHYSICAL MODEL FEASIBILITY STUDY

3.1 INTRODUCTION

In order to evaluate the capability of the active strut assembly to dynamically compensate in a simulated test environment, a generalized "physical test model" was constructed in the Aerojet Controls Laboratory. The physical model included a single degree-of-freedom Aerojet thrust stand, a hydraulic power supply with appropriate delivery piping, a high-pressure gas system for initially charging the pressure accumulators, active strut compensator and calibrator assemblies with the required electro-hydraulic servo valves, electronic control systems, feedback instrumentation, standard recording instrumentation and end recorders. Due to the non-availability of component parts, the physical test model was mechanized with an electrical position-feedback servo system, rather than the mechanical position-feedback servo stage discussed in the previous section. Although the computer model and physical model thus differed in configuration, computer run data illustrated that the outer-loop (position feedback) dynamics did not influence the active strut control system response appreciably; thus the substitution of an electrical outer-loop feedback system for the mechanical feedback stage did not invalidate the computer study.

The one principal problem that was involved in development of the active strut compensator concept was the acquisition of a suitable thrust forcing-function capability. A variety of force calibration approaches were investigated; these include the use of (1) a gas-piston force generator, (2) an impulse pendulum, and (3) an electro-hydraulic ram retraction actuator. Of the three approaches tested, only the impulse pendulum and ram retraction actuator proved satisfactory.

Active strut testing in the Controls Laboratory was conducted in four distinct phases. Phase I consisted of testing conducted upon the "uncompensated" or standard thrust stand assembly. In this series of tests, the test stand was "adjusted" for natural ring frequencies of 16 and 30 hertz. Various types of forcing functions were then applied, and the degree of thrust stand oscillation and force measurement system distortion noted. These Phase I tests formed the basis with respect to which the effectiveness of the active strut configurations could be measured. Phases II, III, and IV consisted of testing conducted upon the compensated thrust stand; in all cases the outer-loop feedback signal was derived from a position potentiometer. Inner loop feedback was derived from a strain gage accelerometer, a crystal accelerometer and a servo accelerometer respectively. Test data illustrated that all compensation modes produced thrust data that were superior to the uncompensated thrust stand system. The active strut configuration that employed the servo accelerometer was observed to yield the most desirable compensation.

3.2 PHYSICAL SYSTEM MECHANIZATION AND FORCE GENERATOR SELECTION

A symbolic block diagram of the active strut compensation approach employed in the feasibility testing of the physical test model is illustrated in Figure 8. As observed, the physical test model differed from the model assumed for analog computer simulation only to the extent that the mechanical feedback servo stage was replaced by an electrical position signal derived from a feedback potentiometer, operating through a standard servo valve. With this exception, however, all other physical characteristics of the developmental model were effectively in accordance with the computer model.

The schematic diagram that illustrates the hydraulic and pneumatic supply system used to mechanize the active strut compensator cylinder and force generator systems is presented in Figure 9. Note that high-pressure nitrogen gas is used to "charge" the accumulators. Once the accumulators are charged with gas and hydraulically filled at the 3000 psi pump discharge pressure,

rapid flow demands required in the active strut compensator and the ram actuator circuits are accommodated by flow directly from the accumulator. In this system, the pump acts simply to slowly replenish the accumulator capacity. The electrical representation indicated in the lower-left portion of Figure 9 indicates a simplified version of the electrical feedback and command voltage supply systems.

A total of three force generator concepts were evaluated in an effort to develop a suitable excitation capability. The first consisted of a "pendulum" force applicator, i.e. an appropriate mass was installed on the end of a pendulus rod, attached to ground by means of a bearing. The ground attachment was placed such that the pendulous mass, when in vertical equilibrium, just touched the thrust stand moving mass at the aft end. Application of the pendulous mass force generator introduced an impulse-like forcing function to the thrust stand mass. However, this forcing function has the undesirable features of exciting all system natural frequencies and is a more severe force environment than that to be expected from a rocket engine.

As illustrated in Figure 10, two additional approaches were mechanized in order to develop a step-like forcing function. The "force generator" shown at the aft end of the thrust stand mass of Figure 10 consisted of an open-ended gas actuator. The "ram generator" shown at the forward end of the Figure 10 thrust stand mass was a double-ended hydraulic actuator that was controlled by an open-loop servo system. The gas actuator assembly was connected rigidly to ground and to the thrust stand mass. The ram generator actuator case was attached rigidly to ground; the piston assembly, however, was connected to the moving thrust stand mass through a bearing surface such that in the "retracted" position, the piston was completely decoupled from the stand.

In simulating the step-like forcing function that exists during the start transient of a high-acceleration rocket motor, the gas actuator force generator was pre-pressurized to an appropriate level, and the ram actuator

was extended until a zero force reading was achieved on the measurement load cell. This calibrator adjustment procedure was accomplished with the active strut compensator servo systems disabled. The active strut was then activated, and the ram actuator was rapidly retracted. For a sufficiently rapid retraction rate, the ram generator was found to be decoupled from the moving thrust stand mass; hence a true gas-actuator-derived step function in force was applied to the thrust stand mass. Thrust, position, and acceleration data derived from this type of step-function excitation test, conducted upon the uncompensated thrust stand configuration, indicated that external damping was introduced through the gas-actuator generator. The effective single degree-of-freedom system damping ratio was increased from 0.03 to about 0.08; this produced a significant and undesirable stabilization of the thrust measurement system.

In order to remove this external damping, a third force excitation concept was developed, in which the gas-actuator force generator of Figure 10 was physically removed, such that the thrust stand mass was no longer coupled to the aft force takeout assembly. The ram generator mechanical length was now increased such that, in the fully extended position, the measurement load cell was placed in tension. Upon rapidly retracting the ram, the uncompensated thrust stand was permitted to "ring out" in a manner similar to that experienced during a true motor test firing. However, rather than stabilizing at a steady state force level, the thrust measurement system stabilized at a zero force level. This final step-like force excitation concept produced data that were similar to those derived in standard thrust stand "twang" testing.

To summarize the types of external force generators that were evaluated during this study program:

(1) The pendulous mass produces an impulse-like force excitation; the thrust measurement system achieves a steady state force level of zero.

(2) The combination of gas-actuator force generator and ram generator release mechanism produces a step-like forcing function through which the thrust measurement system achieves a steady state force level equal to the gas-actuator force input. With this system, however, undesirable external systems damping is provided by the gas-actuator assembly.

(3) By physically removing the gas-actuator, the ram generator produces a step-like force excitation; the thrust measurement system achieves a steady state force level of zero.

Data were derived for both the uncompensated and compensated thrust stand assemblies when excited by all three types of force generator concepts.

Figures 11 through 16 illustrate the physical model mechanization, together with the physical form of the force generator concepts. In Figure 11 the physical appearance of both the impulse pendulum calibrator (shown in the unexcited or vertical position) and the input gas-cylinder actuator is indicated. Note that an external source of high-pressure inert gas is supplied to the gas actuator through a standard regulator and valving arrangement. Also, an external high-pressure volume was supplied to the gas cavity; this volume represented an attempt to minimize interaction between gas-cylinder applied force and motor motion. An input force transducer was installed in the string to provide a redundancy in thrust measurement.

Figure 12 illustrates both the active strut compensation cylinder and the ram calibrator. The active strut compensator is attached to the thrust stand by means of an isolating flexure as shown; the compensator is also coupled to ground through a standard 2000 lbf measurement load cell in series with an isolating flexure. Note that the height of the force measurement strut is adjustable such that a variety of thrust stand natural frequencies could be attained. Standard 5000 psi pressure transducers were mounted on both the extension and retraction ports of the active strut compensator in order to monitor the cylinder cavity pressures.

The ram actuator assembly is shown slightly below the active strut compensator in Figure 12. The ram piston is attached to the thrust stand directly, through a bearing surface as discussed previously. The ram actuator servo valve and position measurement potentiometer installations are also indicated.

A photograph of the principal hydraulic plumbing configuration is illustrated in Figure 13. Note that the position-feedback servo valve is located near the thrust stand and is coupled to the active strut compensator by means of long flex hoses, while the acceleration-feedback servo valve is close-coupled to the compensator. Two pressure accumulators were employed in the final system configuration as shown.

Figure 14 represents a detailed view of the electrical position-feedback system, including the position potentiometer, servo valve assembly, and pressure accumulator, in addition to various hand valves and an inert gas pressure gage. Also, the mounting configurations for two feedback accelerometers are shown, i.e. the accelerations are indicated mounted against the motor retention cradle. Figure 15 indicates the recording system employed, together with electronic servo controllers and power supplies required for control and data acquisition. An overall view of the Controls Laboratory test system is illustrated in Figure 16.

3.3 DISCUSSION OF TRANSIENT FEASIBILITY TEST RESULTS

3.3.1 Uncompensated Test Stand Response

Subsequent to the assembly of all components involved in the Aerojet physical model thrust stand assembly, but prior to the installation of the active strut compensator into the physical thrust stand model, a series of thrust stand calibration tests were conducted. The thrust stand was designed, to some extent, as a "thrust stand simulator". The natural frequency of the

physical model could be varied from approximately 15 hertz to approximately 50 hertz by the process of varying the thrust takeout measurement height. Preliminary dynamic response testing was conducted upon the uncompensated thrust stand system, for thrust stand natural frequencies of approximately 20 and 30 hertz, when perturbed by the three types of force generators discussed previously (i.e. the impulse calibrator, the gas-piston steady state force generator in conjunction with the ram retraction calibrator, and the ram retraction calibrator employed without the gas-piston actuator).

In Figure 17 is illustrated the results of an impulse response test, conducted upon the uncompensated thrust stand, adjusted for a 20 hertz natural ring frequency. It is noted that the measured force, acceleration and position variables exhibit the sustained oscillations characteristics of the conventional uncompensated thrust stand.

Figures 18 through 21 indicate the response obtained from the uncompensated 20 hertz thrust stand when subjected to a series of rapid-release tests, after being initially preloaded into tension. For this application, the ram actuator calibration system was installed, while the gas-actuator calibration system was removed from the system. The ram calibrator was initially extended, placing the normal thrust stand measurement strut in tension. The ram actuator was then retracted rapidly under servo control. Thus, at some arbitrary time, an electrical voltage was impressed across the coils of a servo valve that is coupled hydraulically to the ram actuator piston. The level of the electrical voltage is proportional to the speed of retraction, and hence is roughly proportional to the rise-time of the forcing function excitation. To illustrate, in Figure 18 the ram retraction potential level is 4 volts. The thrust stand response shows an oscillatory nature as expected; however, the fact that only 4 volts were impressed across the ram servo coil caused the relatively low degree of oscillations as indicated in Figure 18. In Figure 19, however, a 6-volt level is impressed across the servo valve coil; hence the

response is considerably more oscillatory. Figures 20 and 21 further illustrate the increased oscillations caused by input voltage levels of 8 and 10 volts respectively.

For the data illustrated in Figures 23 through 26, the ram retraction actuator assembly is employed in conjunction with a gas-cylinder actuator. A pressure level of 200 psi was maintained in the gas-piston actuator cavity; this pressure produced an axial force of approximately 800 lbf. The ram actuator string length was adjusted such that, with 200 psi applied to the gas actuator, a zero thrust level was monitored on the measurement load cell. Rapid retraction of the ram actuator thus had the effect of applying an 800 lbf step to the thrust stand.

The data illustrated in Figure 22 were obtained by removing the ram actuator, installing the gas cylinder actuator, impressing 200 psi across the actuator piston, and applying an impulse force excitation by means of the pendulum assembly. Note that the resulting oscillations in thrust, acceleration and position are heavily damped in comparison to the data illustrated in Figure 17. This additional damping was introduced due to friction associated with the gas-cylinder actuator.

Figures 23 through 26 describe the force, acceleration, and position data that were obtained from the uncompensated 20 hertz thrust stand when excited by step-like thrust calibration forcing functions introduced by the ram generator in conjunction with the gas-cylinder actuator. Again, as the voltage level impressed across the ram generator servo valve increases, the degree of thrust stand oscillation increases, indicating a more and more step-like appearance to the forcing function. Now, however, that the degree of damping for this system is considerably higher than that of the previous data illustrated (Figures 18 through 21), due to the addition of the gas-cylinder actuator.

The information presented in Figures 27 through 35 was derived from preliminary testing of the uncompensated thrust stand, adjusted to exhibit a natural ring frequency of approximately 30 hertz. In Figure 27, the thrust stand is subjected to a pendulum impulse test which, due to the absence of the gas-cylinder actuator installation, caused the thrust stand to oscillate about a zero force value. A series of calibrations were conducted upon the uncompensated 30 hertz thrust stand with the gas cylinder disconnected, as illustrated in Figures 28 through 31. Note that as the voltage level increases across the ram retraction assembly servo valve, the thrust excitation becomes more transient, and hence the thrust stand response exhibits a higher degree of instability and oscillation. From Figure 31, the response of the uncompensated thrust stand is very similar to the response of a linear second order system when excited by a step function. This implies that the force generator, operating upon the uncompensated thrust stand system, is capable of applying a nearly exact step function force excitation.

Figures 32 through 35 describe the results of testing conducted upon the 30 hertz uncompensated thrust stand with a 200 psi pressure applied to the gas-cylinder actuator cavity. Again, one can note that as the ram retraction voltage increases, the thrust measurement system becomes more oscillatory. Also, the high degree of damping that was exhibited by the 20 hertz thrust stand, when coupled to the gas-cylinder actuator is also exhibited by the 30 hertz thrust stand configuration.

3.3.2 Strain Gage Accelerometer Feedback Response

Initial testing of the active strut compensation system was conducted employing a strain-gage accelerometer as the inner-loop acceleration measurement device, together with a 3/4-inch conductive plastic potentiometer as the outer-loop position measurement device. The electrical gains of the two loops K_P and K_A could be varied by the process of increasing or decreasing

amplifier gains associated with the inner and outer loop sensors. In particular, the accelerometer feedback signal was computed directly in terms of volts per G's, while the outer-loop position gain was determined as the amplifier gain employed in the system for a 3/4-inch potentiometer with a 10-volt voltage differential applied across the potentiometer terminals. Thus, for $K_p = 6$, the true electrical position gain is determined as 6 x 10 volts/0.75 inch = 80 volts/inch.

Typical data derived from testing of the active strut system with the strain gage accelerometer are illustrated in Figures 36 through 39 for the 20 hertz thrust stand configuration with the gas-cylinder actuator installed. In Figure 36, for a maximum ram retraction, a position gain of six (representing an electrical gain of 80 volts/inch as described above) and an acceleration gain of 1.5 volts/G, the data appeared as illustrated. Note that the measured thrust signature is significantly improved over that derived under identical conditions for the uncompensated thrust stand configuration. Note also that the position data are extremely sluggish; however, the motor-thrust stand dynamic mass is in fact driven to the pre-fire equilibrium position by the actions of the active strut compensator outer-loop. Two channels of data were unreliable throughout the series of strain gage accelerometer testing, i.e. the ram extension position potentiometer produced erroneous readings, while it was impossible to record the strain gage accelerometer trace due to electrical interaction problems.

Both the position and the acceleration gains are increased (to 8 and 3 respectively) in the system configuration employed to generate the data of Figure 37. For a maximum ram retraction rate, the thrust data indicate a more rapid response (characterized by a higher value of overshoot) while the thrust stand position returns to null much more rapidly than in Figure 36. In Figure 38, an increase in position feedback gain to 10 has the effect of further improving the thrust stand position data; however, thrust measurement oscillations are now noted. Reducing the accelerometer gain results in the response illustrated in Figure 39.

To summarize, the active strut mechanization with an electrical position outer-loop feedback and a strain gage accelerometer inner-loop feedback was capable of significantly improving the response of the original uncompensated thrust stand. However, the system was not optimal, as was shown by additional testing.

3.3.3 Crystal Accelerometer Feedback Response

In order to improve the response characteristics of the active strut compensator system, a crystal accelerometer was substituted for the strain gage accelerometer that had been previously employed in the inner-loop acceleration feedback mechanization. Typical data derived from the developmental testing of this active strut configuration, for both 20 and 30 hertz thrust stands, both with the gas-cylinder actuator concept, are illustrated in Figures 40 through 48. In Figure 40, the step-function response of the compensated system is illustrated, with a low accelerometer gain (K_A = 1); for this inner-loop gain, the response is quite oscillatory and, in fact, approaches that of the uncompensated system. Note that the ram extension position trace is invalid due to intermittent instrumentation difficulties that persisted throughout the crystal accelerometer test series.

The next five runs, Figures 41 through 45, indicate the effect of position-feedback gain upon the overall response characteristics of the active strut compensator system. In Figure 41, the acceleration gain is 3 volts/G, while the position gain is 4; this yields the excellent transient force response as indicated, but produces a thrust stand position signature that exhibits a long trailing edge. In order to eliminate this undesirable characteristics, the outer-loop gain was increased to 5, as illustrated in Figure 42. Although the trailing edge has been reduced somewhat, the characteristic is still apparent. For K_p = 6, as in Figure 43, the response appears optimum, i.e. no trailing edge or undershoot characteristics are present in the position data. Increasing the position gain above 6 produces marked undershoots, as illustrated in Figures 44 and 45. Note that, although the variation in outer-loop gains

has a pronounced effect upon thrust stand position data, the variation has no effect upon the thrust measurement signature. Thus it can be stated that the accelerometer governs the thrust data, while the potentiometer governs the position data. This is again in keeping with the information derived during the analog computer simulation study.

In Figure 46 the 20 hertz thrust stand was compensated by an active strut system that was "tuned" to the optimal position gain, but in which the acceleration gain was 5 volts/G. The crystal accelerometer exhibited sustained resonance during the complete run that was reflected in servo pressures, thrust, etc. The system was clearly only marginally stable.

The crystal accelerometer system was next applied to the compensation of the 30 hertz thrust stand. In Figure 47 the "optimal" system that had been determined in developmental testing of the 20 hertz system (i.e. with $K_p = 6$ and $K_A = 3$) was applied to the 30 hertz thrust stand. Note that only 1000 psi hydraulics were employed in this system, thus reducing the system gains and also reducing the speed of the ram retraction. Note that these gains produced severe oscillations in the force measurement signature and a long trailing edge in position. In an attempt to stabilize the 30 hertz thrust stand system, various combinations of acceleration and position gains were considered. One such combination is illustrated in Figure 48. At a ram retraction rate of only 4 volts, the active strut system became unstable at position and acceleration gains of 6 and 5 respectively; this instability remained throughout the entire run.

To summarize, the active strut mechanization with a crystal accelerometer produced compensated thrust data that were superior to those obtained with the strain gage accelerometer. However, again, the crystal accelerometer system did not represent the optimal configuration, as further developmental testing of the servo accelerometer was to demonstrate.

3.3.4 Servo Accelerometer Feedback Response

Of all the types of accelerometer that were evaluated during the active strut development study, the servo accelerometer produced the most optimum compensator system. Both 20 hertz and 30 hertz systems were compensated with significant improvements being achieved in comparison to the uncompensated configuration.

Figures 49 through 51 illustrate the response data that were obtained in the compensation of the 20 hertz thrust stand, excited by a step function in input force with the gas-cylinder actuator installed. The resulting compensated thrust data produce a single rapid overshoot which returns immediately to the desired thrust level. The thrust overshoot is observed to decrease very slightly with position loop gain; the gains of Figure 51 are optimum for this particular test environment.

In Figure 52 the gas cylinder is disconnected, permitting the thrust stand to "ring out" about a zero steady state force level. The data derived for this system indicates again a single large spike overshoot in measured thrust (caused by the finite servo system bandwidth), with an immediate return to the final steady state operating force level. Figure 53 indicates the results of an impulse test applied to the servo compensated 20 hertz thrust stand configuration.

Due to the failure of the crystal accelerometer to provide compensation at the 30 hertz frequency level, the ability of the servo accelerometer to provide this compensation was of extreme interest. A large number of developmental tests were conducted in order to determine the optimum servo accelerometer and position feedback gains for this thrust stand configuration. In Figure 54 a low pressure test with an acceleration gain of 10 volts/G indicated a condition of impending instability. The lowering of the acceleration gain to 7.5 volts/G, as indicated in Figure 55, produces a less oscillatory system, while decreasing the acceleration gain still further (to 5.0 volts/G)

produces a more oscillatory system (Figure 56). These results are due to the fact that at high acceleration feedback gains, the servo system is approaching marginal stability; at low gains the system is approaching the uncompensated system; at median gains, however, the accelerometer feedback mechanism achieves maximum effectiveness. Based upon these data, the servo pressure was increased to 2800 psi, and after conducting a series of developmental tests, isolated the optimum 30 hertz active strut system of Figure 57. Note that the thrust measurement system response is characterized by one very rapid thrust overshoot, followed by an immediate return to the input thrust level. The position data indicate a reasonably rapid thrust stand return to equilibrium. Figures 58 through 61 indicate the response of the active strut compensator to ram retraction rates of decreasing magnitude. Note that the thrust overshoot decreases with ram retraction rate. The final development test data, illustrated in Figure 62, indicates the optimum system response to an impulse excitation.

To summarize, the combination of electrical position feedback (outer-loop) and inner-loop acceleration feedback derived from a servo accelerometer was observed to yield the optimum active strut compensator system.

3.4 COMPUTER DERIVED FREQUENCY RESPONSE DATA

The data illustrated to this point describe the effectiveness of the active thrust strut compensator in significantly increasing the thrust measurement system transient response characteristics. In an effort to present these data in the frequency domain, a computerized approach was applied as follows: Thrust data were recorded on high-speed magnetic tape. The tape was then played back through a high-speed digitizer. Digital thrust data were next analyzed in an automatic digital computer routine, employing the "fast Fourier transform" approach, assuming a step function input thrust excitation. With this assumption regarding the input force excitation, amplitude ratio data were calculated by the computer for both the uncompensated thrust stand and the compensated stand assembly.

The resulting frequency response data are illustrated in Figure 63. It is observed that the uncompensated thrust stand system exhibits a +16 db resonance at 16 hertz; the +16 db value is consistent with data derived for conventional thrust measurement systems from purely dynamic considerations. This implies that the assumption of a step function input excitation is reasonably correct, i.e. if the ram retraction calibrator were not introducing a step-like forcing function, the computed uncompensated thrust stand resonance would be in error accordingly.

Both amplitude ratio curves illustrated in Figure 63 were normalized to 0 db at 1 hertz in order to remove undesirable "bias" from the data. With this known physical reference, it is observed that the uncompensated thrust stand amplitude ratio curve passes through +4 db at approximately 12 hertz, reaches a +16 db resonance peak at 16 hertz, reduces to -4 db at 22 hertz, shows a second resonance at approximately 30 hertz, and is -16 db at 45 hertz. Conversely, the servo compensated thrust stand system is within the band of ±4 db from DC through 45 hertz. The great improvement previously noted in transient response realized through the application of the active strut compensator is thus due to (1) the elimination of the thrust stand resonance, and (2) an extension of the usable thrust stand bandwidth. With respect to these criteria, the former eliminates the "ringing" that characterizes the uncompensated (conventional) thrust measurement system, while the latter greatly improves the ability of the thrust measurement system to accurately portray transient thrust information.

SECTION IV
SOLID ROCKET MOTOR TESTING WITH ACTIVE STRUT COMPENSATION

4.1 INTRODUCTION

Although the active strut concept was determined to be capable of significantly improving rocket motor thrust data in a laboratory environment, the final proof of conceptual feasibility required the actual application of the strut in the captive test firing environment. For this purpose the physical test model that had been employed in laboratory development was disassembled and reassembled in the Aerojet solid rocket motor test facility.

Figures 64 and 65 illustrate the physical thrust stand system incorporating the active strut compensator as installed in the solid rocket motor test bay. The rocket motor shown secured to the thrust stand is typical of those that were available for developmental testing of the active strut compensator system and consisted of propellant-development grains that were designed to fire for a two-second duration and generate approximately 300 pounds of thrust. Figure 66 illustrates the active strut compensator assembly and ram force calibrator, together with associated servo valves and plumbing. Figure 67 indicates the position-feedback potentiometer, servo valve, accumulator, and miscellaneous electrical wiring and hydraulic/pneumatic plumbing.

4.2 DATA DERIVED FROM UNCOMPENSATED SOLID ROCKET MOTOR TESTING

A series of short duration (two seconds) solid rocket motors were statically test fired upon the uncompensated thrust stand system in order to form a base reference for later comparisons. Data derived from a typical rocket motor firing, employing this configuration, are illustrated in Figure 68. As was the case in laboratory testing of the uncompensated thrust stand system, the firing data of Figure 68 illustrate that severe oscillations occur

in recorded thrust. Thrust stand ringing occurs throughout the entire solid rocket motor test duration. Chamber pressure data suggest that the start transient of propellant-development solid rocket motors is characterized by a rapid thrust rise time (25 milliseconds) and an initial force overshoot. Acceleration and position data are derived from the servo accelerometer and the feedback potentiometer.

In all cases of uncompensated thrust stand testing, it was observed that stand oscillations produced slightly negative force levels during and immediately following the motor start transient. The form of the force signature during these periods of zero-crossing indicate that the thrust stand system had been adequately assembled, i.e. no apparent dead-band about the zero force level is observed to exist.

After satisfactorily testing a number of solid rocket motors on the uncompensated thrust stand system, the active strut compensator was installed, but for the subsequent test firing the compensator was hydraulically locked such that no active compensation was possible. In this mode of operation, the compensator functioned as an in-line hydraulic damper. Test data derived from this solid rocket motor firing are illustrated in Figure 69. Note that although the resulting thrust stand oscillations are damped more rapidly in comparison to the uncompensated stand data of Figure 68, the improvement in response is attributed only to a reduction of the characteristic resonant peak amplitude shown in the frequency response diagram of Figure 63. Thus, as anticipated, thrust stand response is improved with the introduction of a passive damper, but the response is not improved significantly.

4.3 DATA DERIVED FROM COMPENSATED SOLID ROCKET MOTOR TESTING

Following completion of the solid rocket motor firing employing the compensator damper approach, a series of development motors were statically test fired employing the active strut compensator concept developed in the Controls Laboratory. In particular, identical control system gains were

inserted in the control system, and ram retraction calibration testing conducted to insure that the slight increase in mass had not seriously affected the initial design. In this context, it should be noted that the additional motor weight had the effect of lowering the thrust stand ring frequency; however, since the thrust measurement strut height was adjustable, this increase in mass was compensated by a slight increase in effective strut spring constant in order to maintain the 16 hertz natural frequency system.

Data derived from a typical compensated solid rocket motor captive test are shown in Figure 70. Note that the initial peak in chamber pressure is much more severe than previously noted in Figure 68. The active strut compensation test program confirmed, as illustrated in test data such as that of Figure 70, that significant improvements in rocket thrust measurements are possible. Problems that had been anticipated by some sources regarding the inability of a ground-reference system to function correctly under the severe dynamic test environment were found not to exist. Although slight shifts in the steady state motor position occurred, with respect to the initial equilibrium position, these shifts were on the order of a few thousandths of an inch; the shifts are considered to arise due to dead-band and hysteresis in the servo valves, slight electrical biases, etc.

In observing the compensated data of Figure 70 in comparison to the uncompensated data of Figure 68, it is noted that the initial portions of the two runs are quite similar, indicating that the active strut compensator does not become totally effective for some small period of time following a motor generated thrust variation. Further, it is noted that the initial acceleration surge, following motor ignition, is more severe for the compensated stand than for the uncompensated stand. This initial positive acceleration is made more severe by the compressibility of the actuator hydraulic fluid, i.e. the load strut reaction must be transmitted through the hydraulically coupled piston-cylinder actuator. Compressibility of the hydraulic oil in this coupling system

permits the rocket and thrust stand mass to rapidly accelerate initially; once the fluid is placed in compression, however, the total restraining force consists of dynamic as well as static contributions. This in turn causes the large returning (negative) acceleration observed clearly in Figure 70, and results in the correspondingly large thrust measurement system overshoot. The force overshoot produced by the active strut system is thus a result of a negative "rebound" acceleration which, in turn, is caused by the initial positive acceleration surge. The response of the active strut compensator is thus observed to be critical in terms of minimizing the initial acceleration surge.

SECTION V
SUMMARY OF RESULTS AND CONCLUSIONS

The technique whereby an active strut compensator assembly is inserted into the typical rocket thrust measurement system in order to increase the bandwidth of that system has been shown to be both feasible and physically realizable with state-of-the-art hardware. Data have been gathered for a 2000 lbf thrust stand compensation system that demonstrate significant improvements in both thrust stand damping and usable bandwidth. The extension of this technique from the low-thrust environment (up to 2000 lbf) to a higher-thrust environment (20,000 lbf and above) is also feasible, although certain problems of a "scaling" nature will possibly arise.

During analog computer simulation studies conducted upon a generalized thrust stand and active strut compensation system, a variety of control system modes were identified and studied. It was affirmed that a purely mechanical-position feedback mode of stabilization gave rise to a marginally stable (highly oscillatory) response. The introduction of velocity feedback, or a lead compensator in the thrust stand position feedback signal, produced a slight improvement in stability; the general oscillatory nature of the response however remained. The introduction of an inner loop compensation servo, driven by a signal proportional to achieved thrust stand acceleration was observed to greatly improve stability while also permitting the system bandwidth to be extended.

In testing of the physical model that was characterized during analog computer simulation, the differing performance obtained from a variety of physical accelerometers was observed to be critical. In particular, the standard strain gage accelerometer response was such that the resulting thrust measurement system was not optimum from a dynamic point of view. However, it should be

noted that even this non-optimum response represented a great practical improvement over the uncompensated (conventional) rocket motor thrust measurement system. Although the crystal accelerometer and charge amplifier combination represented an improvement over the strain gage accelerometer in terms of the compensated thrust stand response, the unit was susceptible to noise disturbances and again did not produce an optimum response. The application of a servo accelerometer to sense motor-generated acceleration proved to yield the most desirable compensated thrust measurement system response; due to the higher frequency response of this acceleration-measurement device, the inner-loop acceleration gain could be increased over that of the strain gage or crystal devices. This higher inner-loop gain resulted in a more clearly defined capability for the extension of rocket-motor-derived thrust data.

Testing of the active strut concept in conjunction with a group of propellant-development solid rocket motors produced data that verified earlier laboratory results. The comparison of thrust data derived from compensated and uncompensated thrust measurement systems illustrated that both the damping and the bandwidth of the force measurement system had been significantly improved.

Throughout the analog computer simulation studies the active strut compensation configuration was assumed to consist of an electronic acceleration inner-loop feedback, together with a mechanical position outer-loop feedback. This combination was considered for all analog computer simulation runs. In physically implementing the results of the analog computer runs, it was unfortunately not possible to investigate the mechanical-position outer-loop concept. Rather, a standard electrical potentiometer was employed as an outer-loop position sensor, with the resulting error signal being impressed across the coils of a standard servo valve. Although this represented a non-optimum approach to the measurement and application of a position error signal, the physical thrust stand test results were in essential agreement with those data predicted through computer simulation. This fact correlated with conclusions

derived from the computer simulation, i.e. that reasonably small lags and gain variations in the outer loop (and resulting non-optimal position variations during and immediately subsequent to thrust transients) did not appreciably influence the type of thrust data obtained. Thus, if the active strut system is capable of responding to motor-generated acceleration signals, the outer-loop position signal servo need be of only low gain and limited response. This statement was again reflected in the large response variations produced by relatively small variations in accelerometer gains and response.

Certain sources had indicated that a critical problem area would exist with respect to referencing the motor-thrust stand dynamic mass to the "ground" environment that exists during a rocket motor static test firing. Thus, the thought was proposed that the vibrational conditions encountered during the static test firing of rocket motors would preclude the sensing of a local reference ground for purposes of providing a stabilizing feedback signal. Data derived during the static testing of propellant-development solid rocket motors using the active strut illustrated, however, that the use of a reference ground during motor firing presented no difficulties. In all cases the motor-thrust stand dynamic mass was returned, by actions of the active strut compensator, to within a few thousandths of an inch of the original pre-fire equilibrium reference. Further, the derived solid rocket motor thrust signature did not exhibit local irregularities to any appreciable extent.

As mentioned previously, the extension of the low-thrust active strut system to the higher-thrust environment required for practical thrust stand applications may present problems of a "scaling" nature. It was observed that the response of the inner acceleration loop components was critical in producing an optimum thrust measurement capability. In scaling the low-thrust active strut system to the higher thrust levels, the problem of component response becomes highly important. Since the deflections of the moving thrust stand and motor masses do not increase appreciably with an increasing thrust (i.e. measurement strut rigidity increases with thrust level, thus maintaining total

strut deflections about the same), the high-thrust active strut must possess roughly the same dynamic response as the low-thrust strut. This implies that the components that comprise the high-thrust active strut must also be capable of the same dynamic response characteristics as the similar components that comprised the low-thrust active strut in order to provide the same overall compensation capability. This is obviously impossible to achieve for all system components, i.e. a 30 gpm servo valve simply does not have the response of a 3 gpm valve. For this reason, certain components of the high-thrust system must be of higher response than the counterparts of the low-thrust system described in this report. Thus, in order to yield a high-thrust active strut compensator with an ability to improve transient force measurements to a degree consistent with the unit herein described, certain components or subsystems must function with a higher frequency response than the corresponding components or subsystems of the 2000 lbf active strut. Since the low-thrust active strut system was not optimized from a hydraulic design point of view, this area represents one of possible improvement, i.e. the active strut components could be repositioned in the high-thrust design to minimize line volumes and fluid acceleration requirements, thus improving response. Further, the hydraulic oil used in the low-thrust system was susceptible to aeration difficulties, lowering the fluid bulk modulus. In the high-thrust design, a de-aeration system would maintain a high bulk modulus and hence increase overall systems response.

APPENDIXES

I. ILLUSTRATIONS

II. EQUATIONS OF THE MATHEMATICAL MODEL

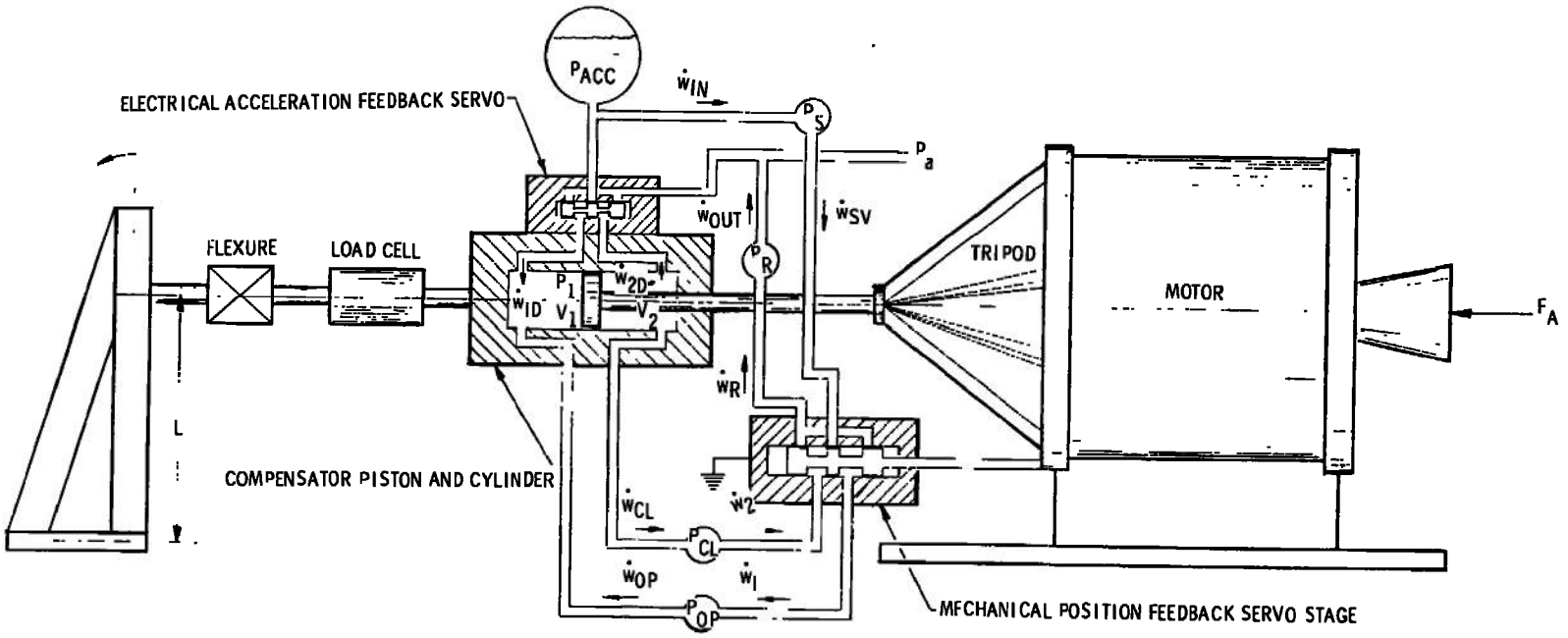

Fig. 1 Active Strut Functional Diagram - Computer Model

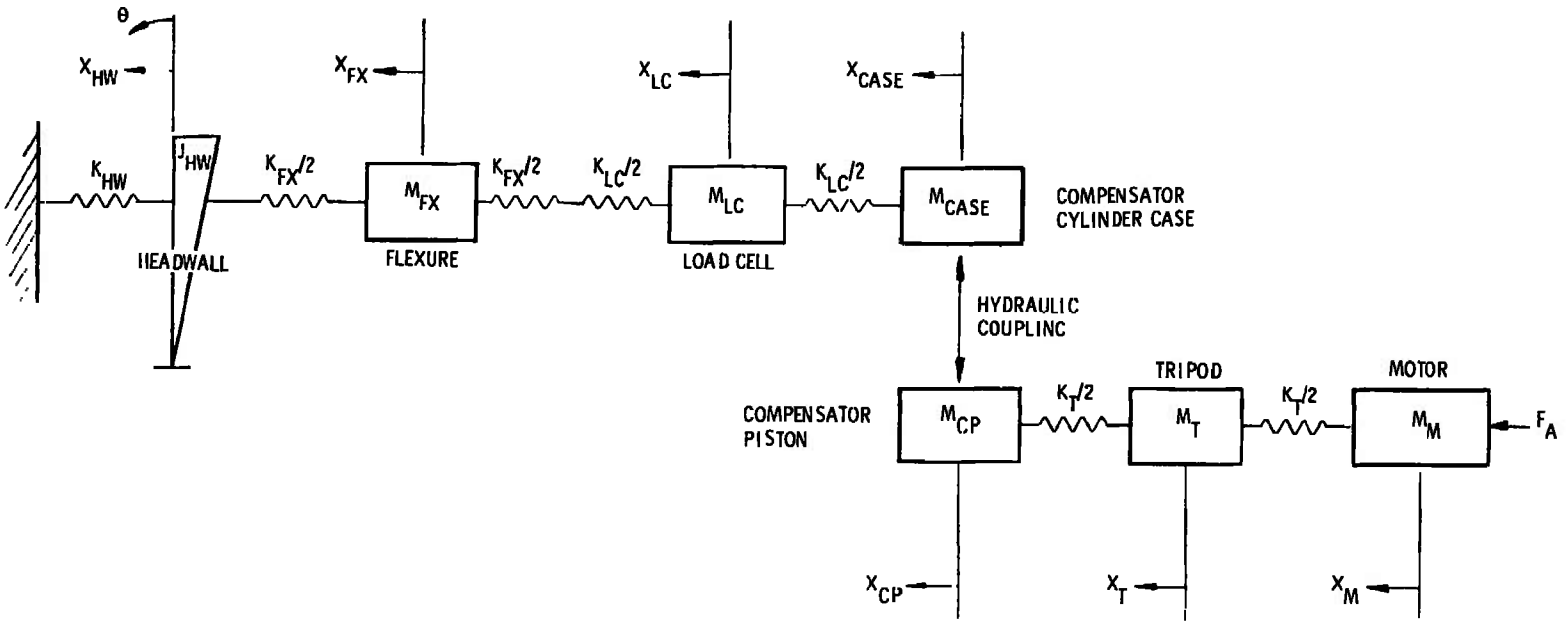

Fig. 2 Mechanical Dynamic Block Diagram for Computer Simulation

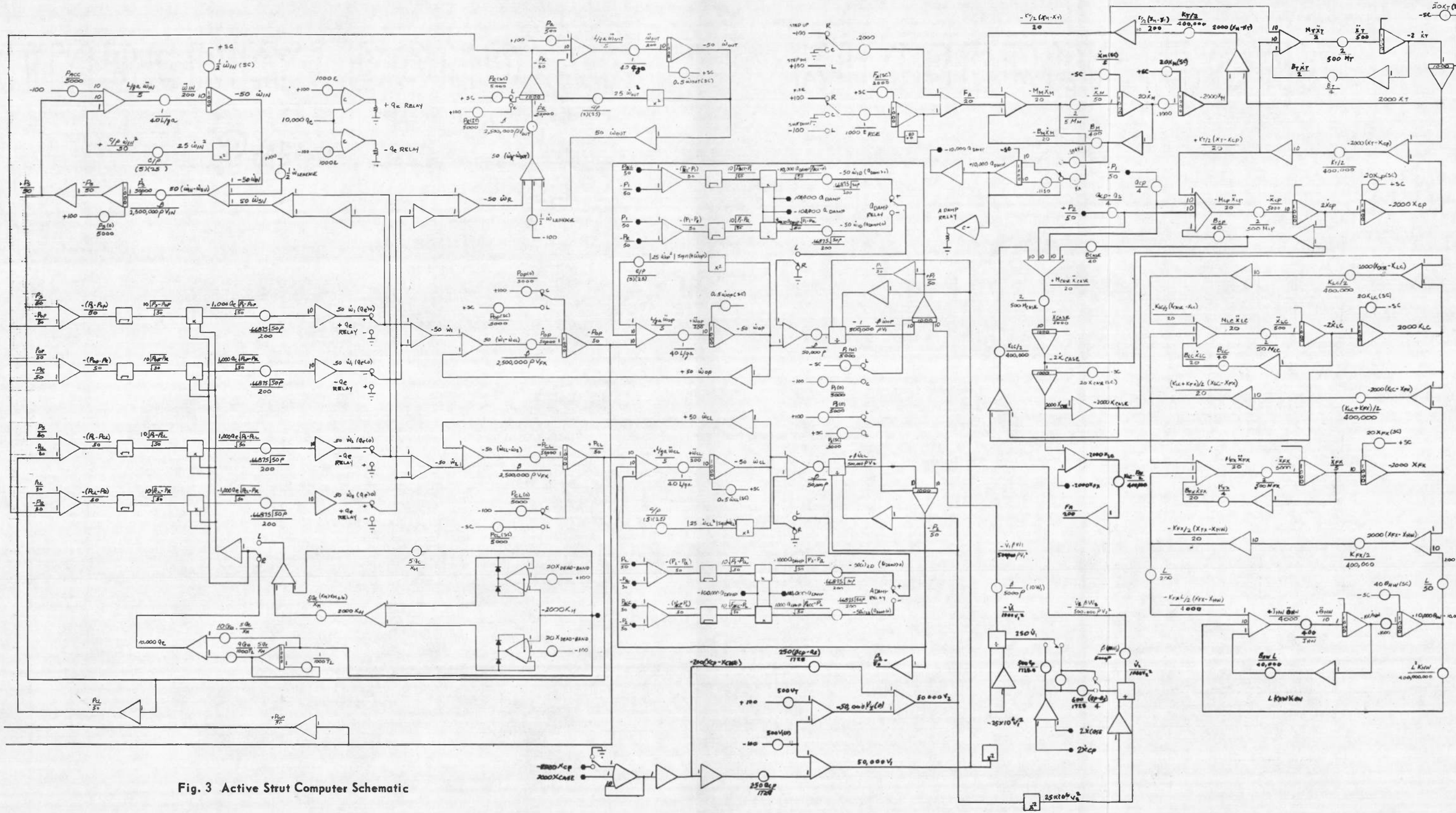

Fig. 3 Active Strut Computer Schematic

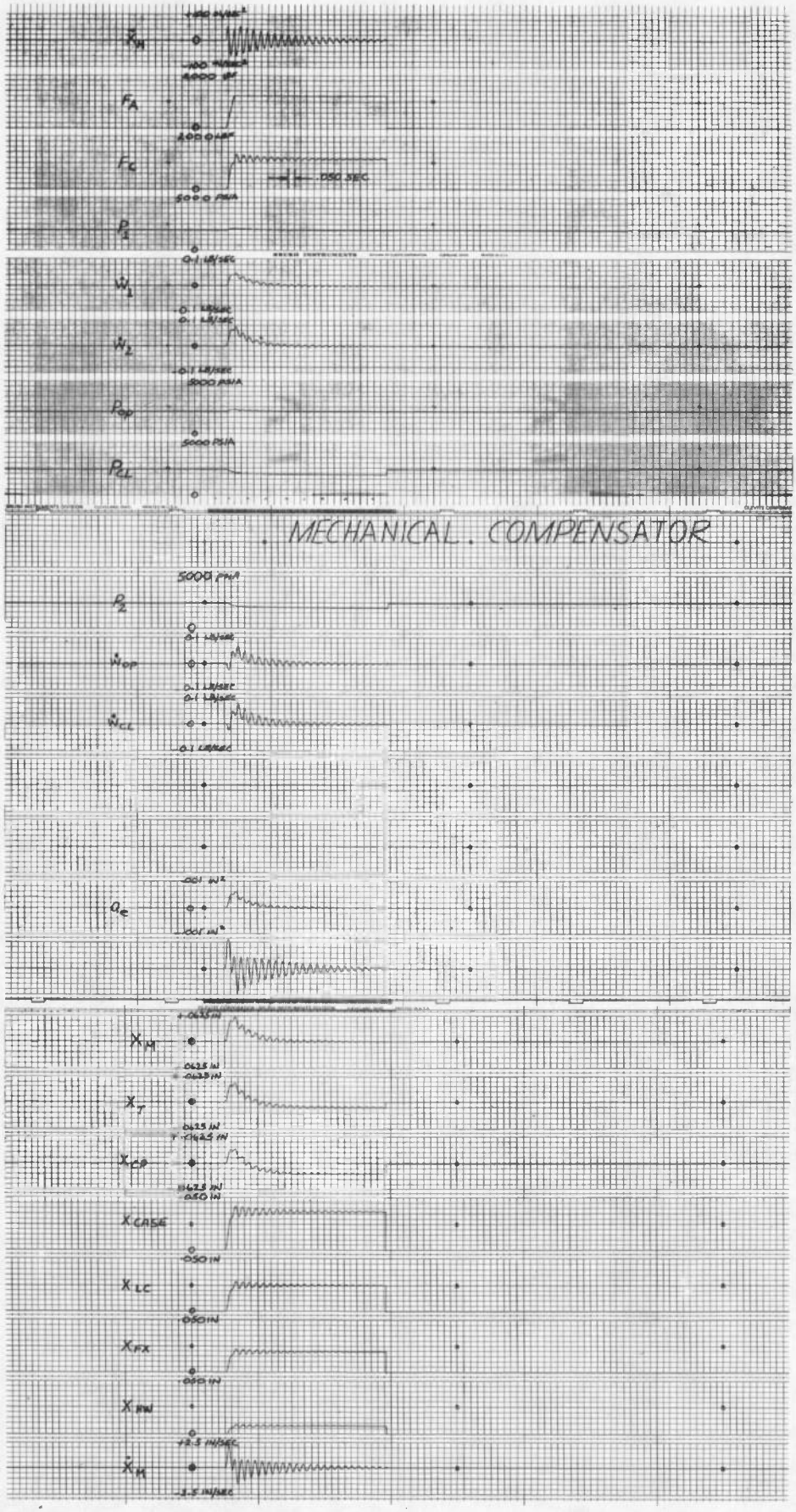

Fig. 4 Computer Response Data - Mechanical Compensator System

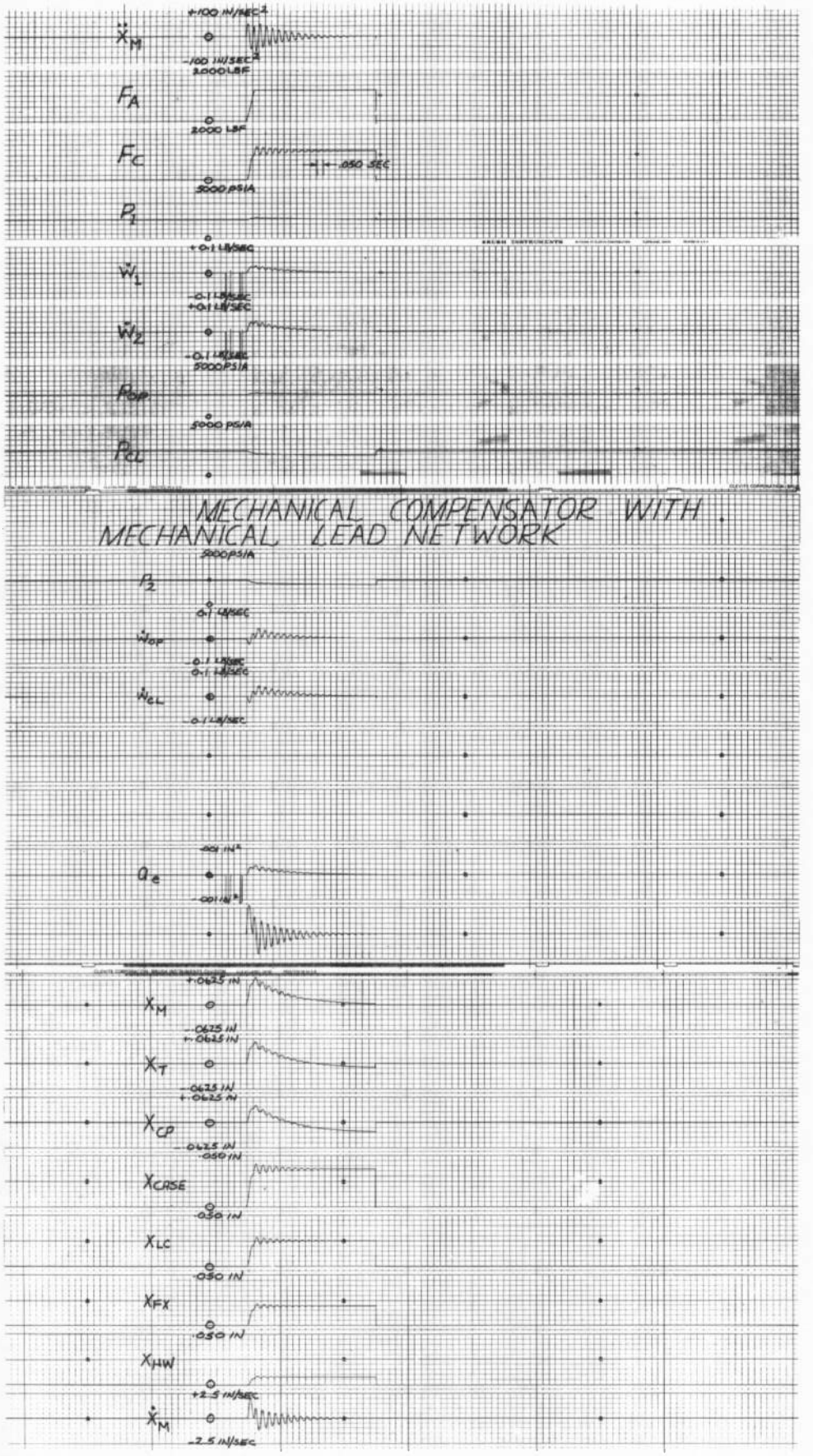

Fig. 5 Computer Response Data - Mechanical Compensator with Mechanical Lead Network

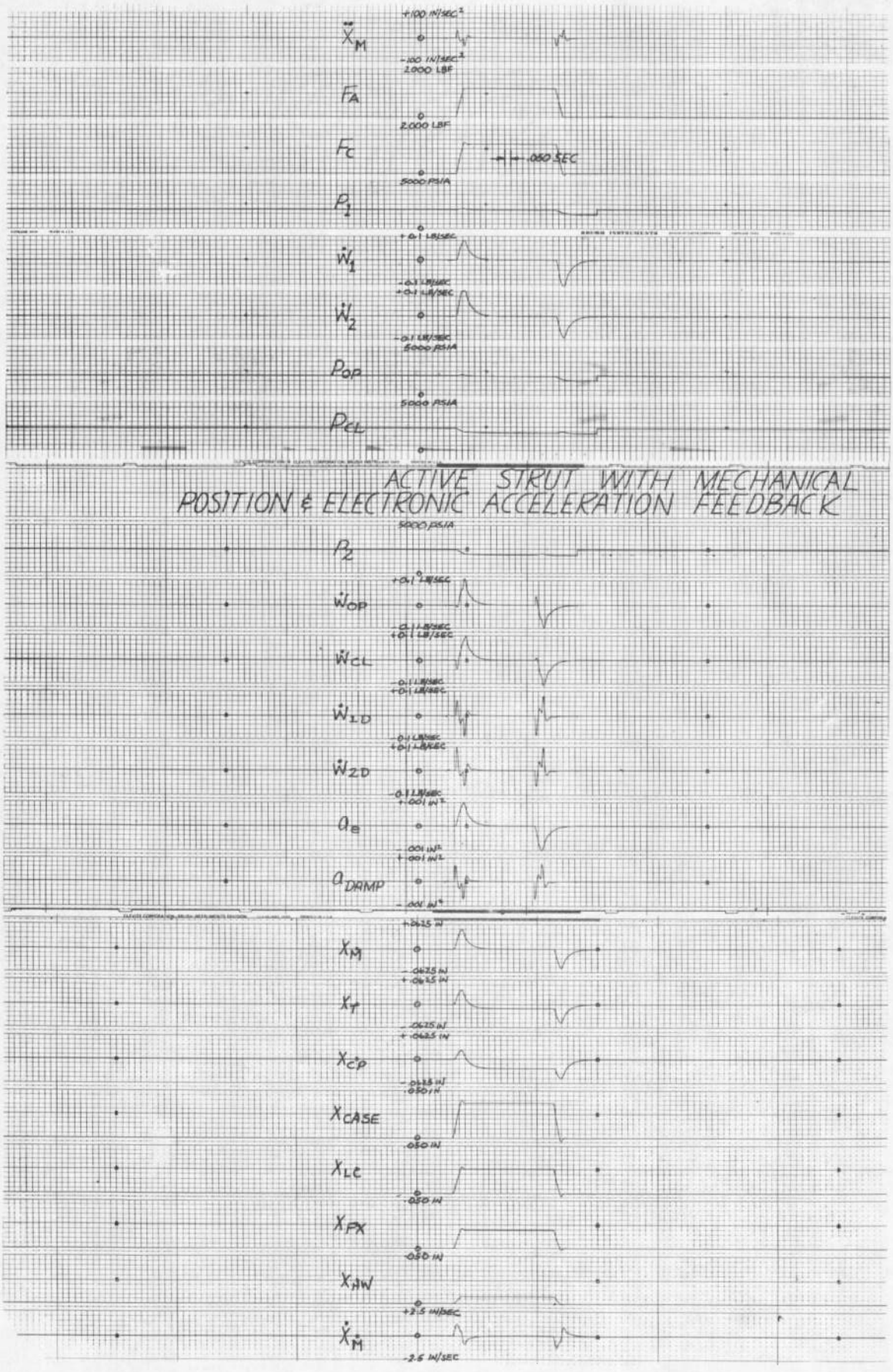

Fig. 6 Computer Response Data - Active Strut with Mechanical Position and Electronic Acceleration Feedback

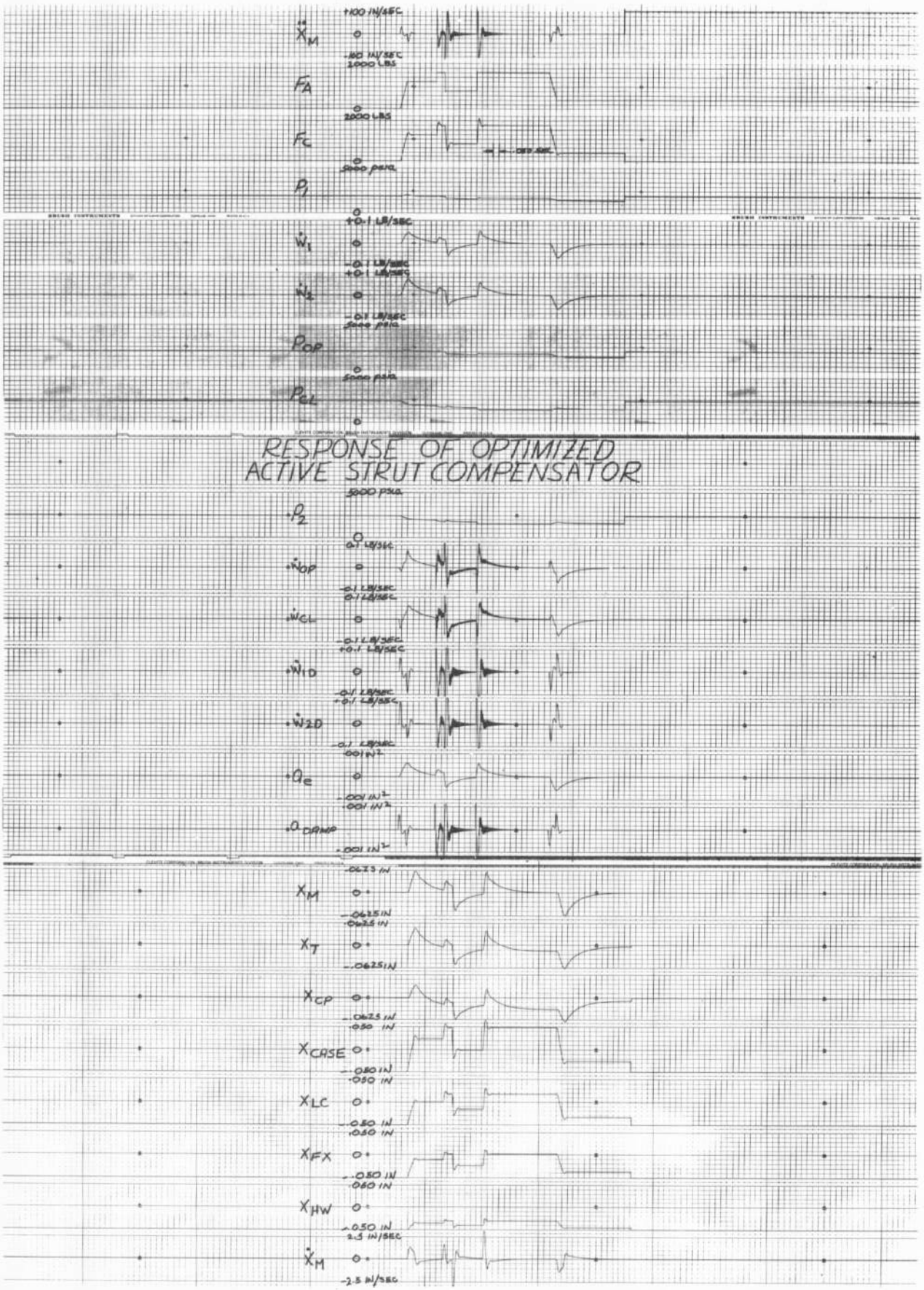

Fig. 7 Computer Response Data - Response of Optimized Active Strut Compensator

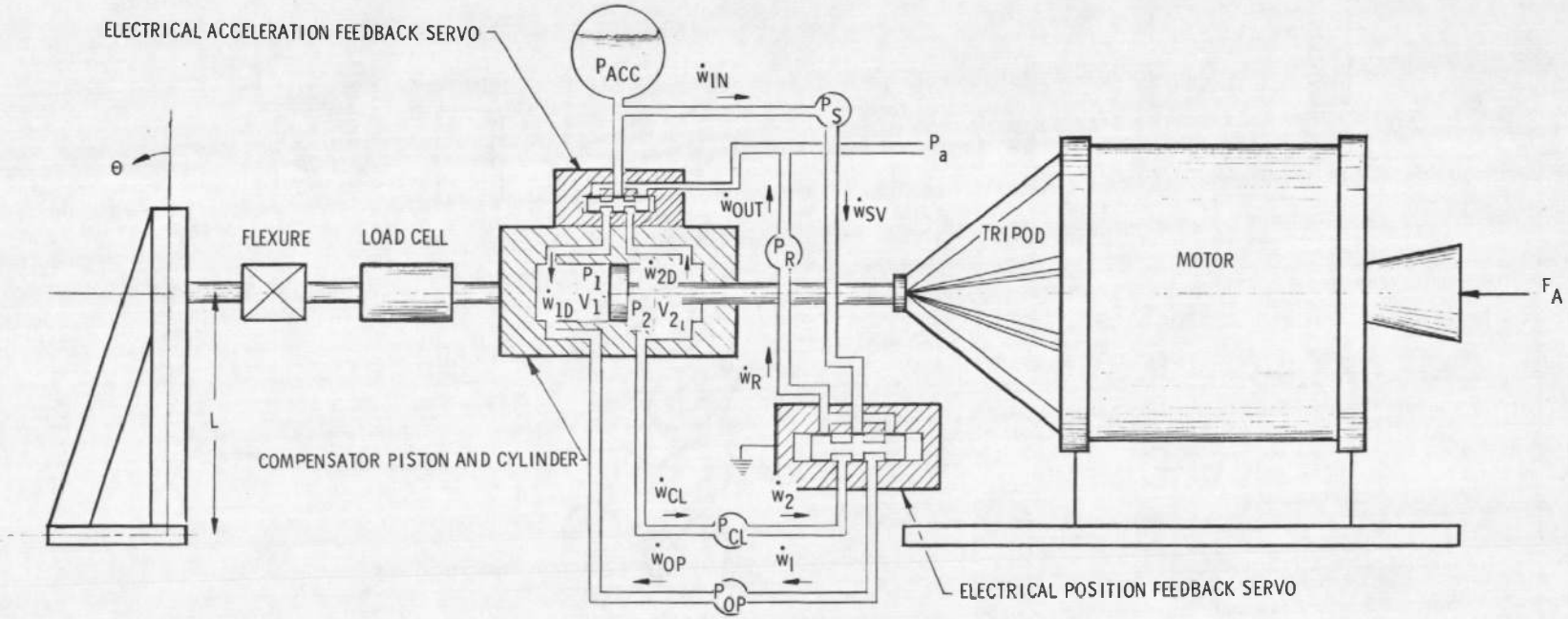

Fig. 8 Active Strut Functional Diagram - Physical Model

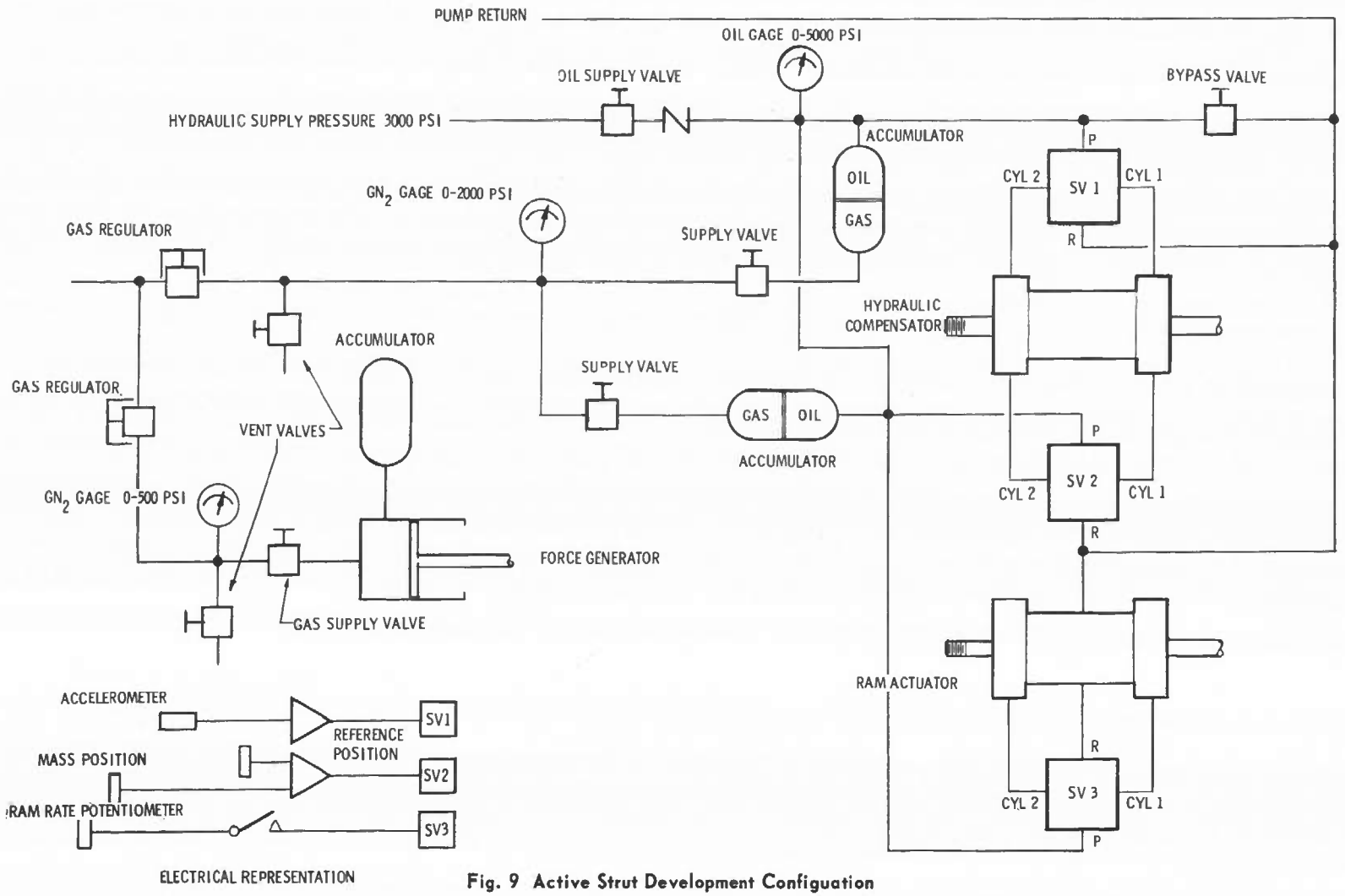

Fig. 9 Active Strut Development Configuation

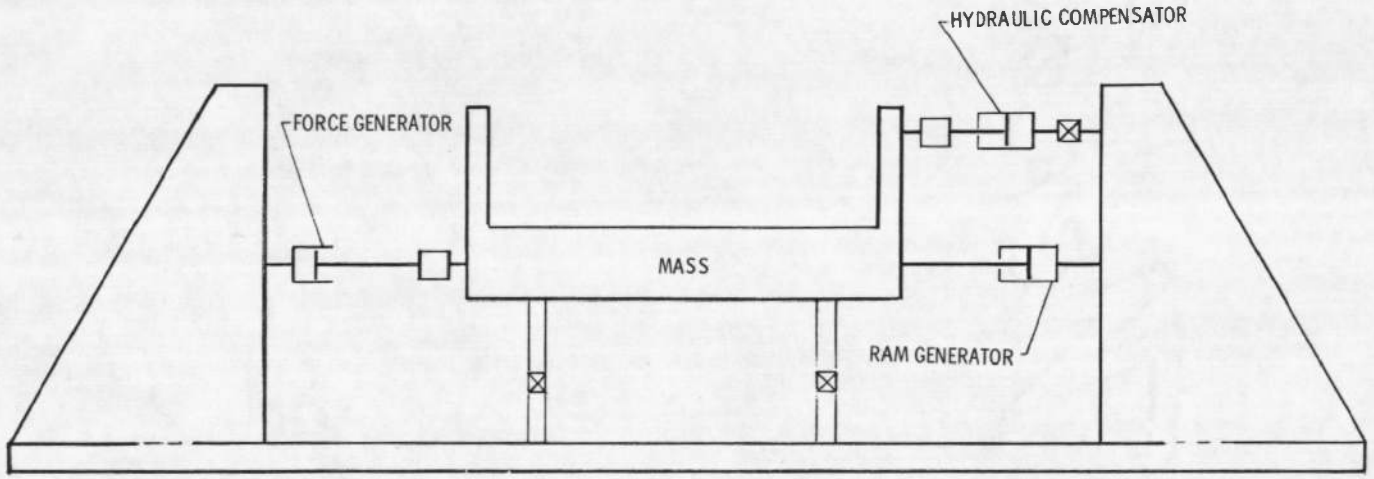

Fig. 10 Component Location for Compensating Strut Testing

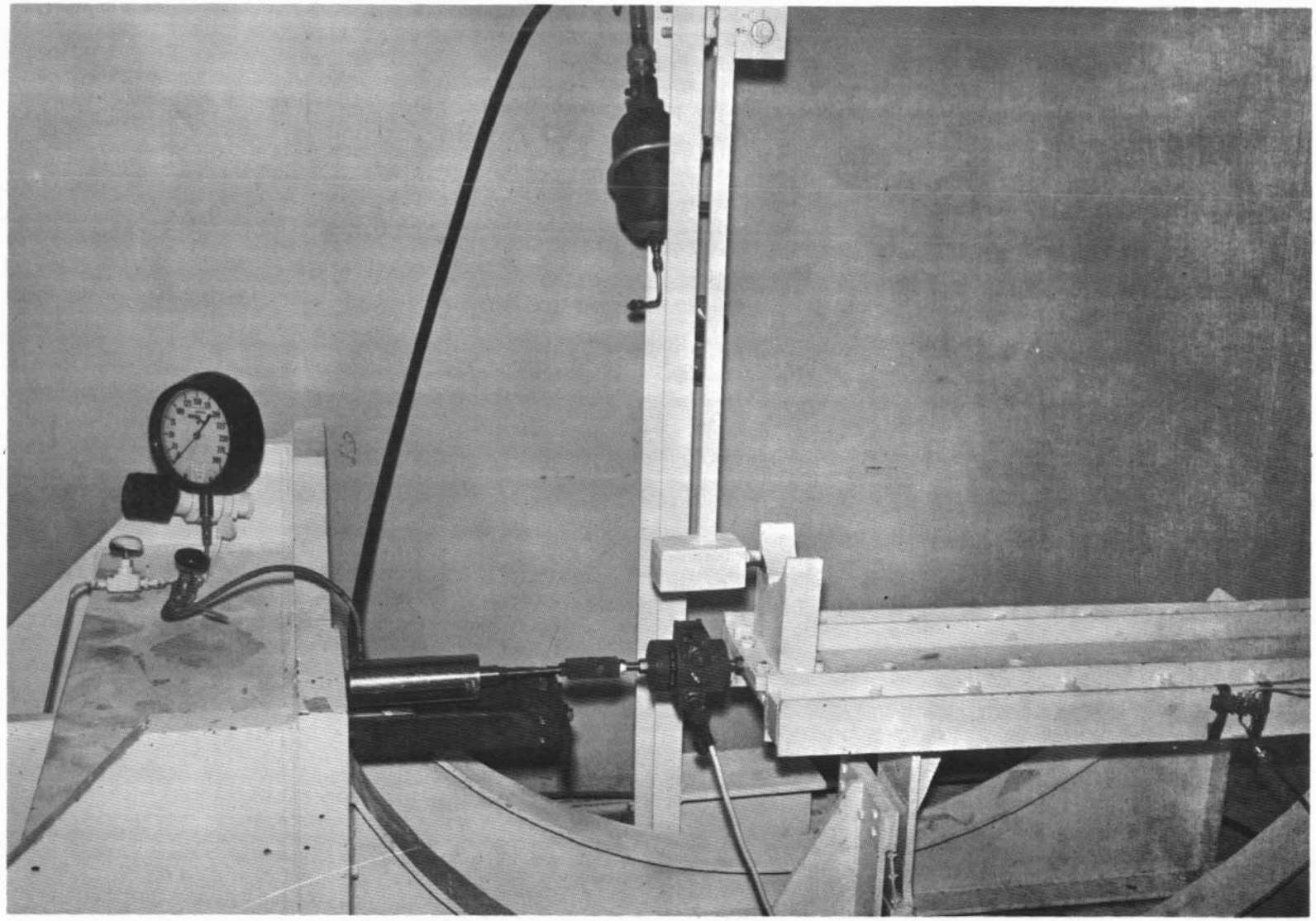

Fig. 11 Gas-Cylinder and Impulse Calibration Assemblies

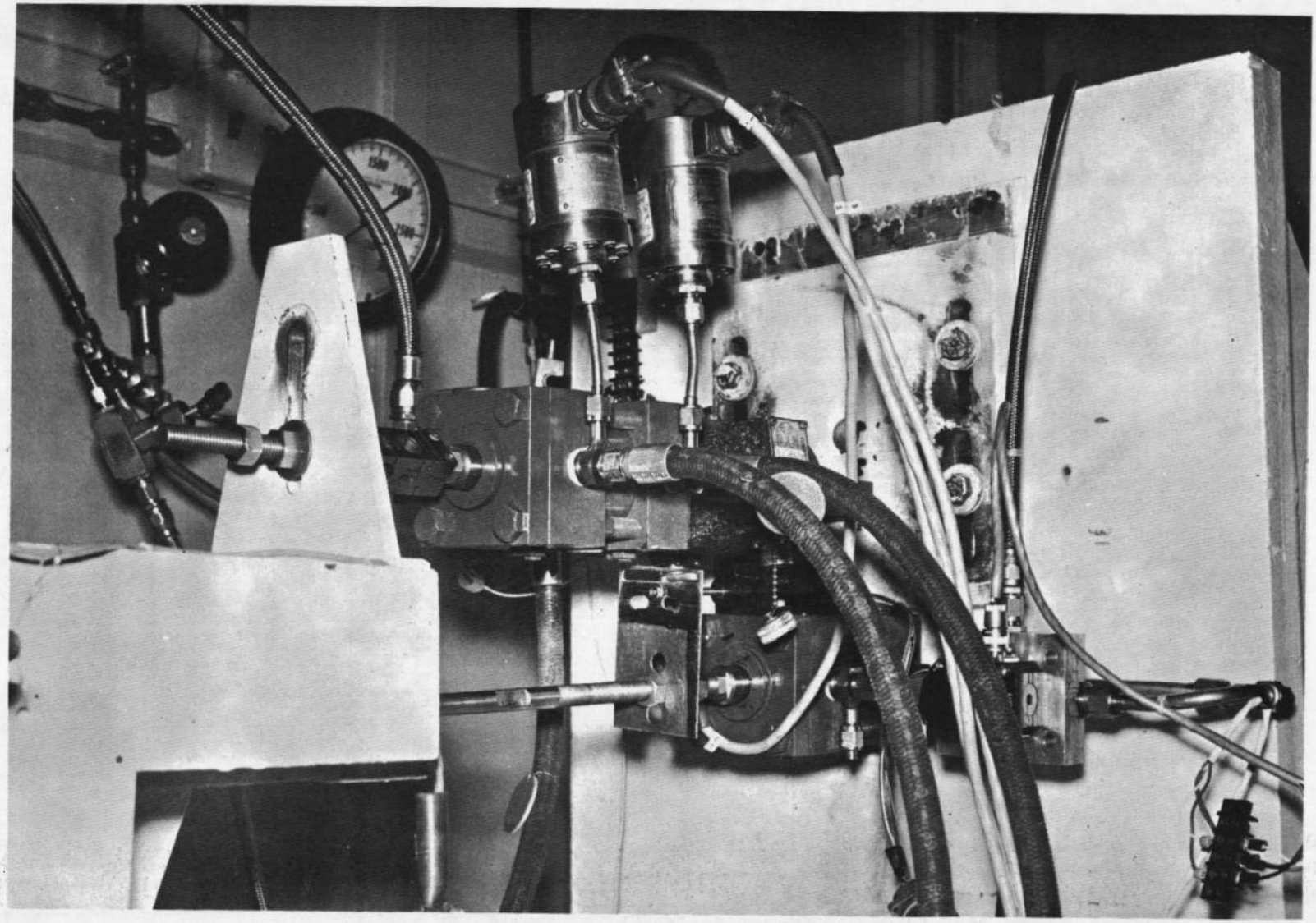

Fig. 12 Active Strut Compensator and Ram Retraction Force Generator

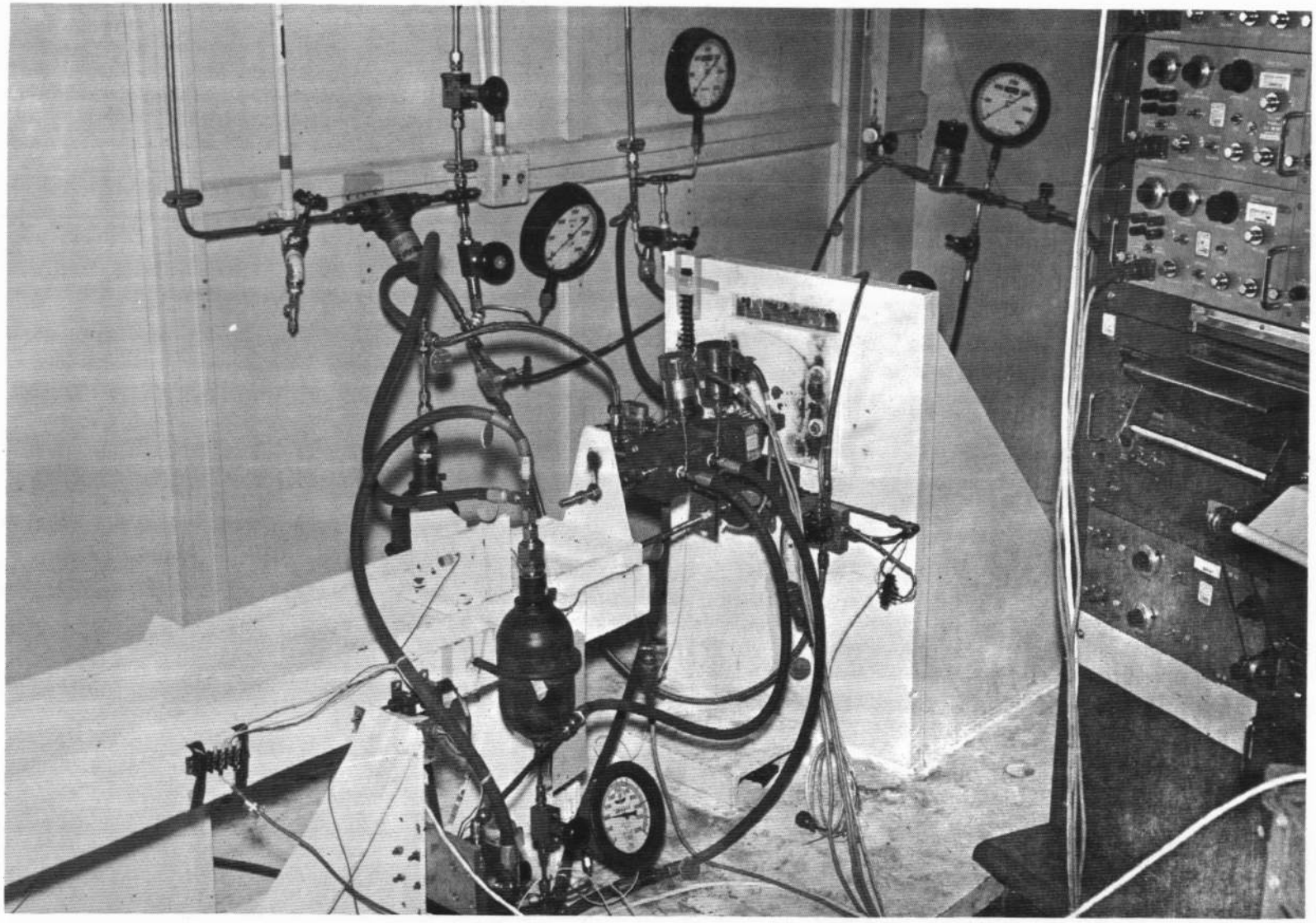

Fig. 13 Active Strut Model Showing Hydraulic Systems

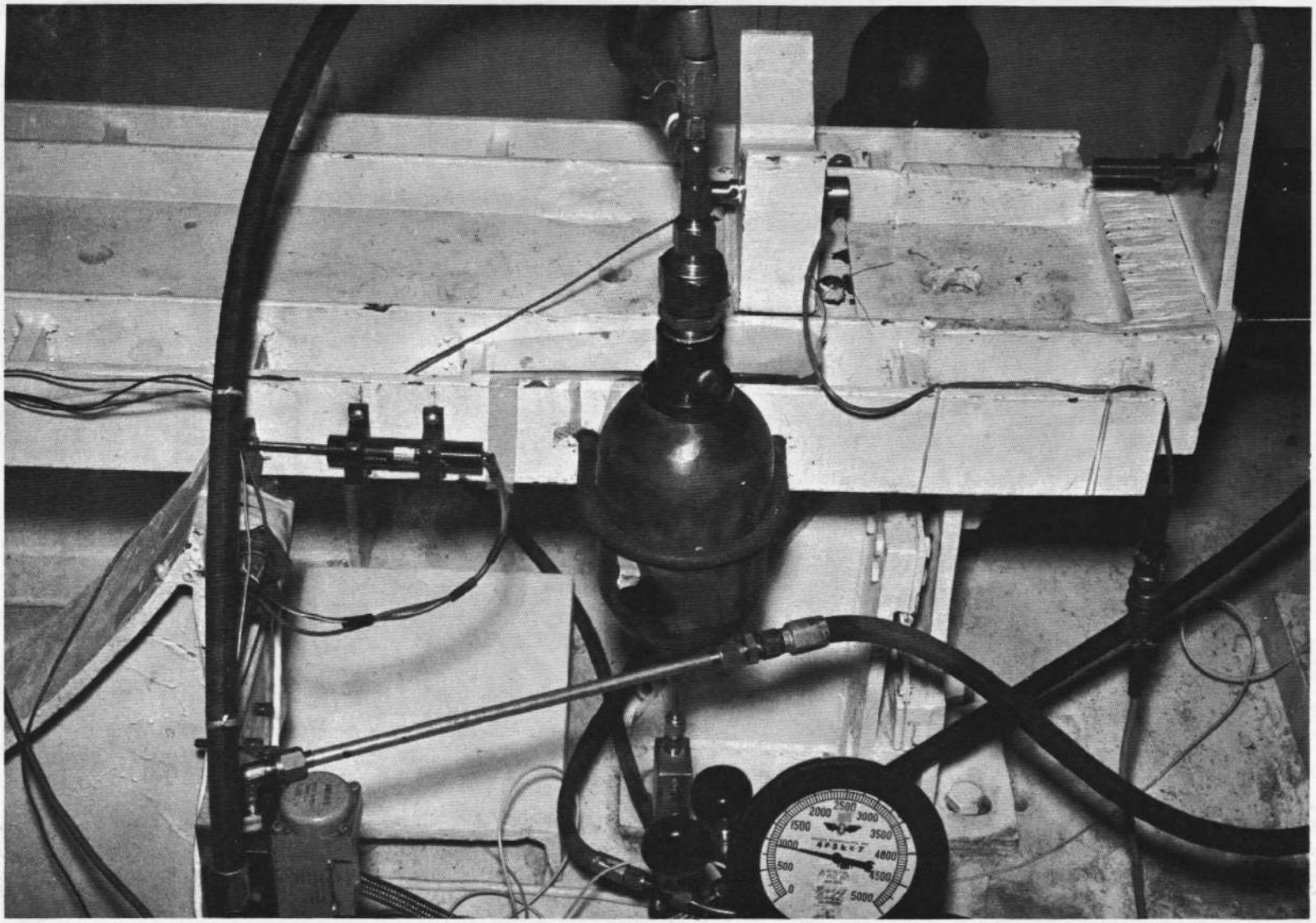

Fig. 14 Electrical Position Feedback Configuration

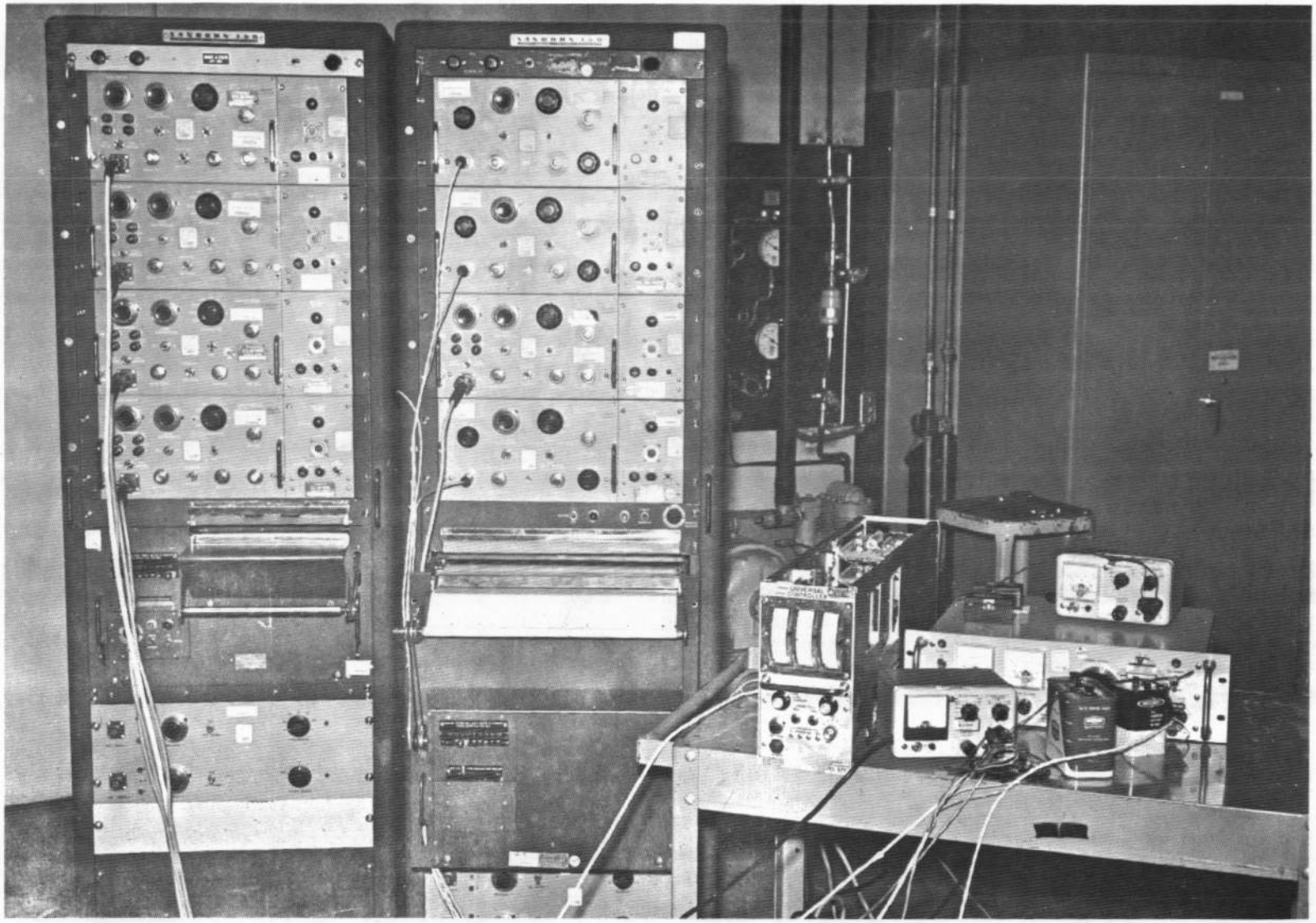

Fig. 15 Electronics and Recorders

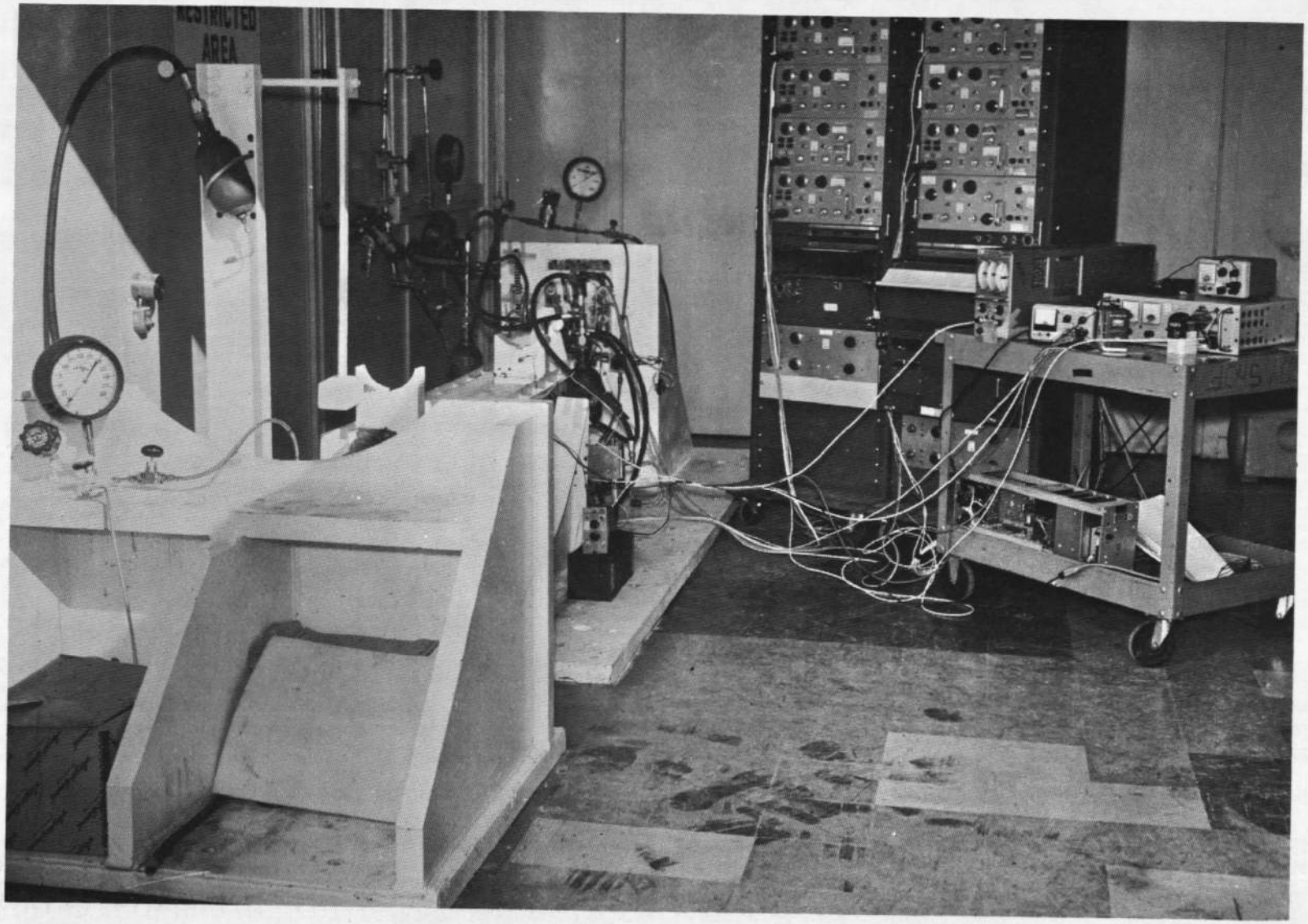

Fig. 16 Overall View of Controls Laboratory Physical Model

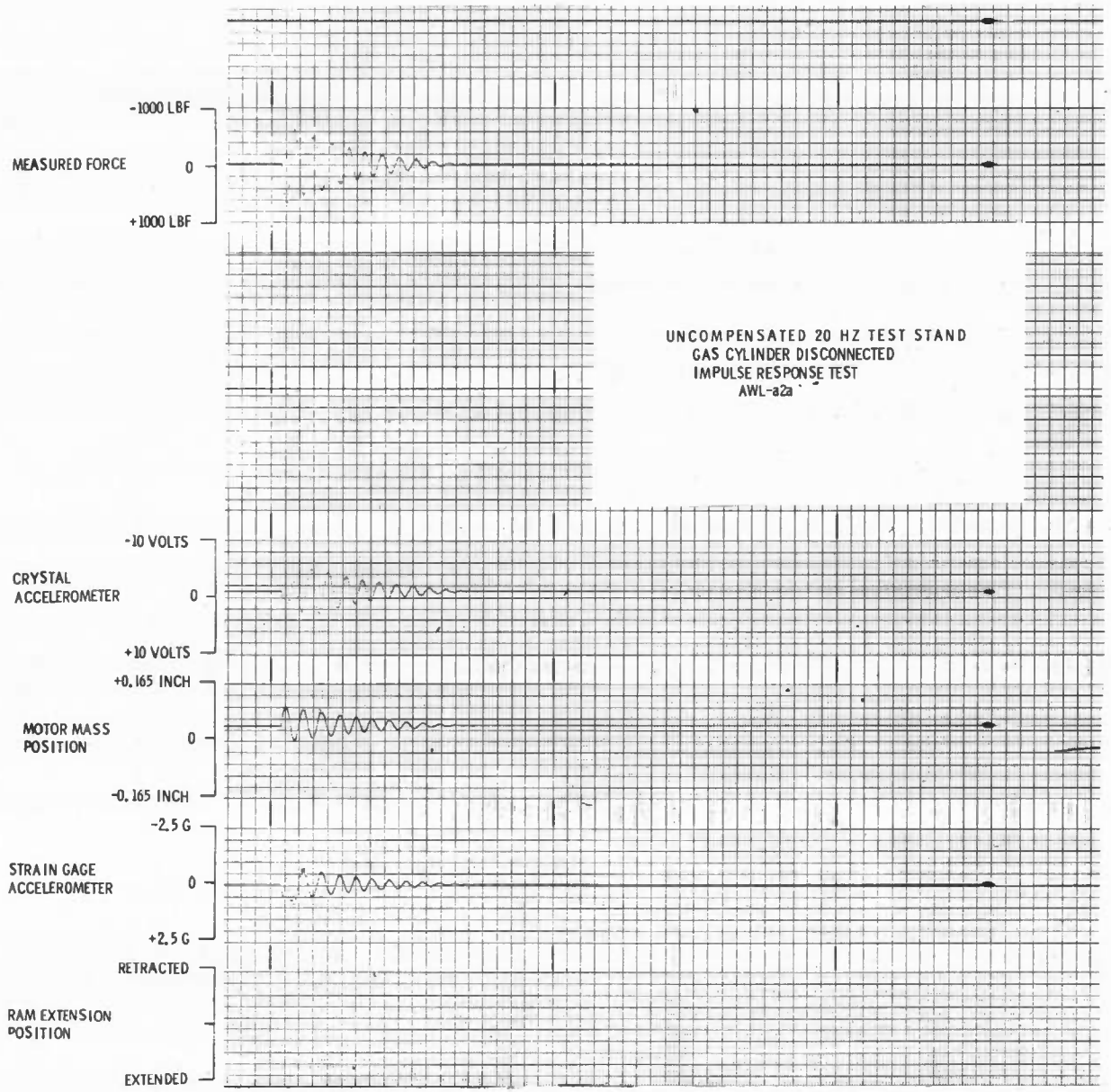

Fig. 17 Impulse Response Test - Uncompensated 20 Hertz Test Stand with Gas Cylinder Disconnected

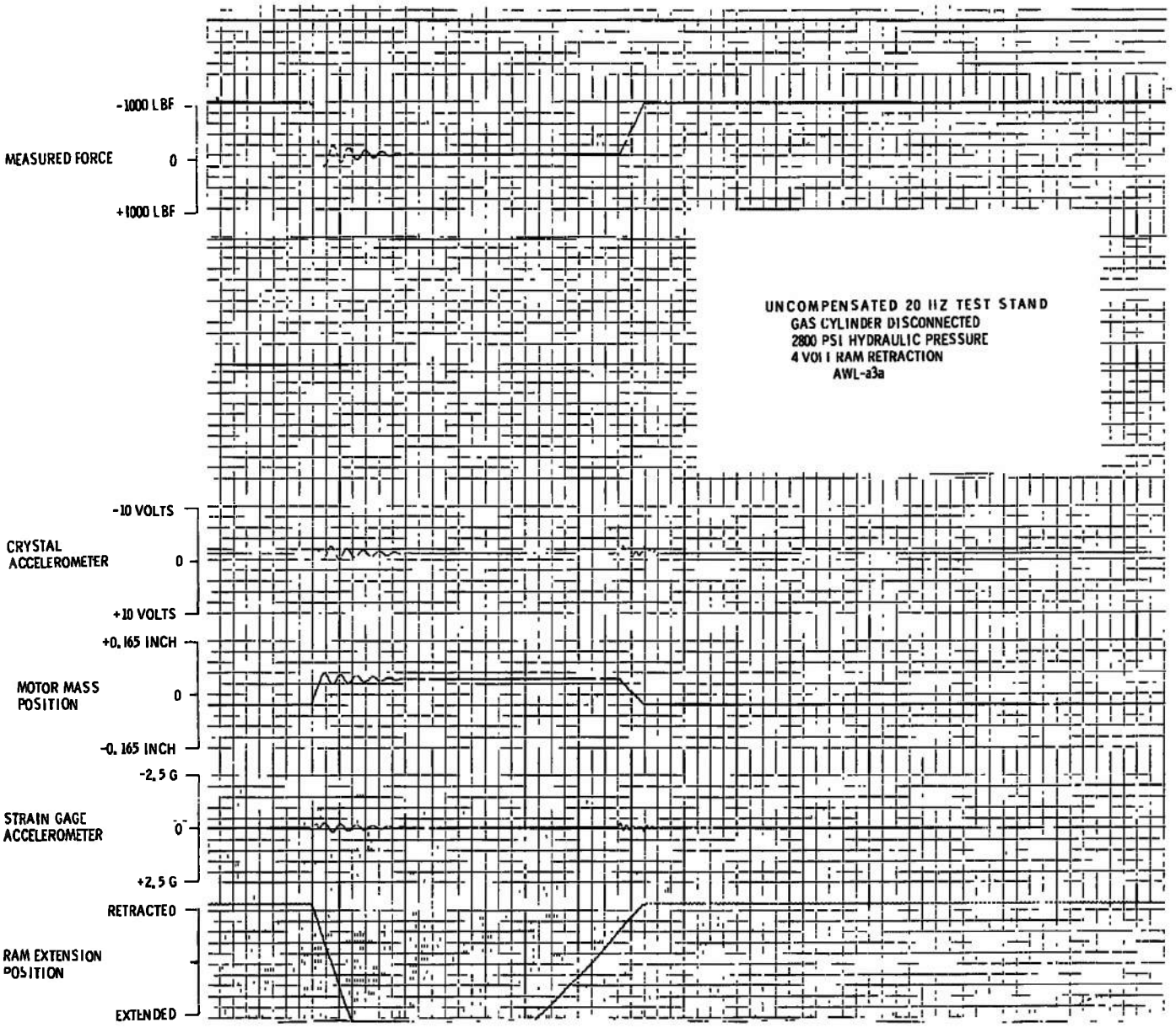

Fig. 18 Ramp Response Test—Uncompensated 20 Hertz Test Stand with Gas Cylinder Disconnected and 4-Volt Ram Retraction Rate

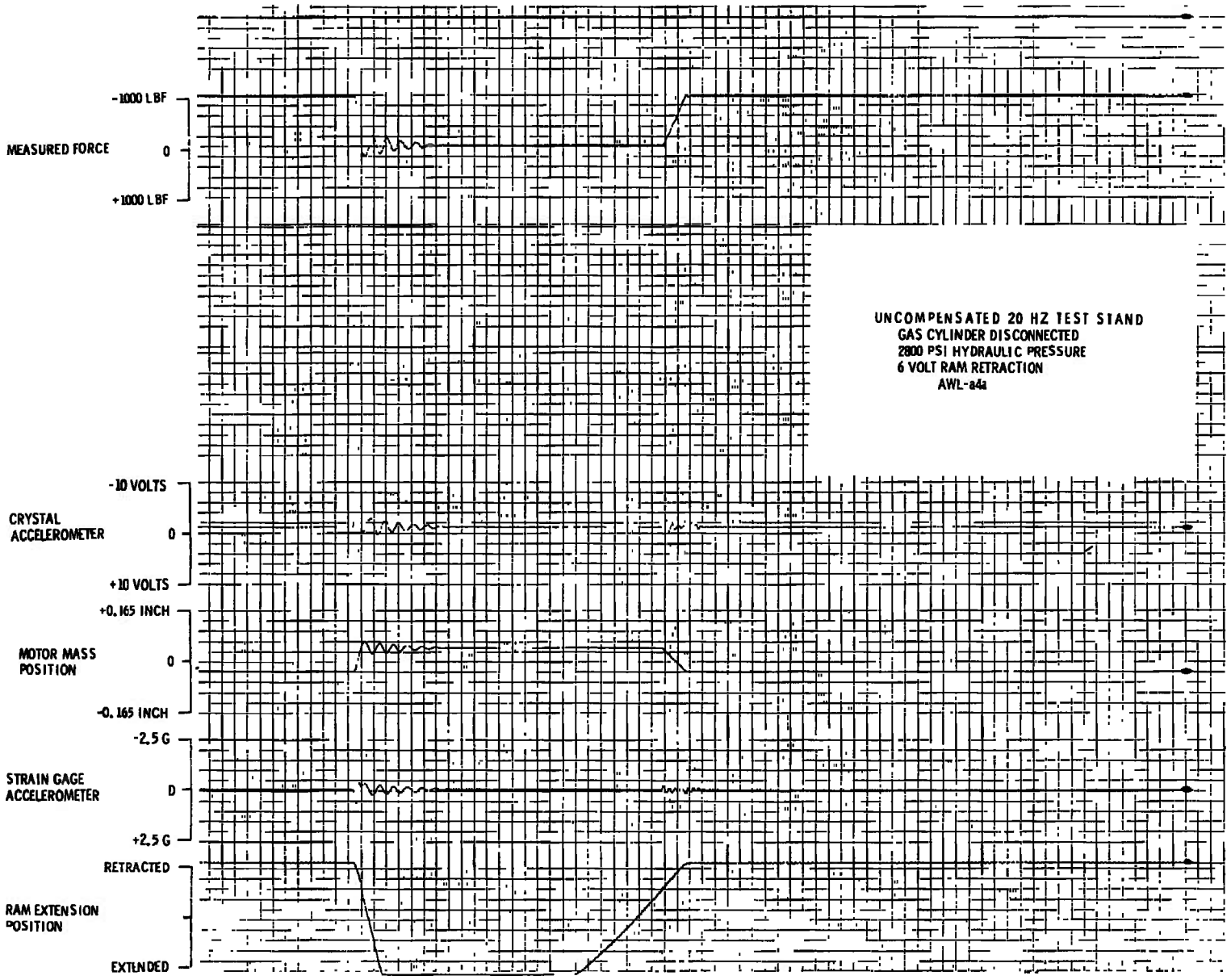

Fig. 19 Ramp Response Test–Uncompensated 20 Hertz Test Stand with Gas Cylinder Disconnected and 6-Volt Ram Retraction Rate

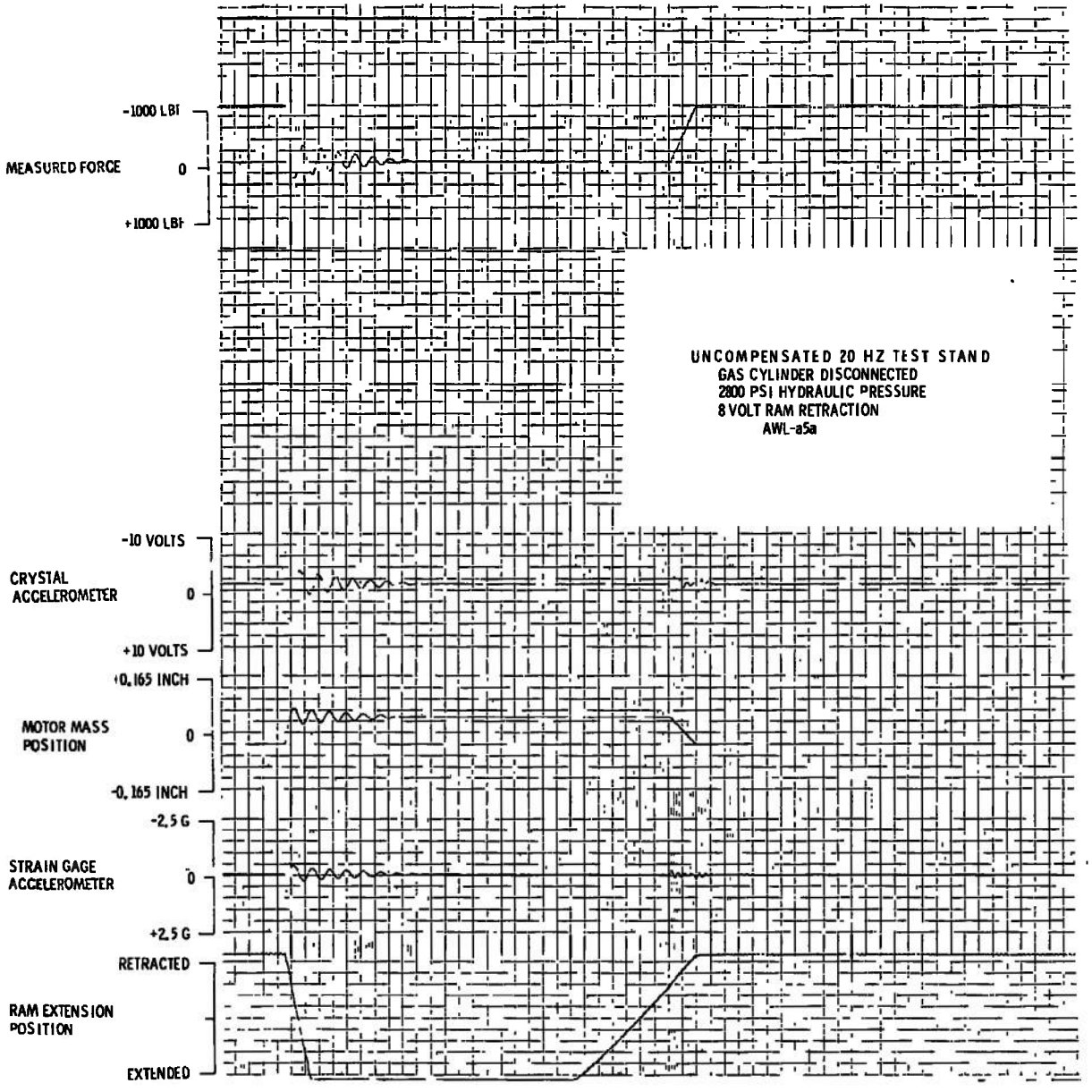

Fig. 20 Ramp Response Test - Uncompensated 20 Hertz Test Stand with Gas Cylinder Disconnected and 8-Volt Ram Retraction Rate

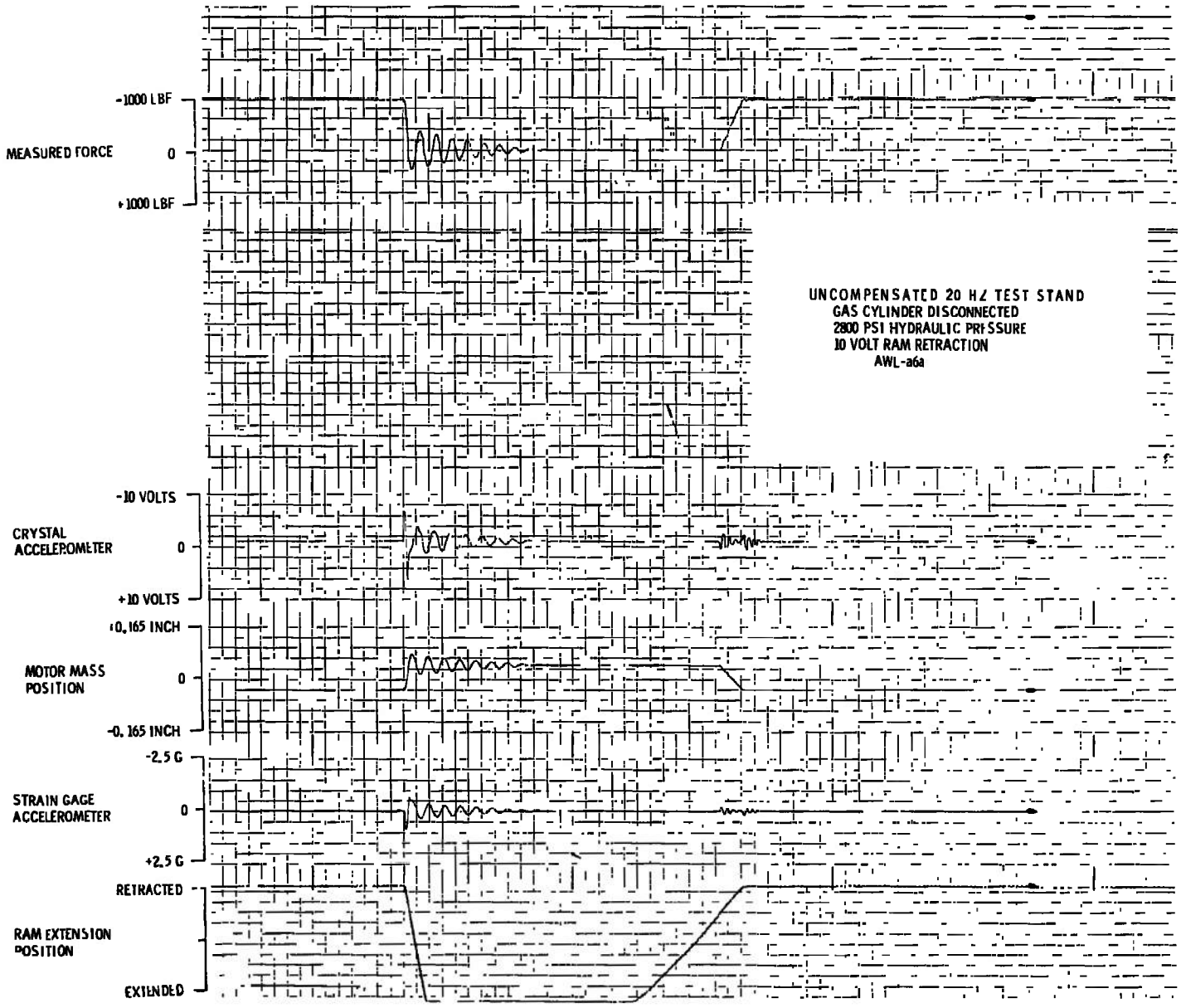

Fig. 21 Ramp Response Test - Uncompensated 20 Hertz Test Stand with Gas Cylinder Disconnected and 10-Volt Ram Retraction Rate

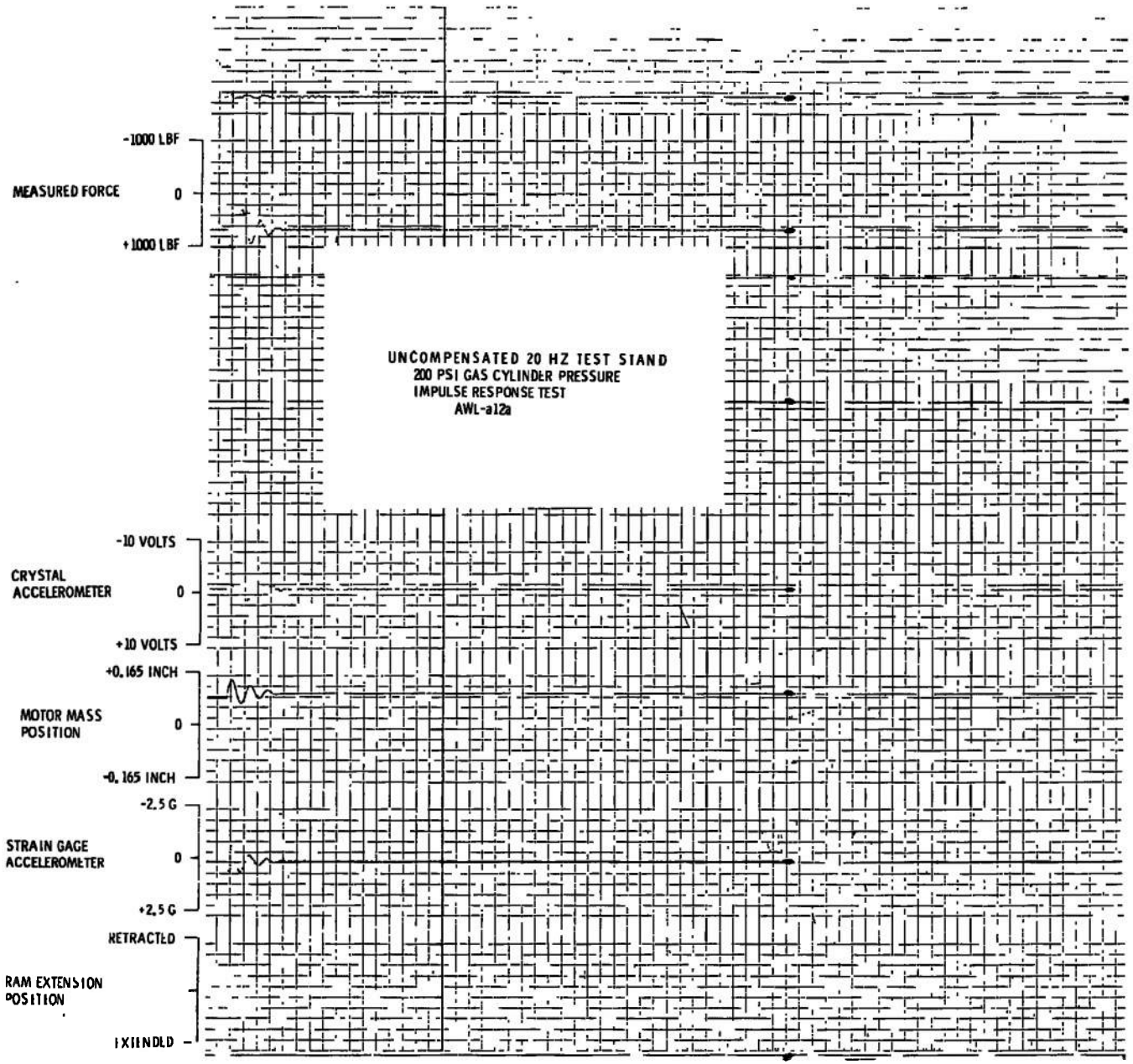

Fig. 22 Impulse Response Test - Uncompensated 20 Hertz Test Stand with 200 psi Gas Cylinder Pressure

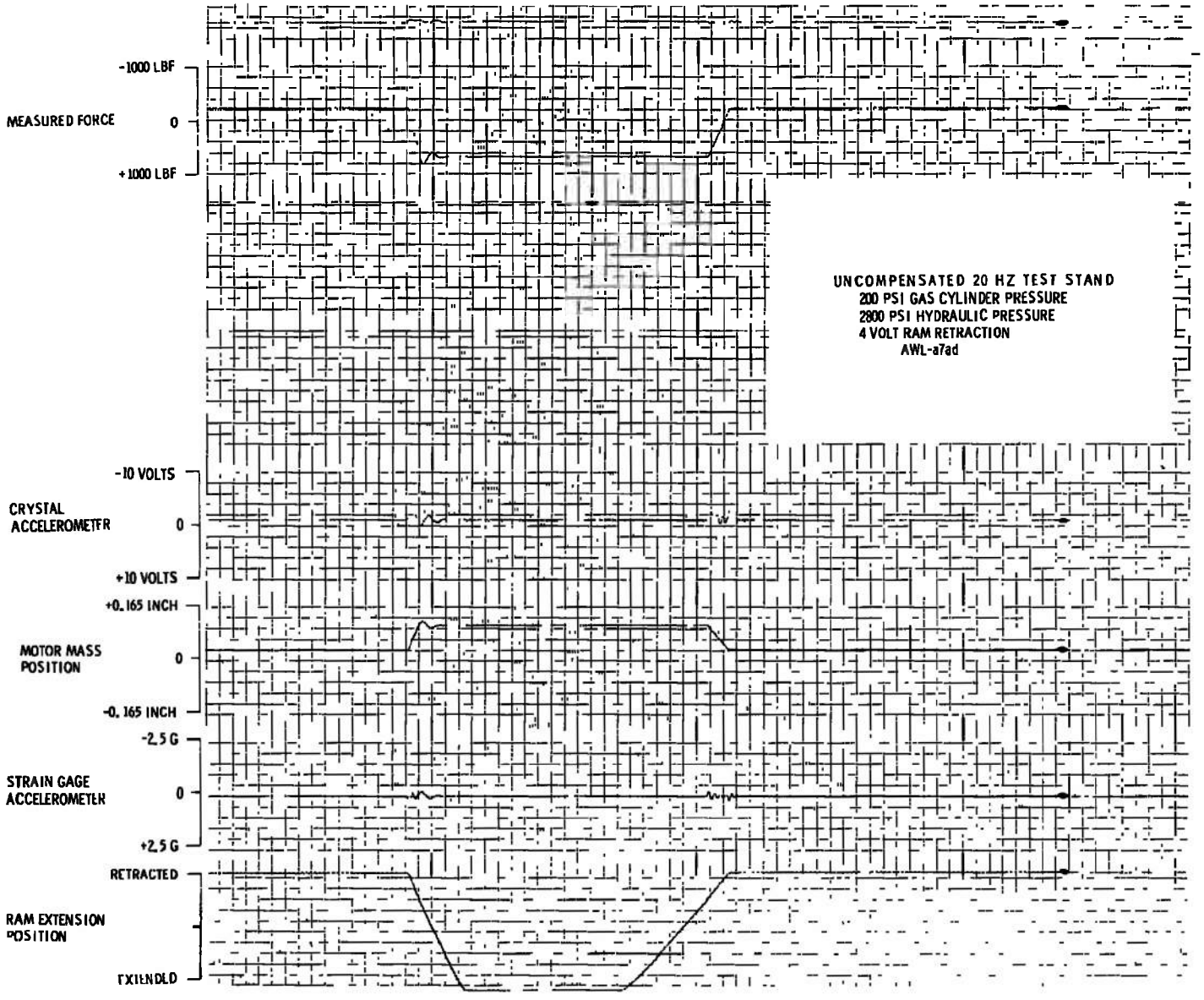

Fig. 23 Ramp Response Test - Uncompensated 20 Hertz Test Stand with 200 psi Gas Cylinder Pressure and 4-Volt Ram Retraction Rate

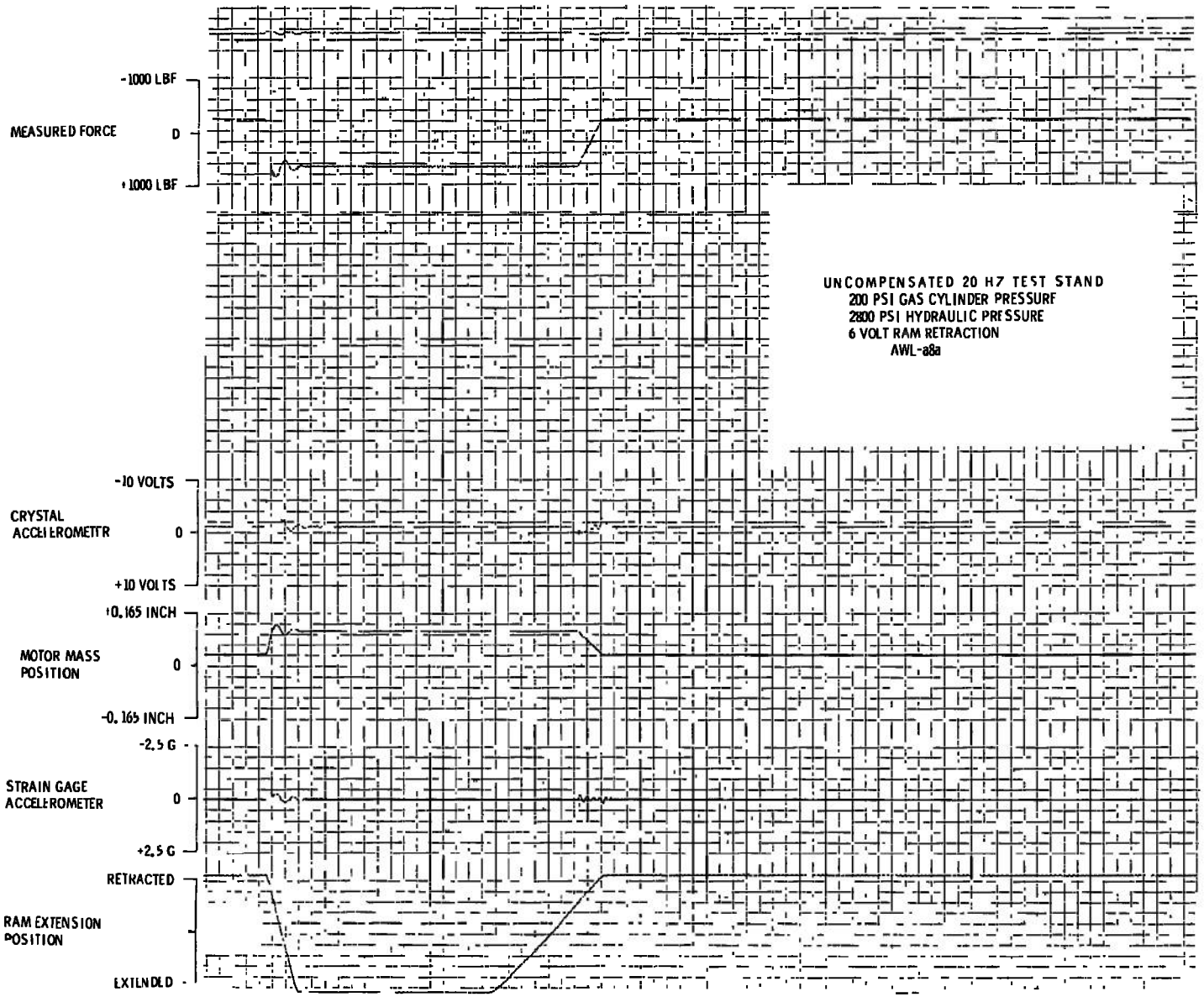

Fig. 24 Ramp Response Test - Uncompensated 20 Hertz Test Stand with 200 psi Gas Cylinder Pressure and 6-Volt Ram Retraction Rate

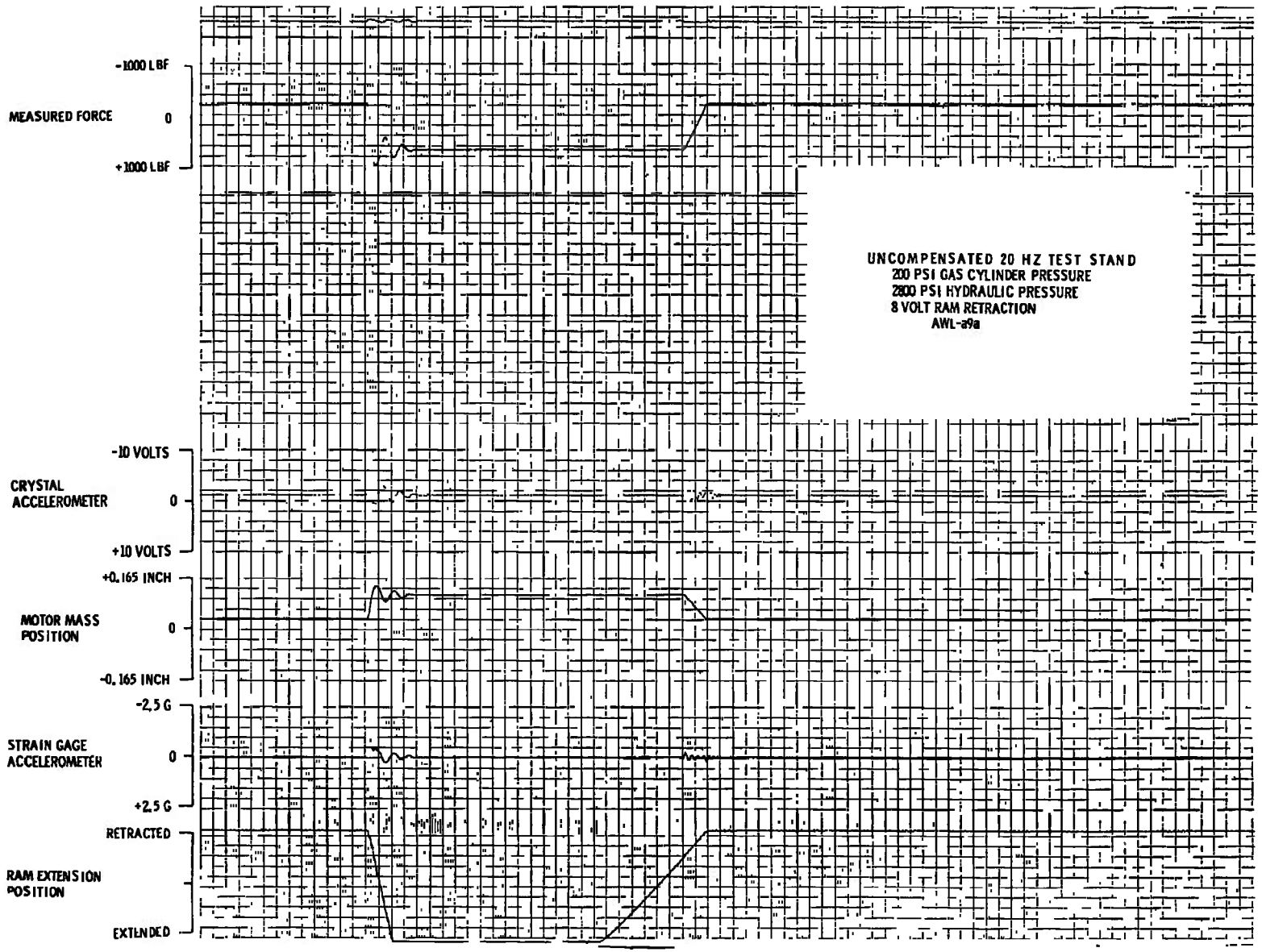

Fig. 25 Ramp Response Test - Uncompensated 20 Hertz Test Stand with 200 psi Gas Cylinder Pressure and 8-Volt Ram Retraction Rate

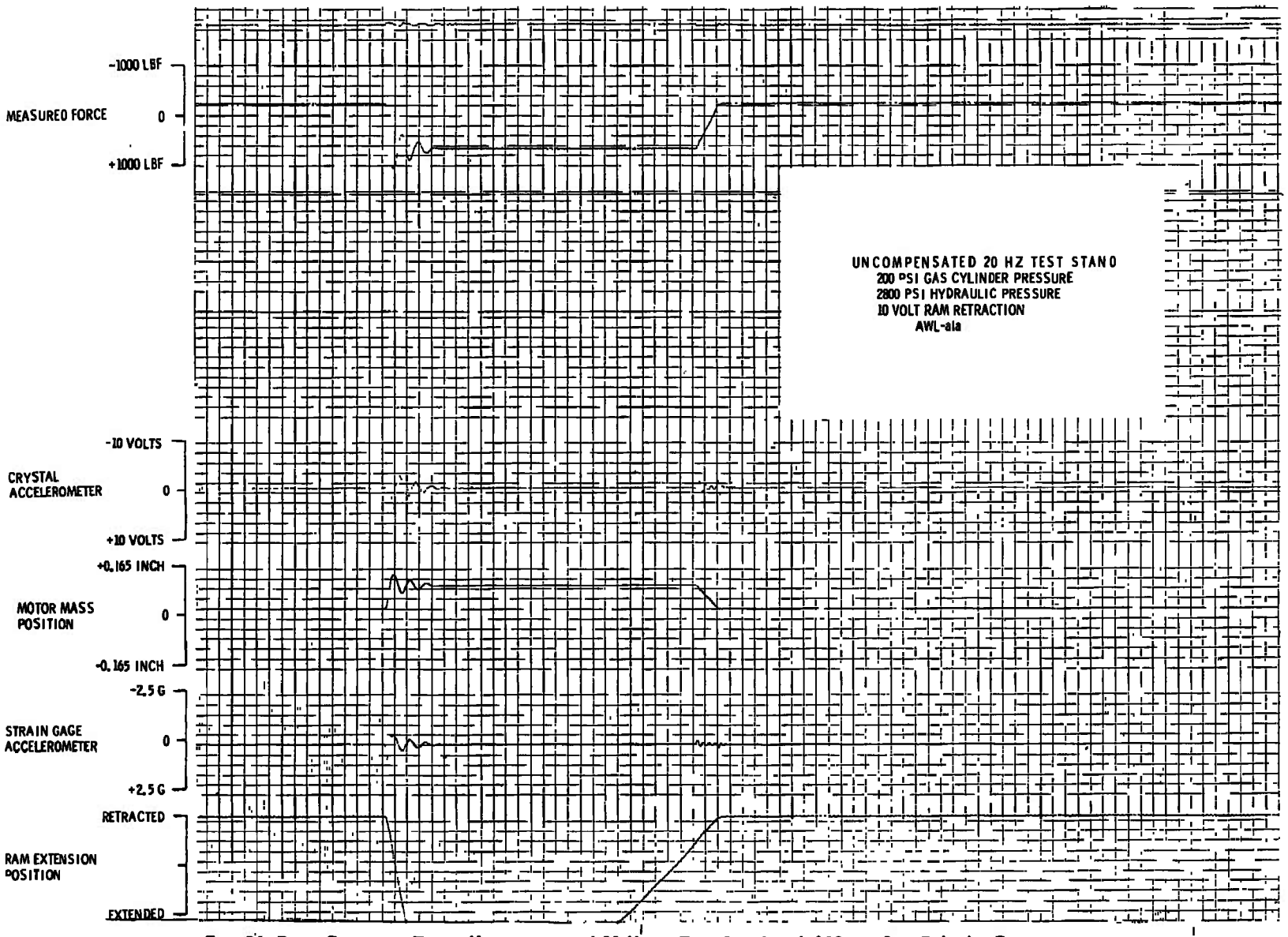

Fig. 26 Ramp Response Test - Uncompensated 20 Hertz Test Stand with 200 psi Gas Cylinder Pressure and 10-Volt Ram Retraction Rate

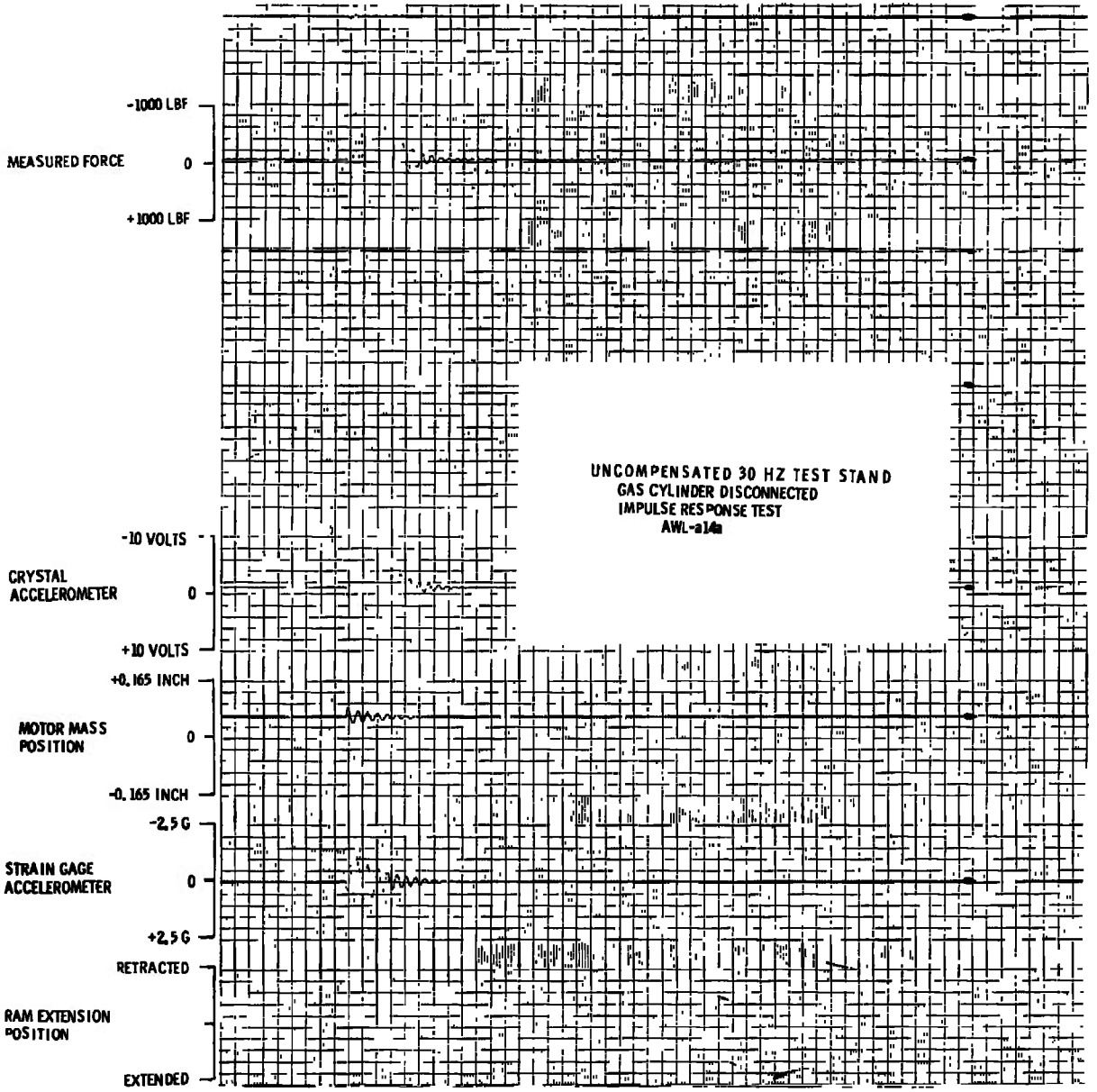

Fig. 27 Impulse Response Test - Uncompensated 30 Hertz Test Stand with Gas Cylinder Disconnected

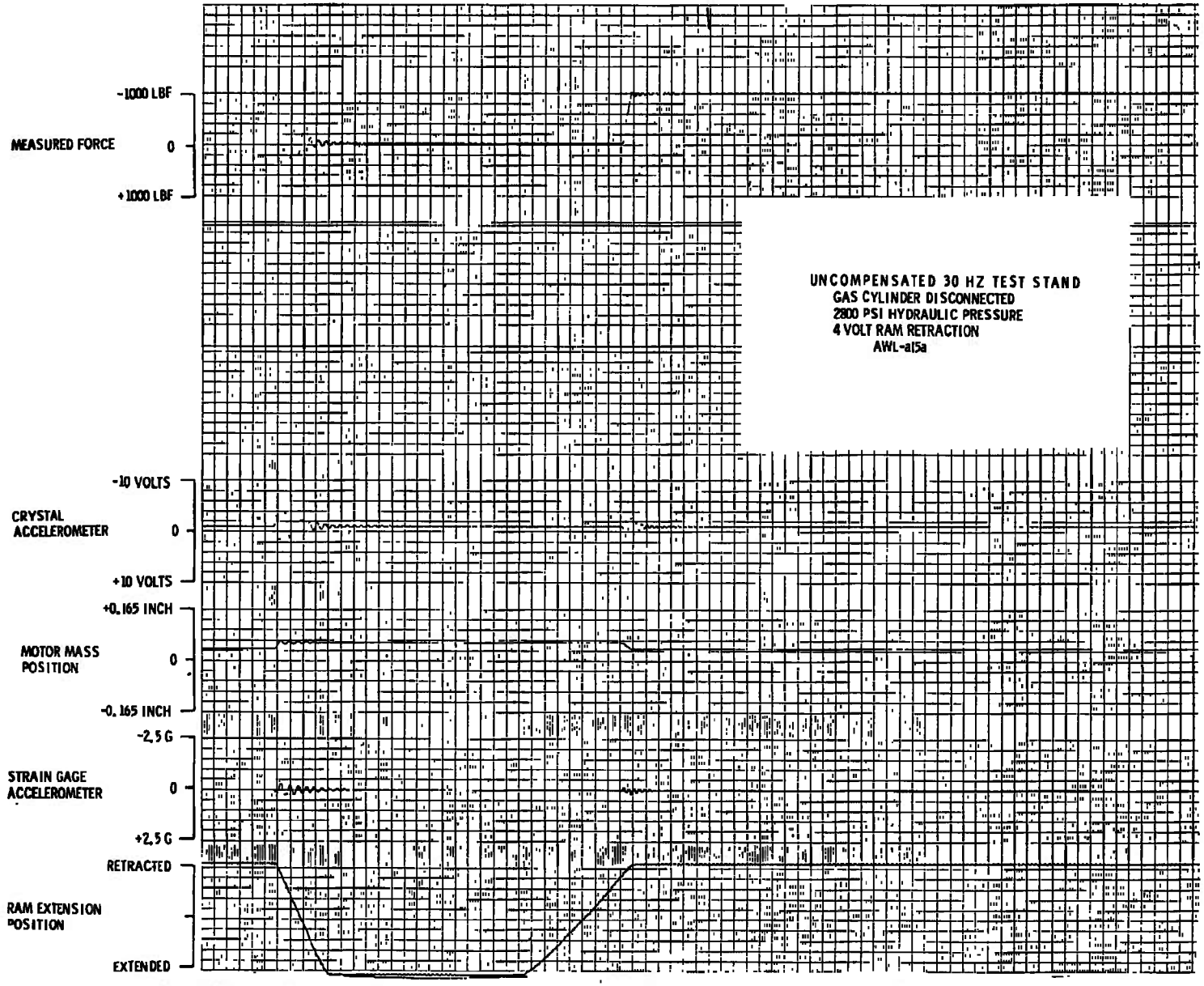

Fig. 28 Ramp Response Test - Uncompensated 30 Hertz Test Stand with Gas Cylinder Disconnected and 4-Volt Ram Retraction Rate

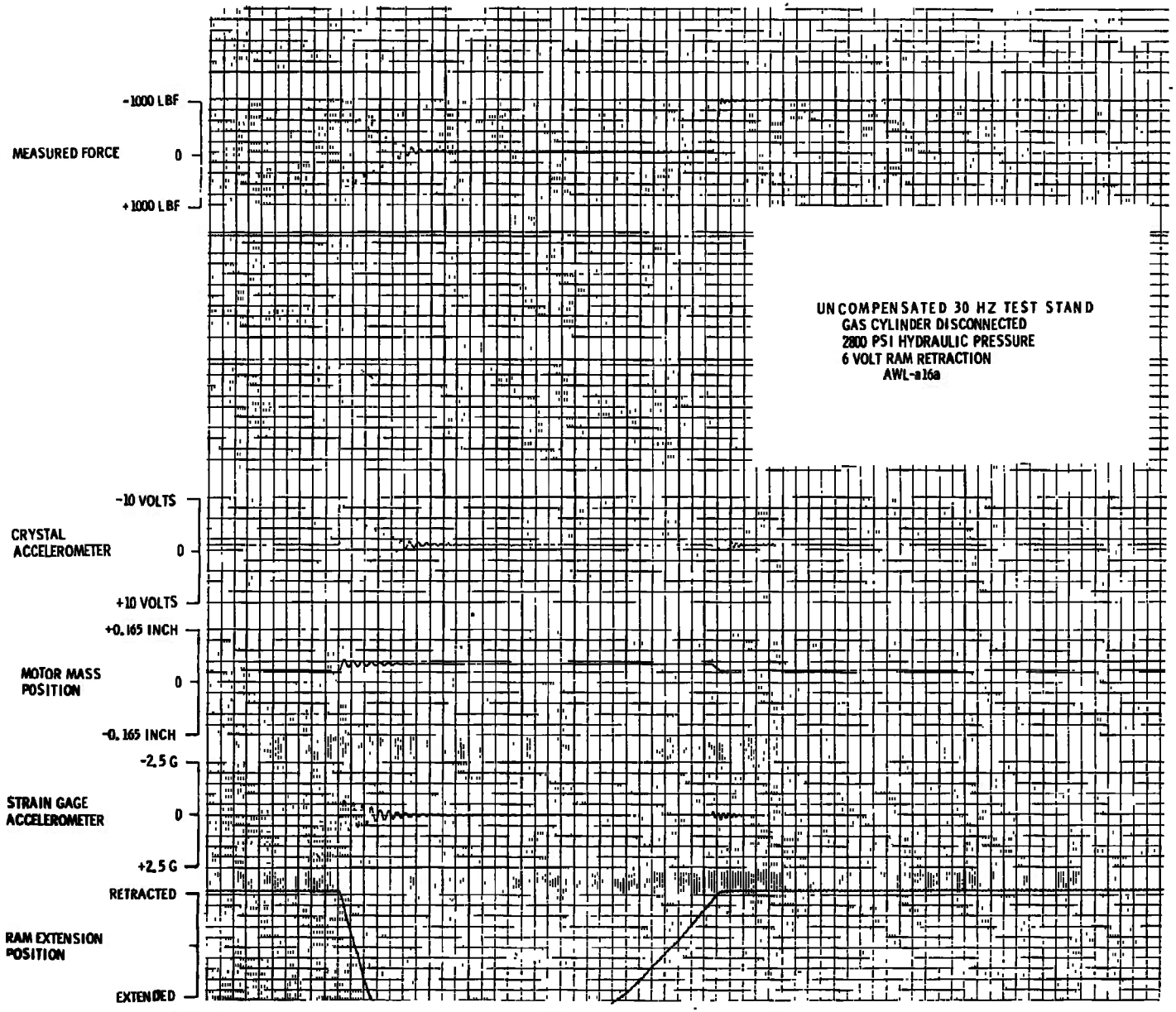

Fig. 29 Ramp Response Test - Uncompensated 30 Hertz Test Stand with Gas Cylinder Disconnected and 6-Volt Ram Retraction Rate

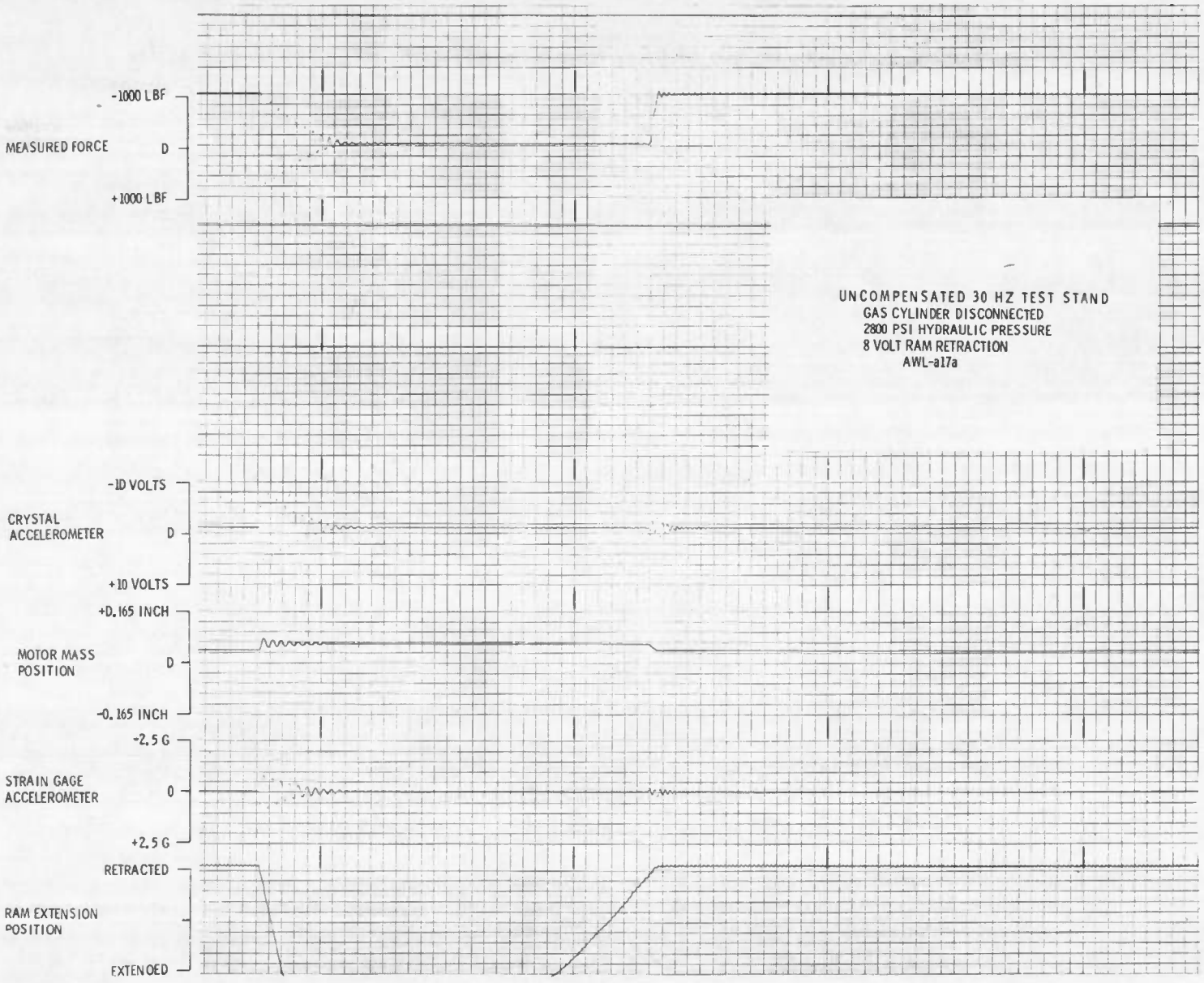

Fig. 30 Ramp Response Test - Uncompensated 30 Hertz Test Stand with Gas Cylinder Disconnected and 8-Volt Ram Retraction Rate

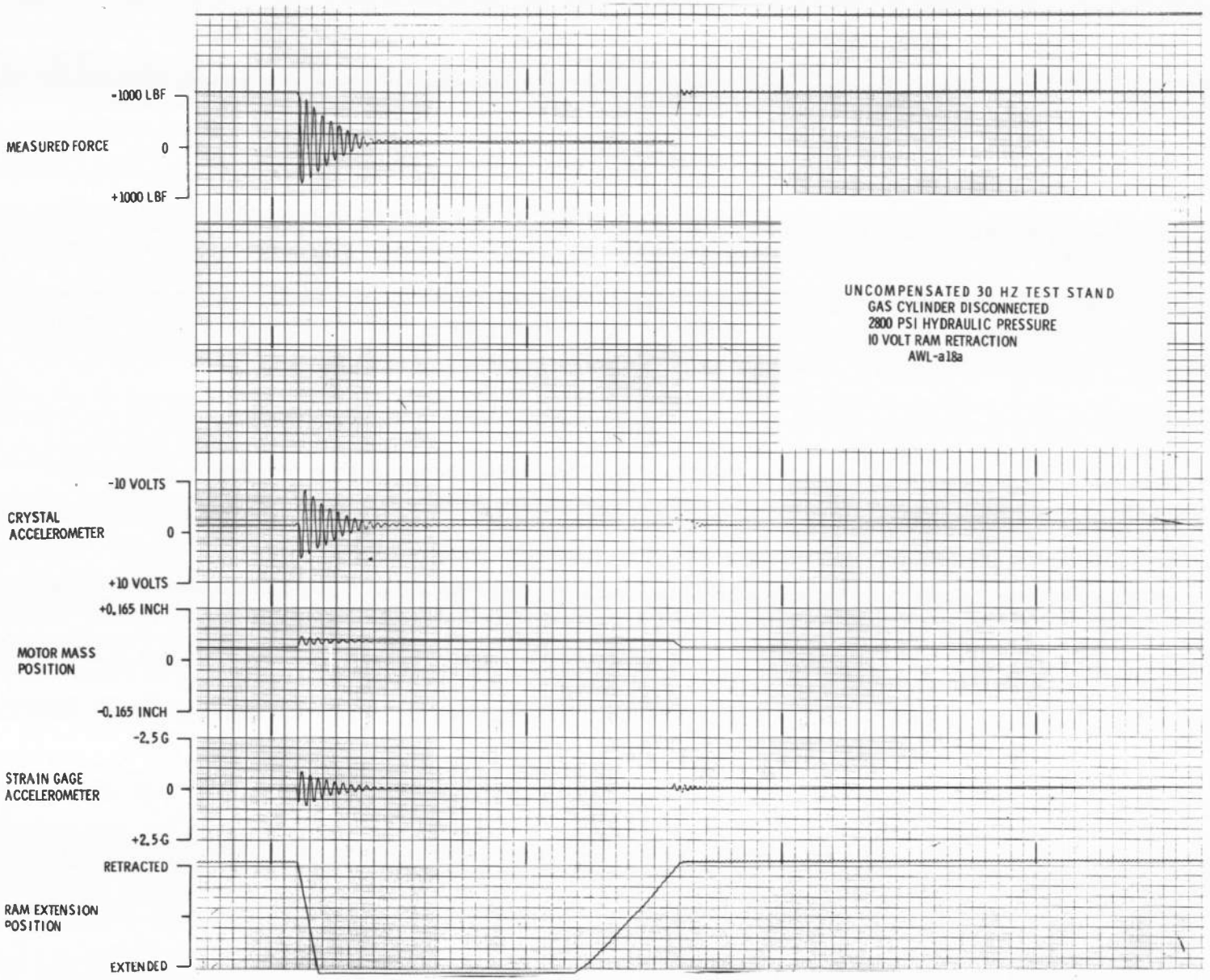

Fig. 31 Ramp Response Test - Uncompensated 30 Hertz Test Stand with Gas Cylinder Disconnected and 10-Volt Ram Retraction Rate

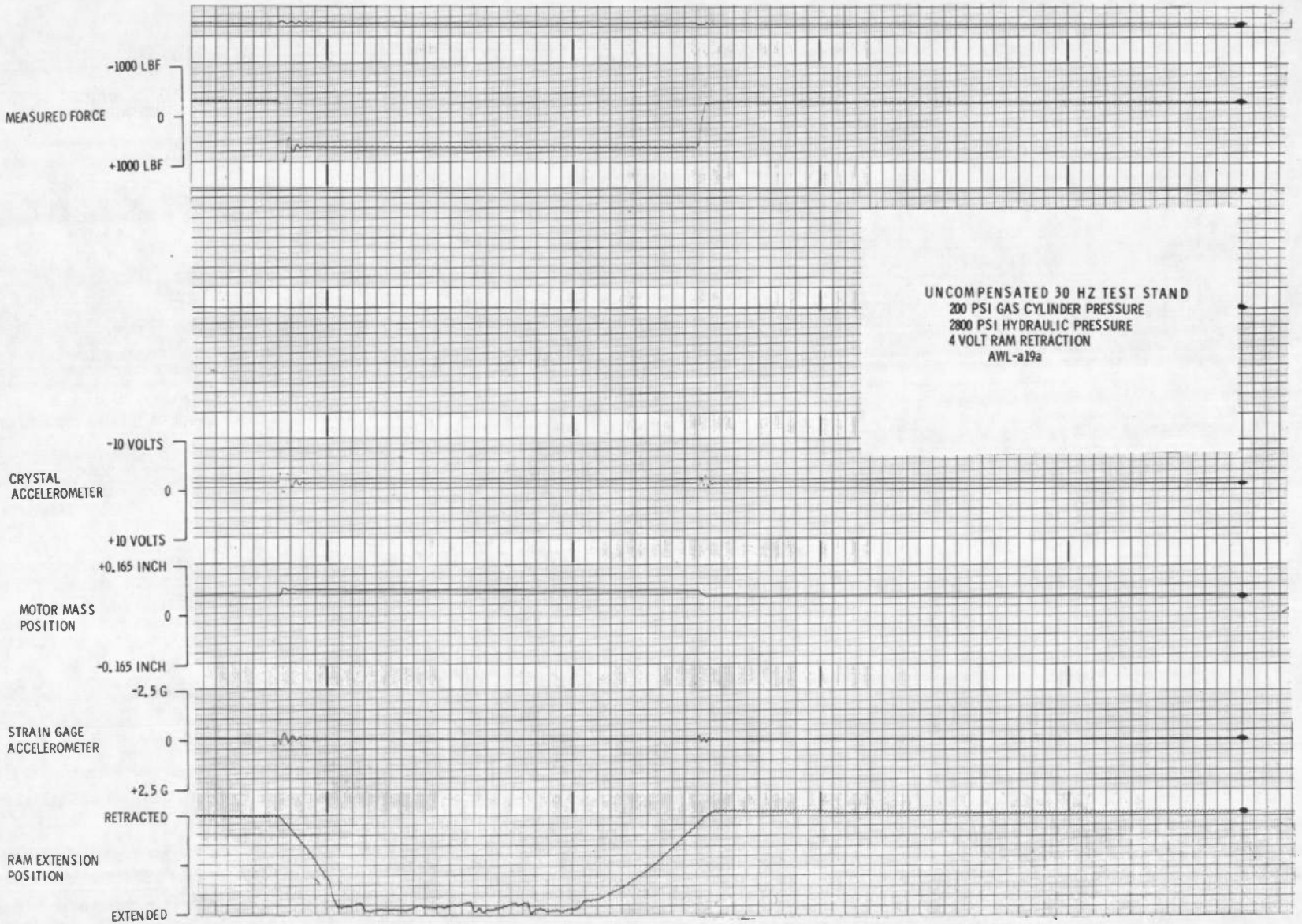

Fig. 32 Ramp Response Test - Uncompensated 30 Hertz Test Stand with 200 psi Gas Cylinder Pressure and 4-Volt Ram Retraction Rate

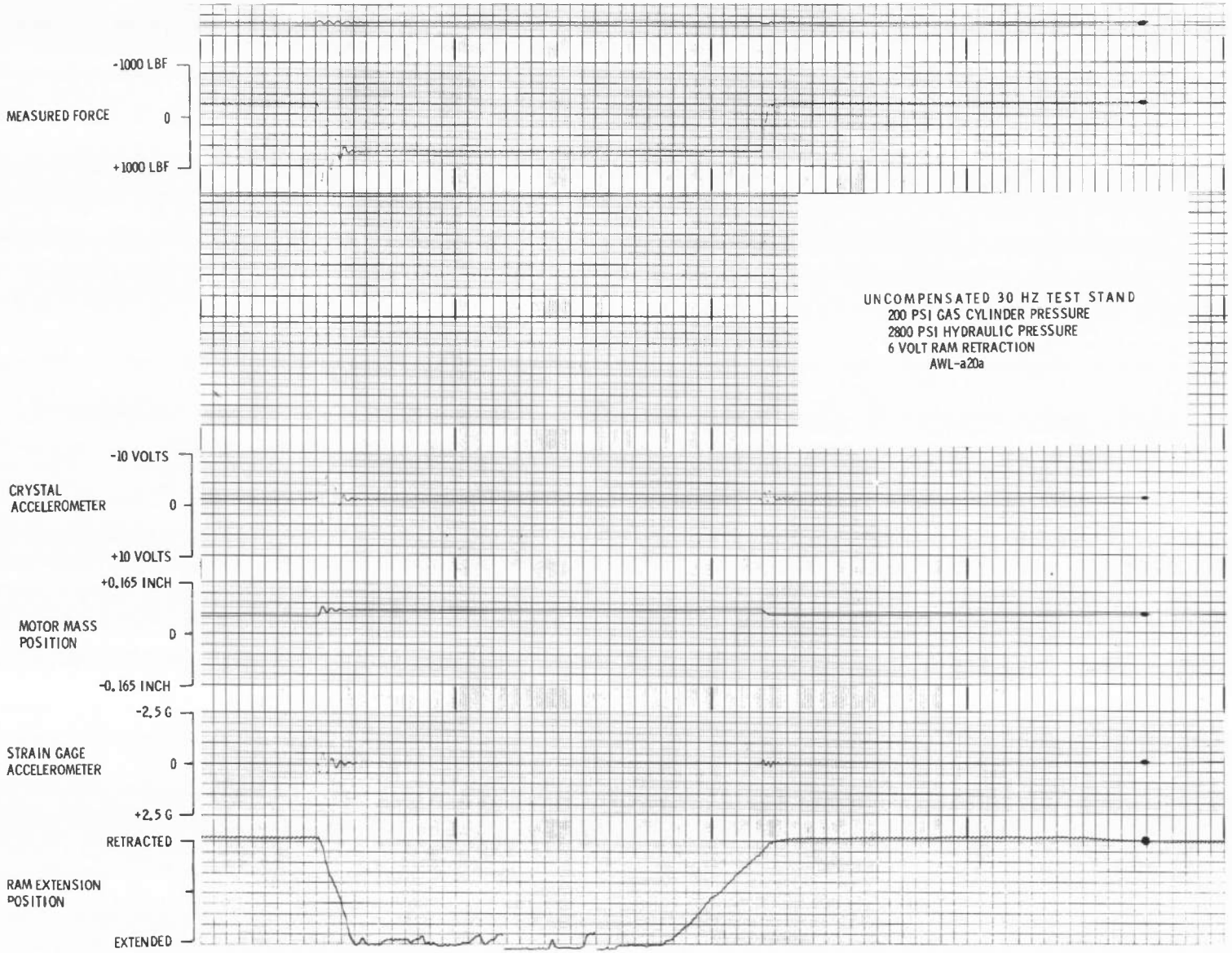

Fig. 33 Ramp Response Test - Uncompensated 30 Hertz Test Stand with 200 psi Gas Cylinder Pressure and 6-Volt Ram Retraction Rate

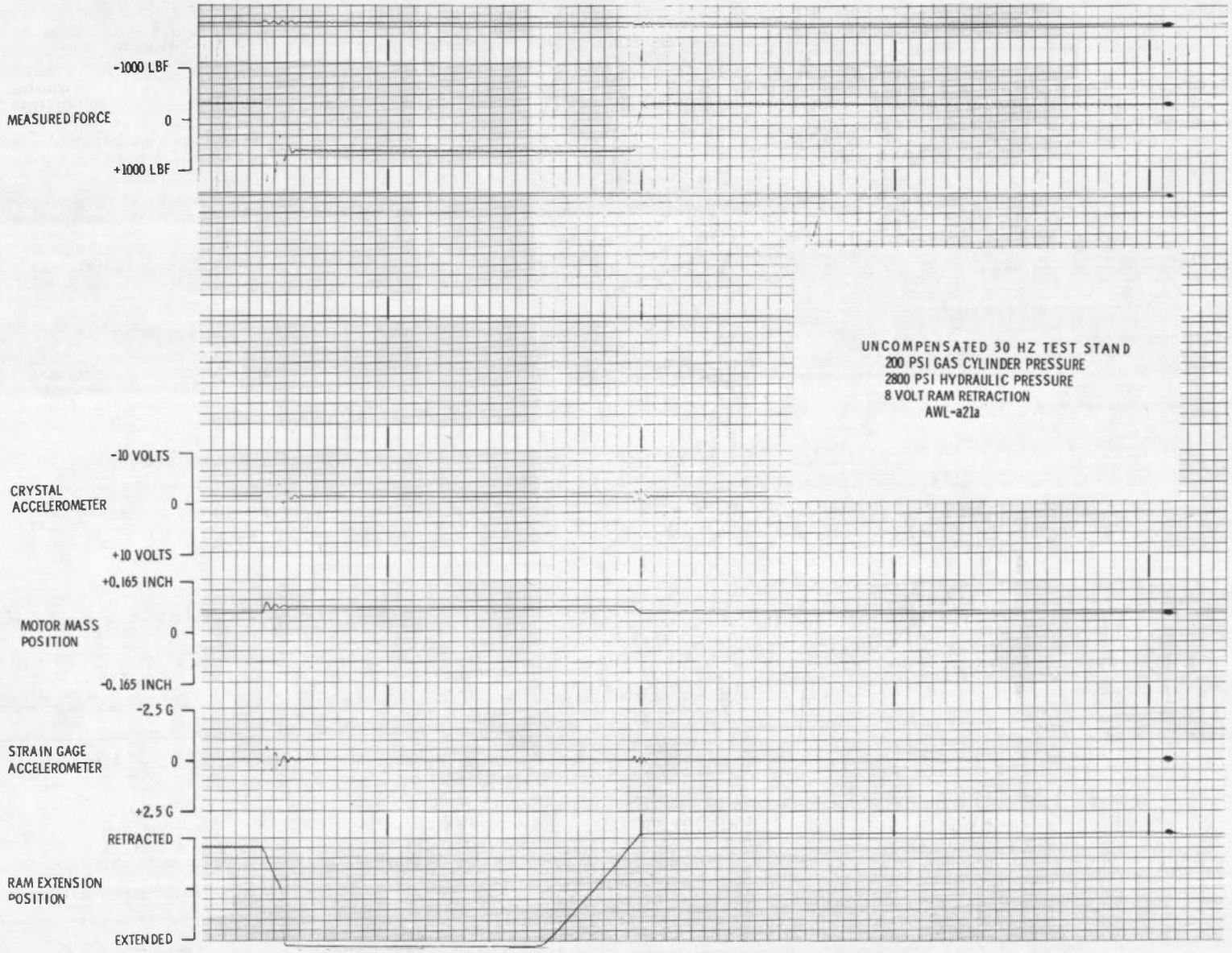

Fig. 34 Romp Response Test - Uncompensated 30 Hertz Test Stand with 200 psi Gos Cylinder Pressure and 8-Volt Rom Retraction Rote

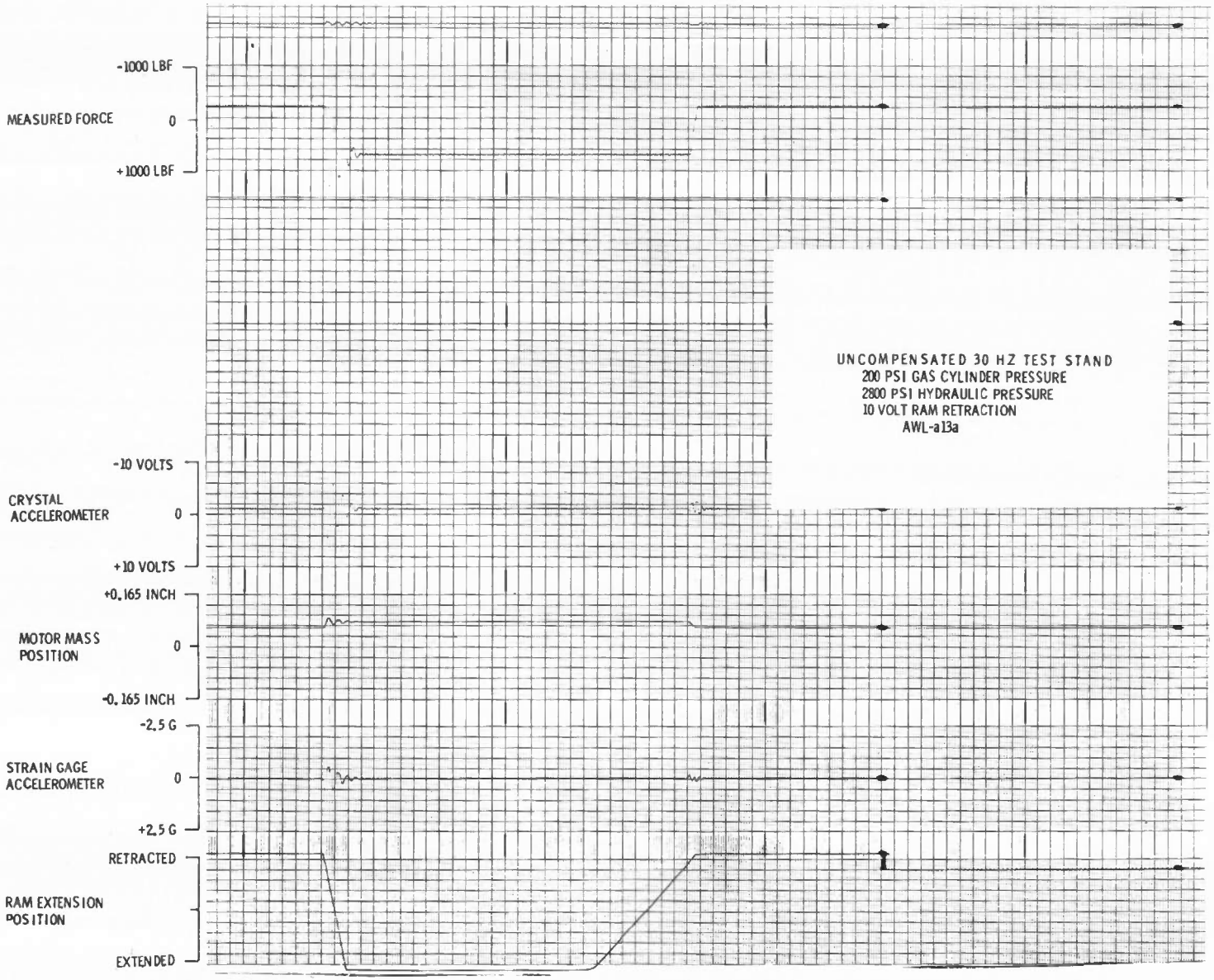

Fig. 35 Ramp Response Test - Uncompensated 30 Hertz Test Stand with 200 psi Gas Cylinder Pressure and 10-Volt Ram Retraction Rate

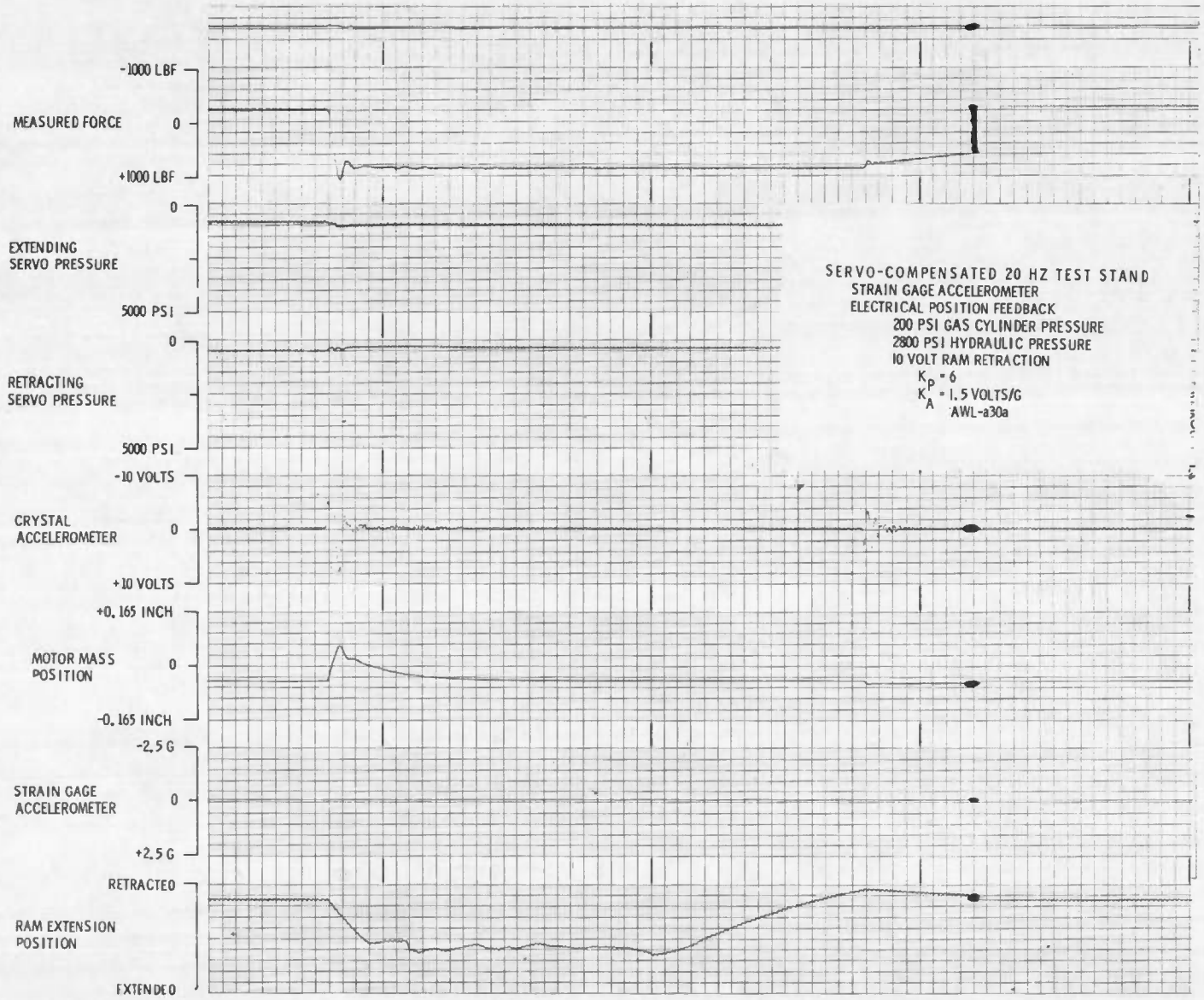

Fig. 36 Active Strut Response Data with Strain Gage Accelerometer Feedback - 20 Hertz Test Stand with 200 psi Gas Cylinder Pressure

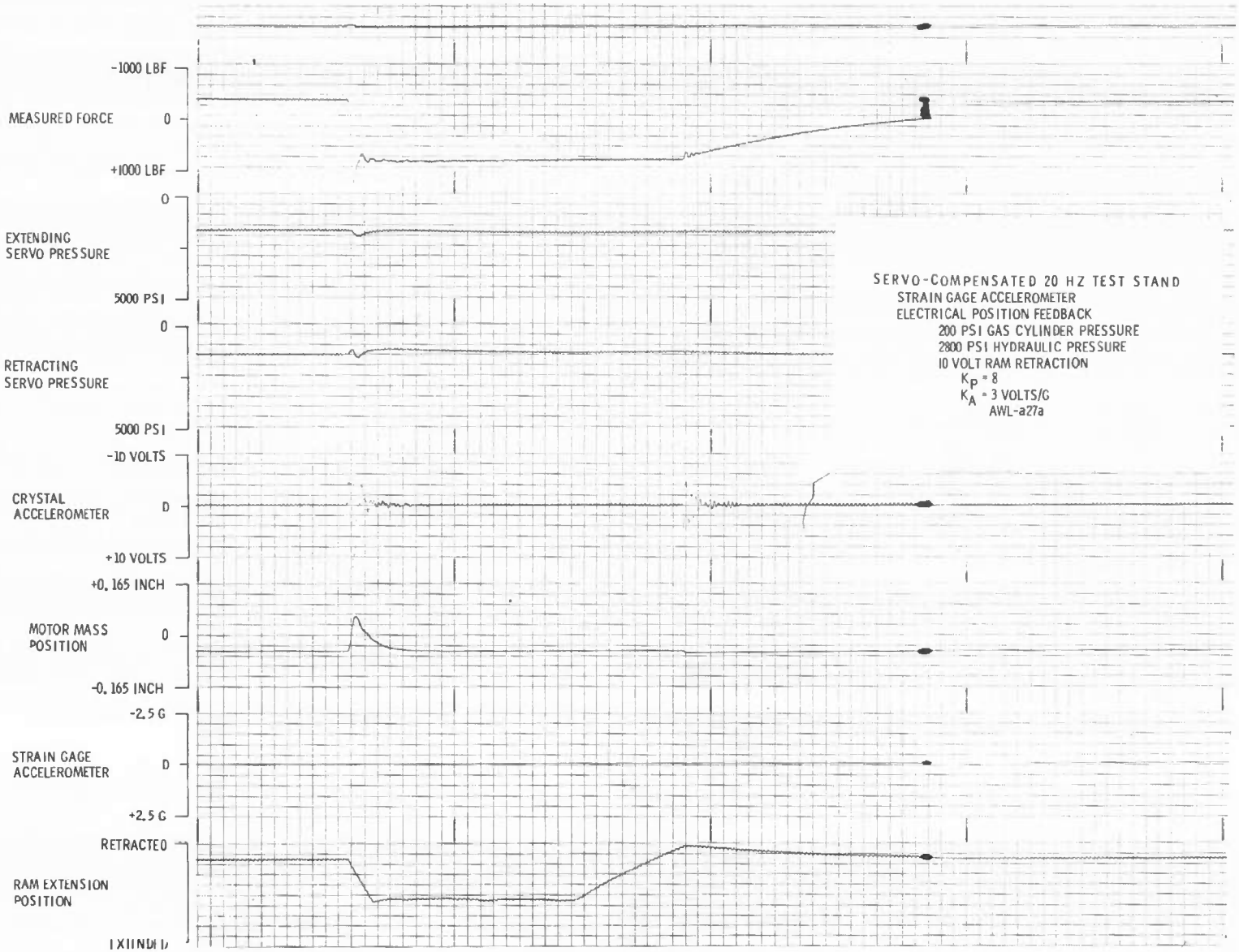

Fig. 37 Active Strut Response Data with Strain Gage Accelerometer Feedback - 20 Hertz Test Stand with 200 psi Gas Cylinder Pressure

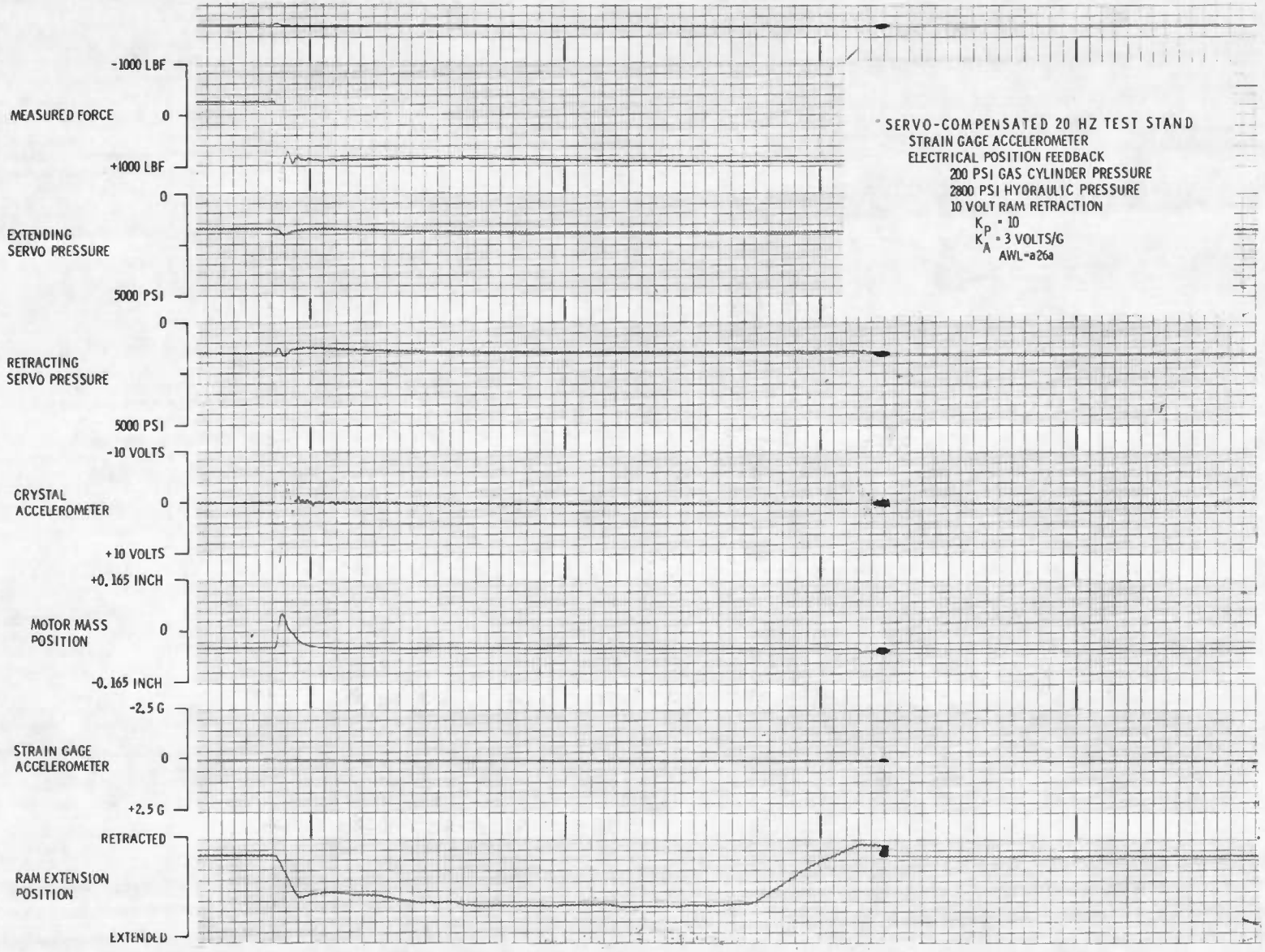

Fig. 38 Active Strut Response Data with Strain Gage Accelerometer Feedback - 20 Hertz Test Stand with 200 psi Gas Cylinder Pressure

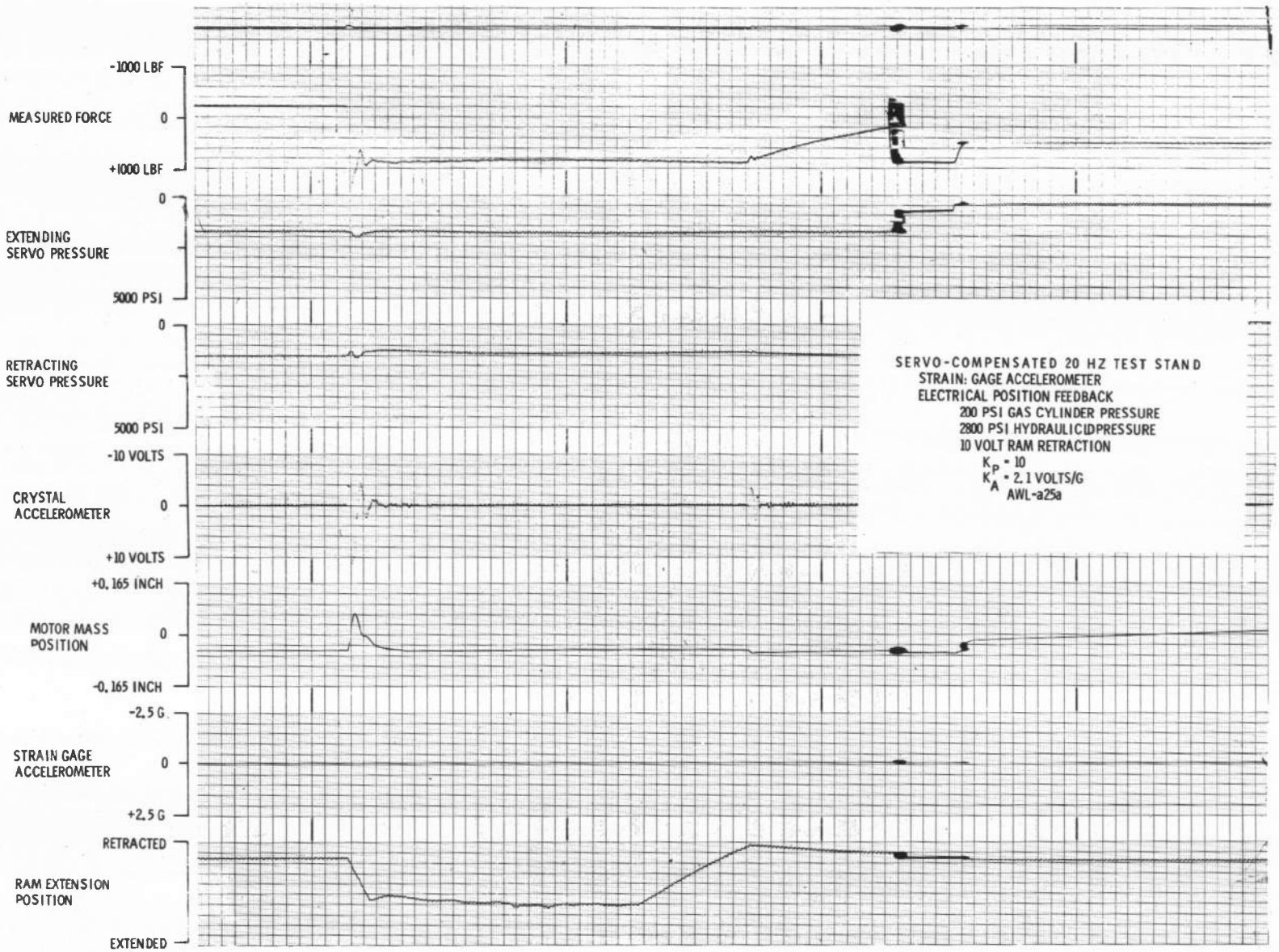

Fig. 39 Acitve Strut Respanse Data with Strain Gage Accelerometer Feedback - 20 Hertz Test Stand with 200 psi Gas Cylinder Pressure

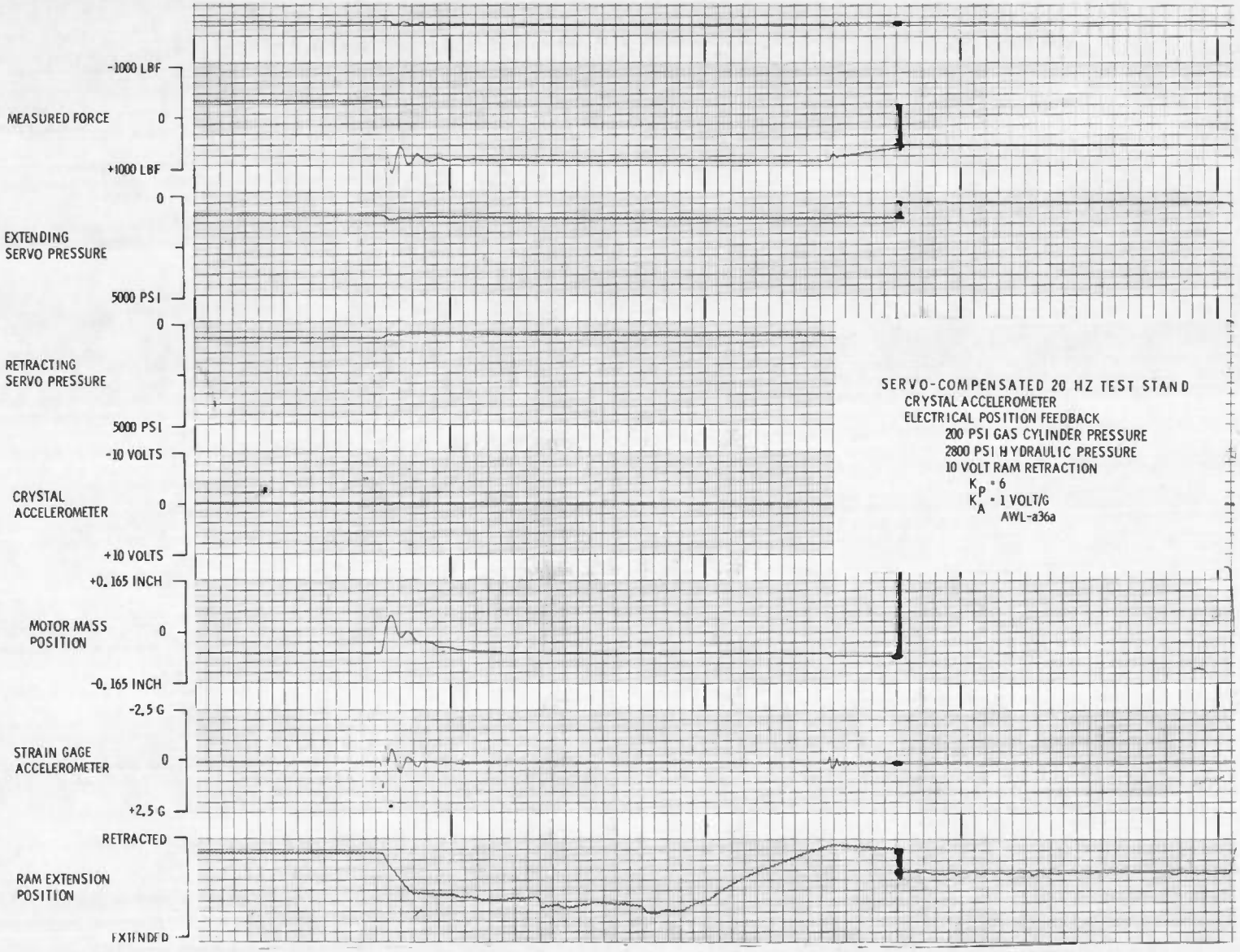

Fig. 40 Active Strut Response Data with Crystal Accelerometer Feedback - 20 Hertz Test Stand with 200 psi Gas Cylinder Pressure

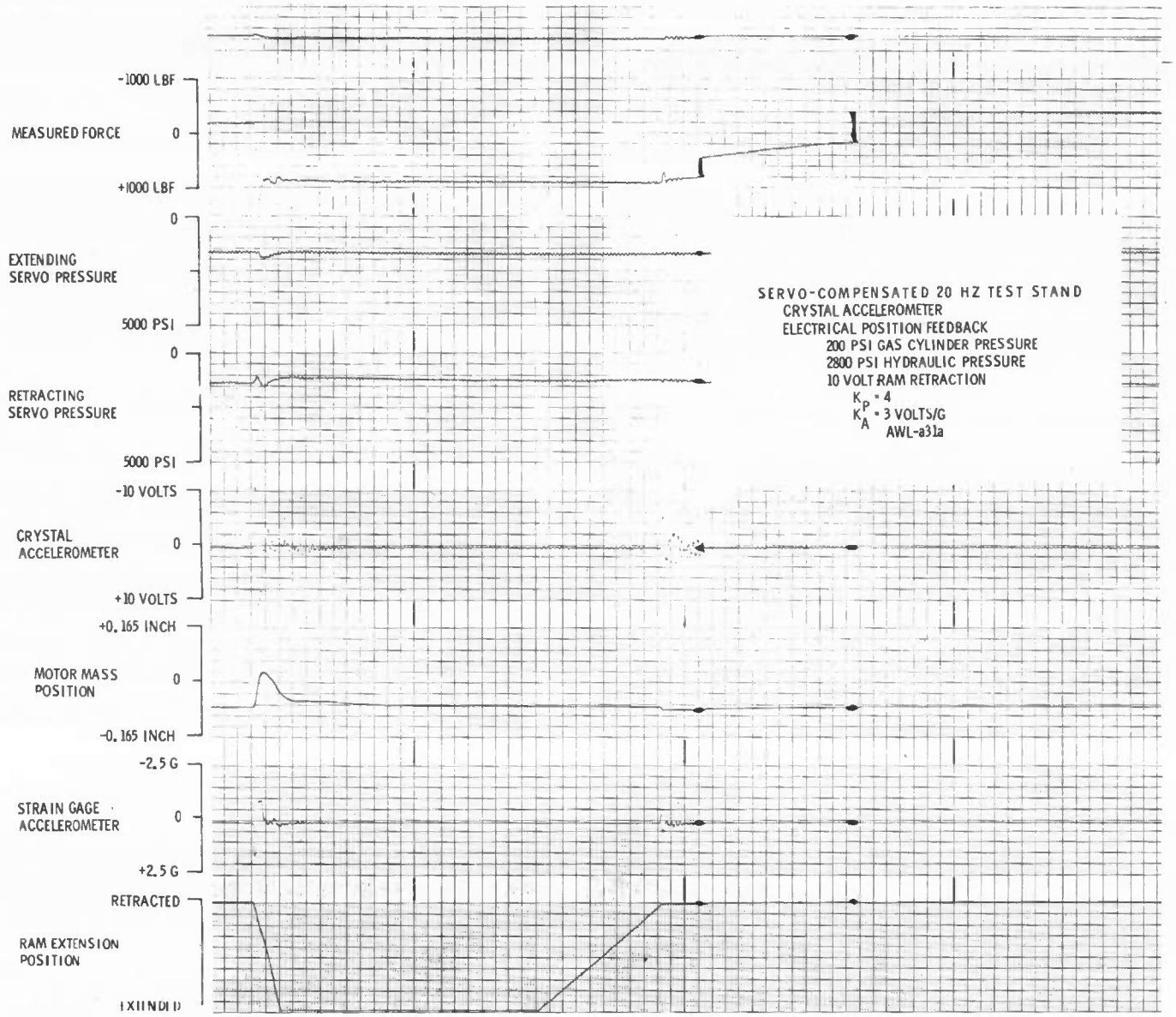

Fig. 41 Active Strut Response Data with Crystal Accelerometer Feedback - 20 Hertz Test Stand with 200 psi Gas Cylinder Pressure

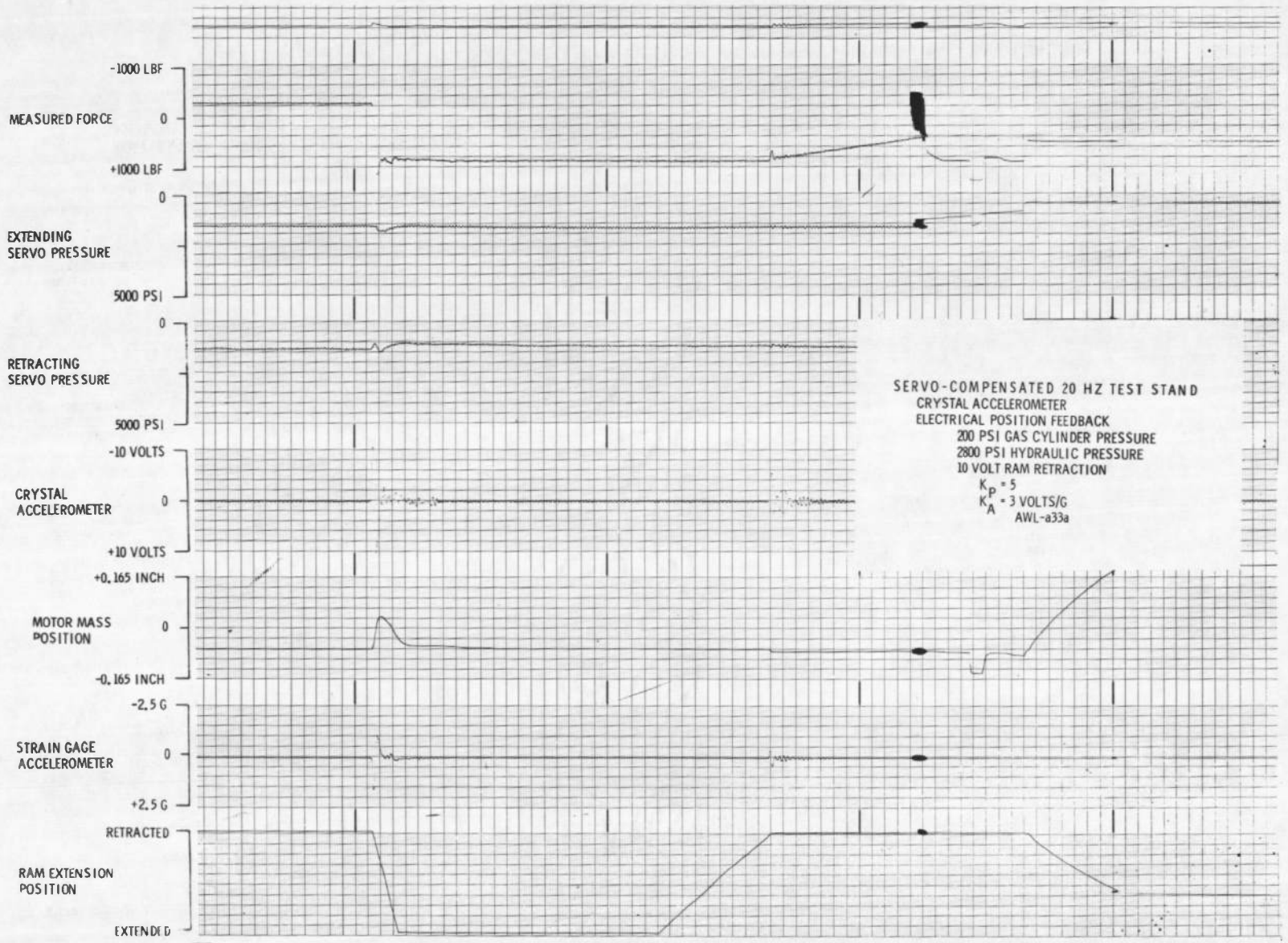

Fig. 42 Active Strut Response Data with Crystal Accelerometer Feedback - 20 Hertz Test Stand with 200 psi Gas Cylinder Pressure

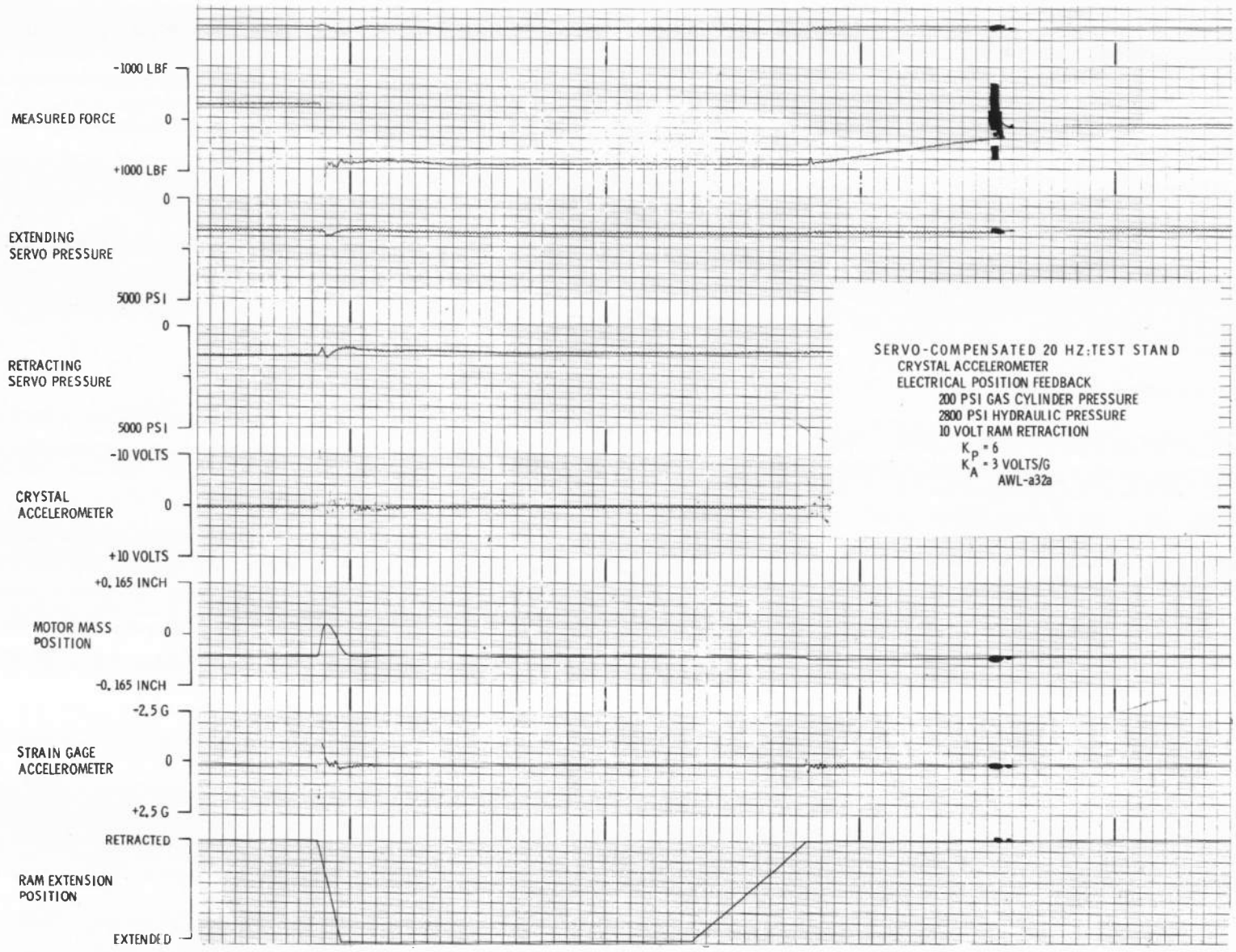

Fig. 43 Active Strut Response Data with Crystal Accelerometer Feedback - 20 Hertz Test Stand with 200 psi Gas Cylinder Pressure

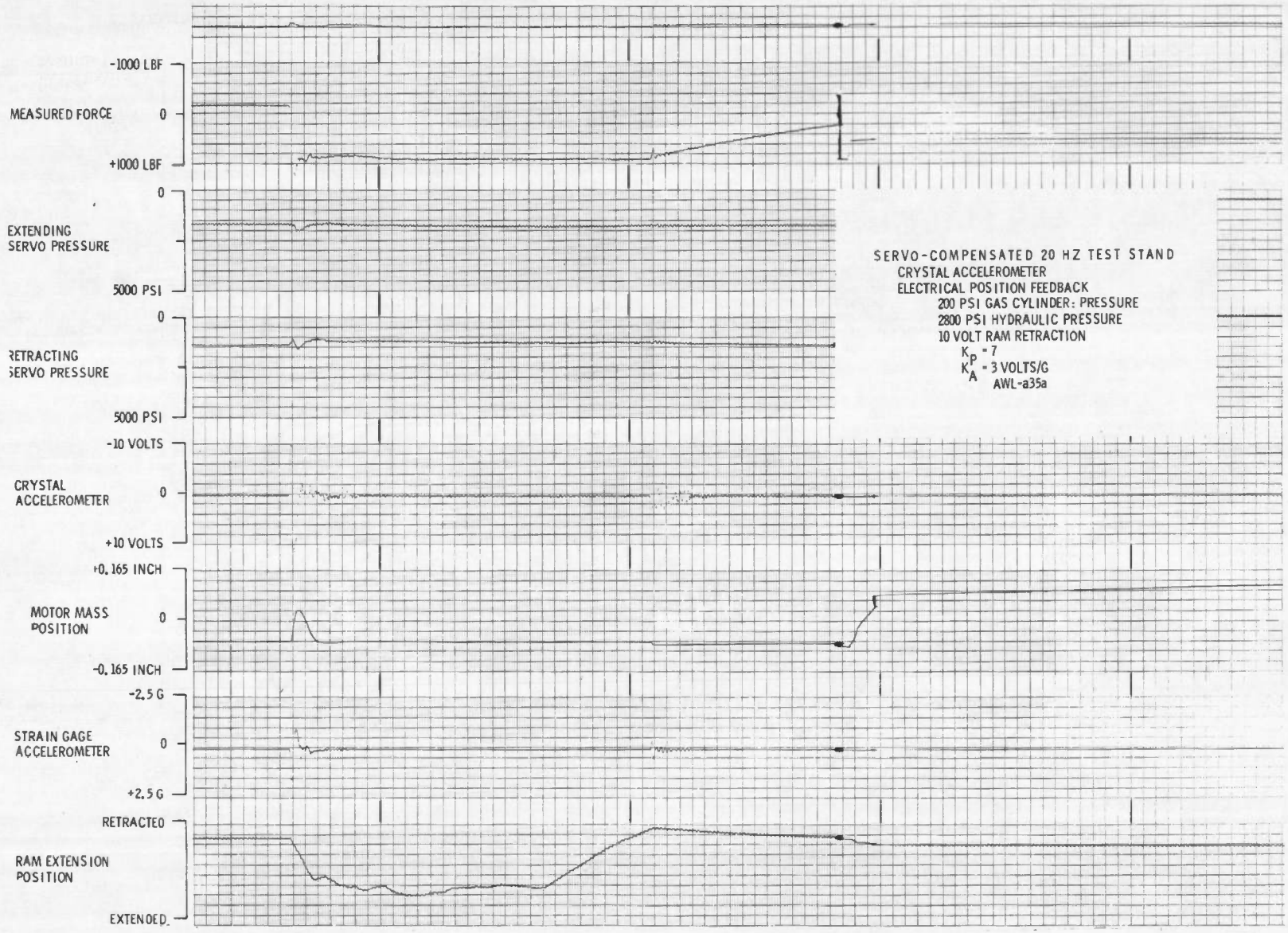

Fig. 44 Active Strut Response Data with Crystal Accelerometer Feedback - 20 Hertz Test Stand with 200 psi Gas Cylinder Pressure

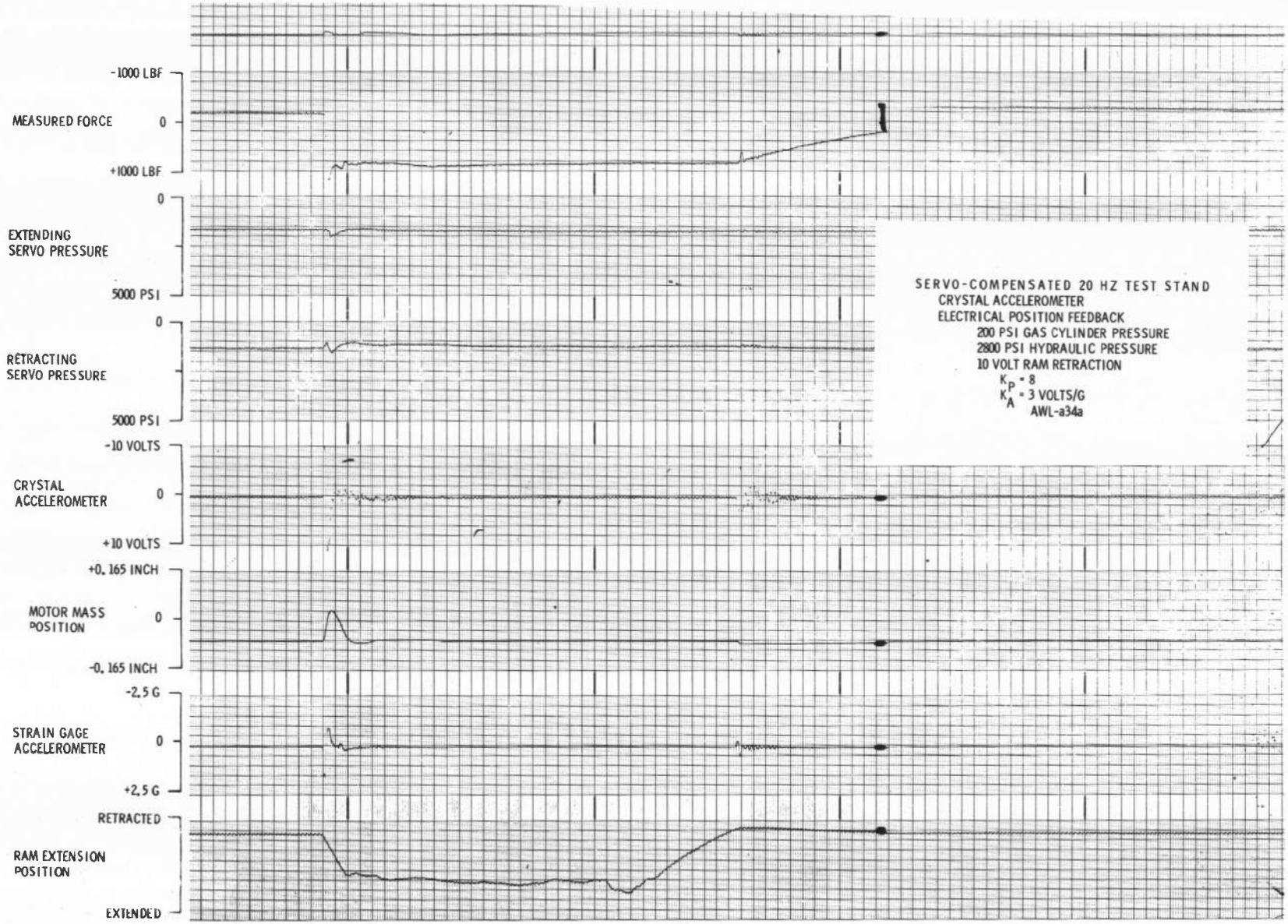

Fig. 45 Active Strut Response Data with Crystal Accelerometer Feedback - 20 Hertz Test Stand with 200 psi Gas Cylinder Pressure

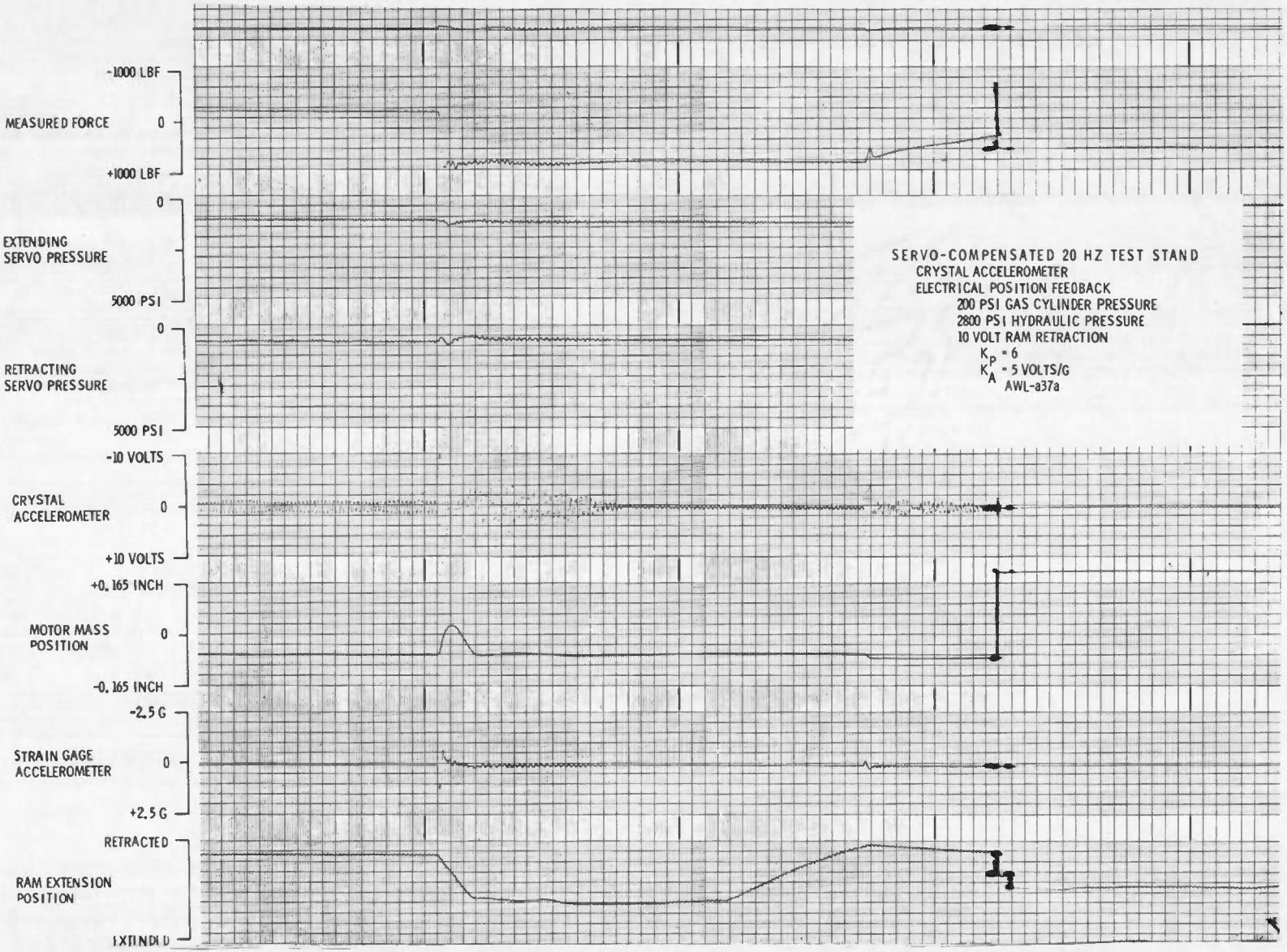

Fig. 46 Active Strut Response Data with Crystal Accelerometer Feedback - 20 Hertz Test Stand with 200 psi Gas Cylinder Pressure

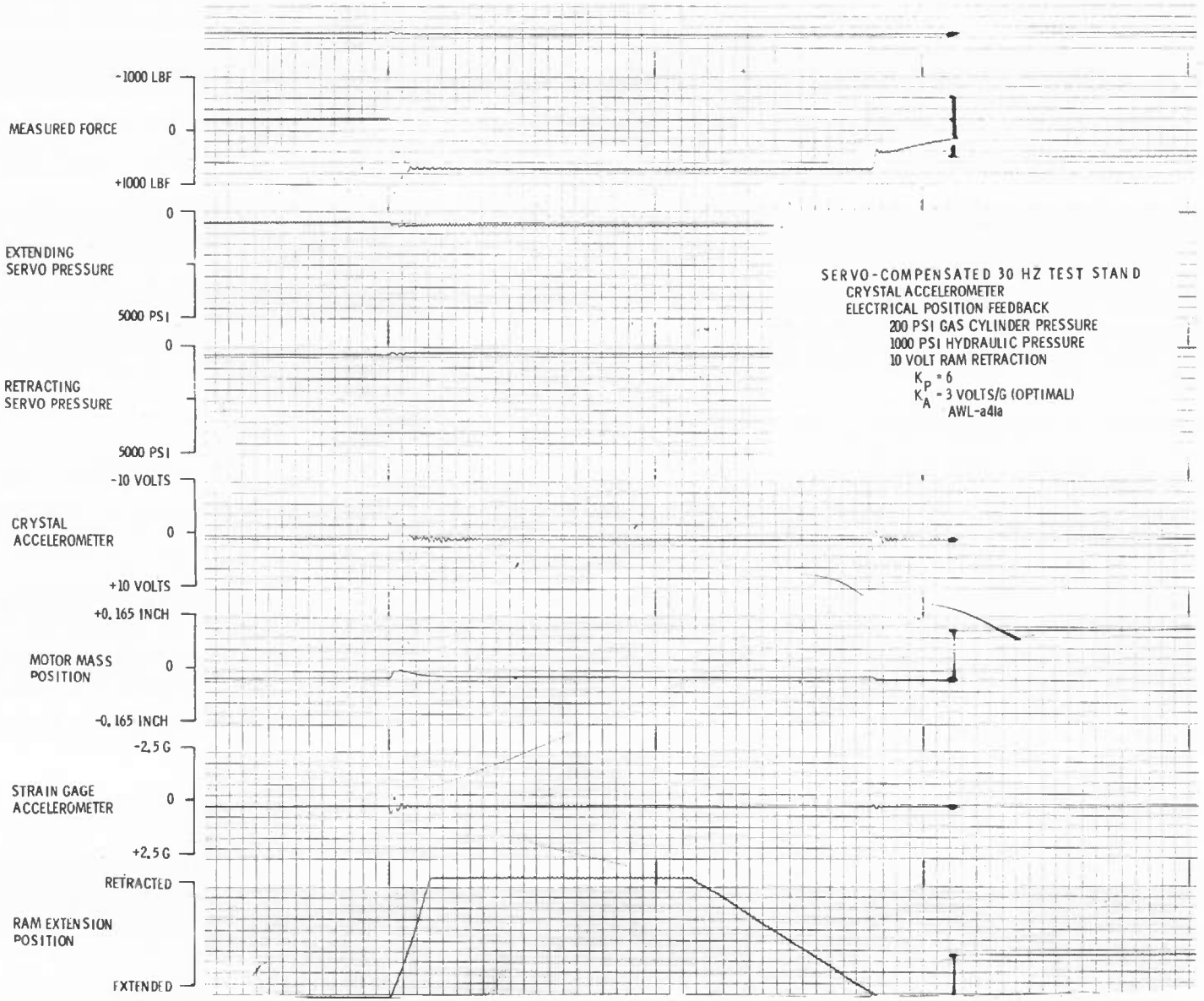

Fig. 47 Active Strut Response Data with Crystal Accelerometer Feedback - 30 Hertz Test Stand with 200 psi Gas Cylinder Pressure

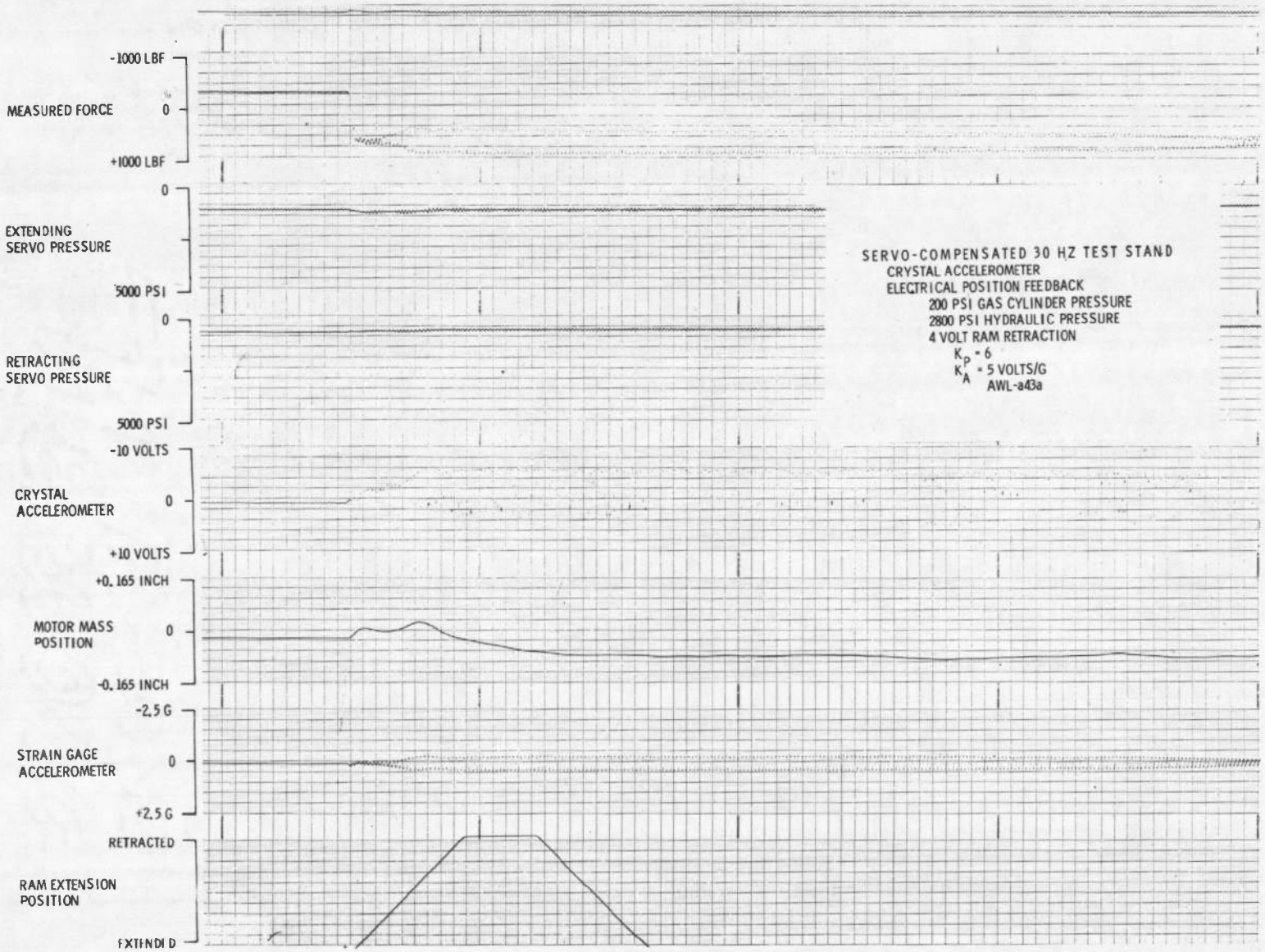

Fig. 48 Active Strut Response Data with Crystal Accelerometer Feedback - 30 Hertz Test Stand with 200 psi Gas Cylinder Pressure

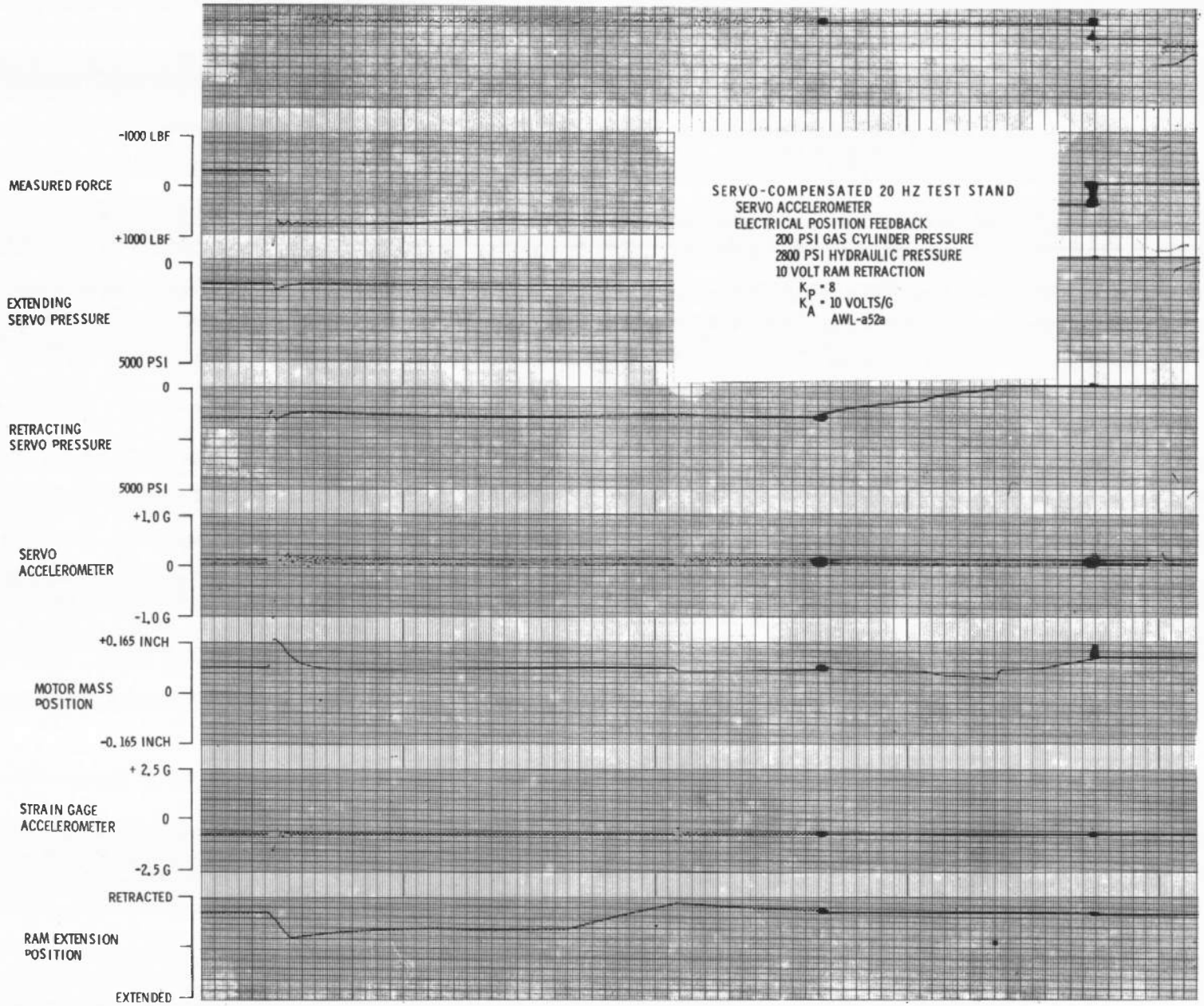

Fig. 49 Active Strut Response Data with Servo Accelerometer Feedback - 20 Hertz Test Stand with 200 psi Gas Cylinder Pressure

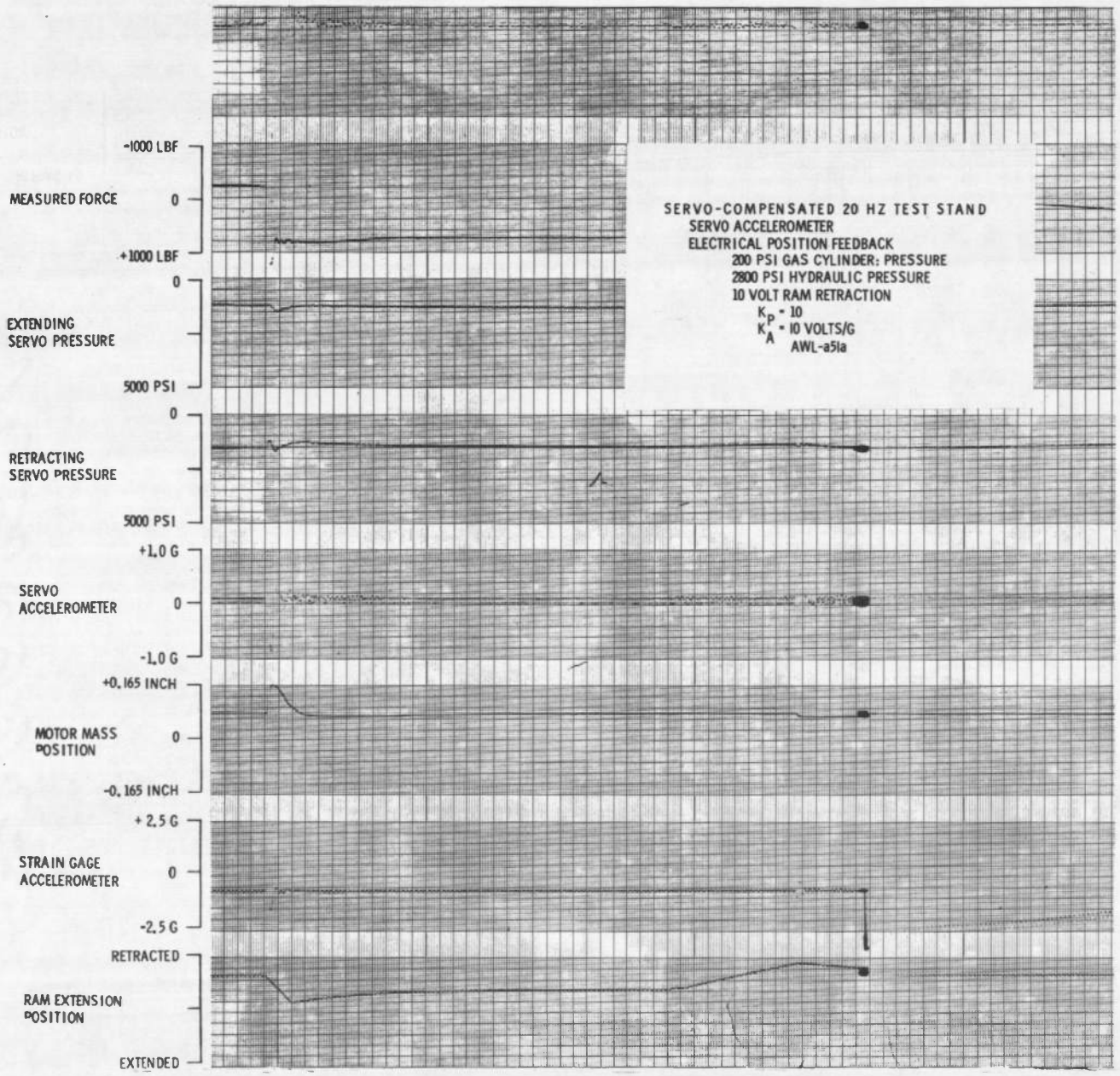

Fig. 50 Active Strut Response Data with Servo Accelerometer Feedback - 20 Hertz Test Stand with 200 psi Gas Cylinder Pressure

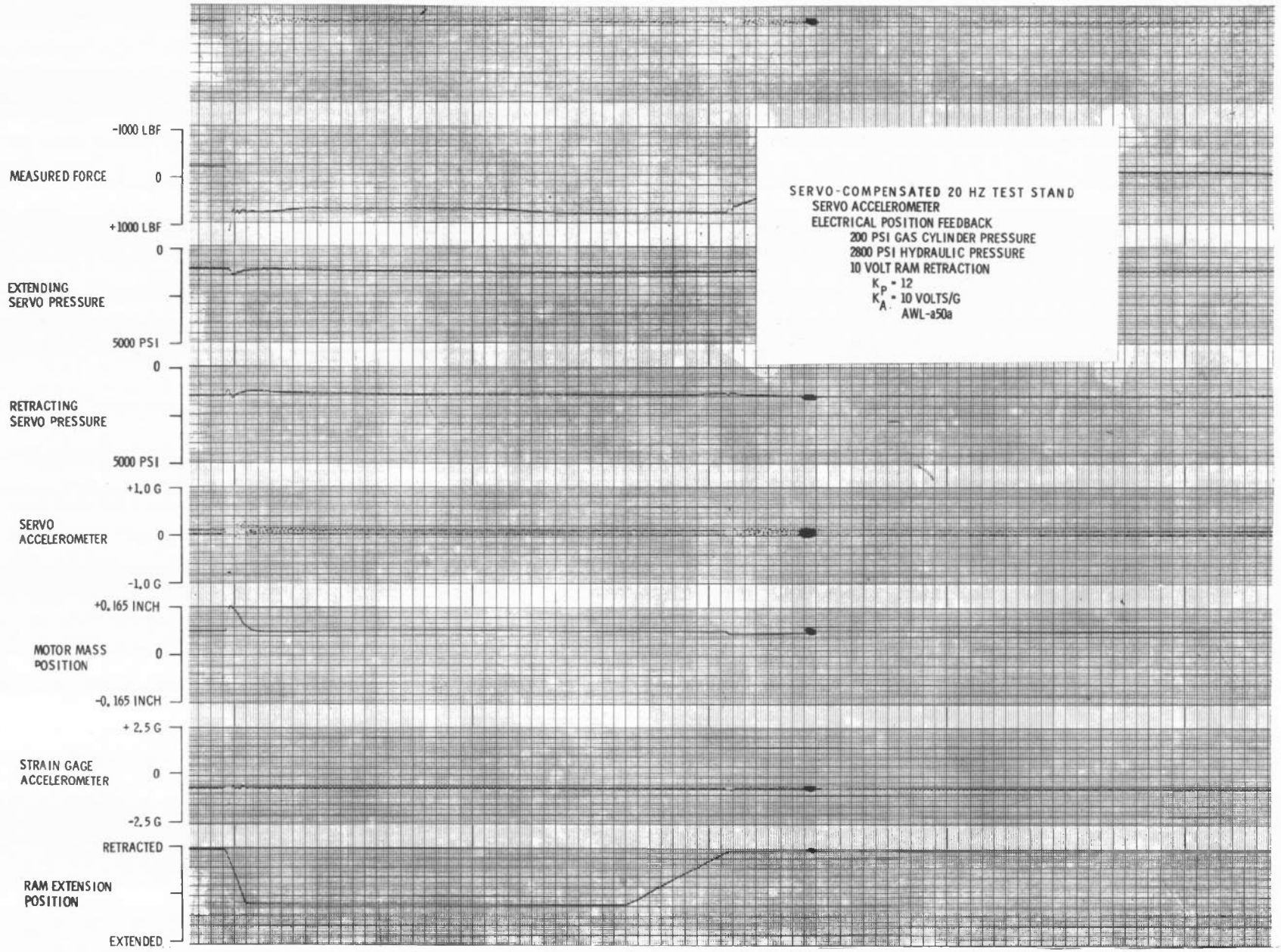

Fig. 51 Active Strut Response Data with Servo Accelerometer Feedback - 20 Hertz Test Stand with 200 psi Gas Cylinder Pressure

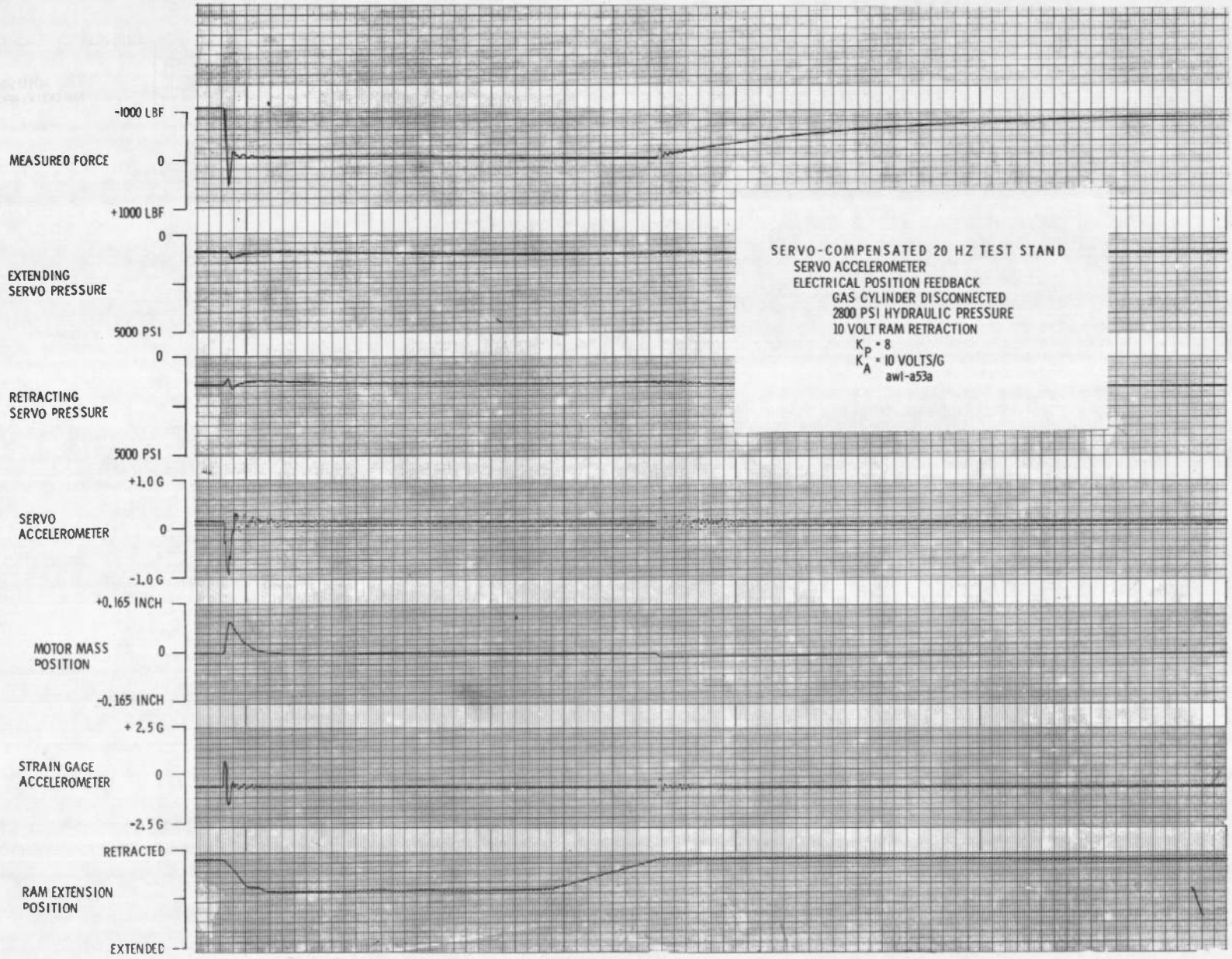

Fig. 52 Active Strut Response Data with Servo Accelerometer Feedback - 20 Hertz Test Stand with Gas Cylinder Disconnected

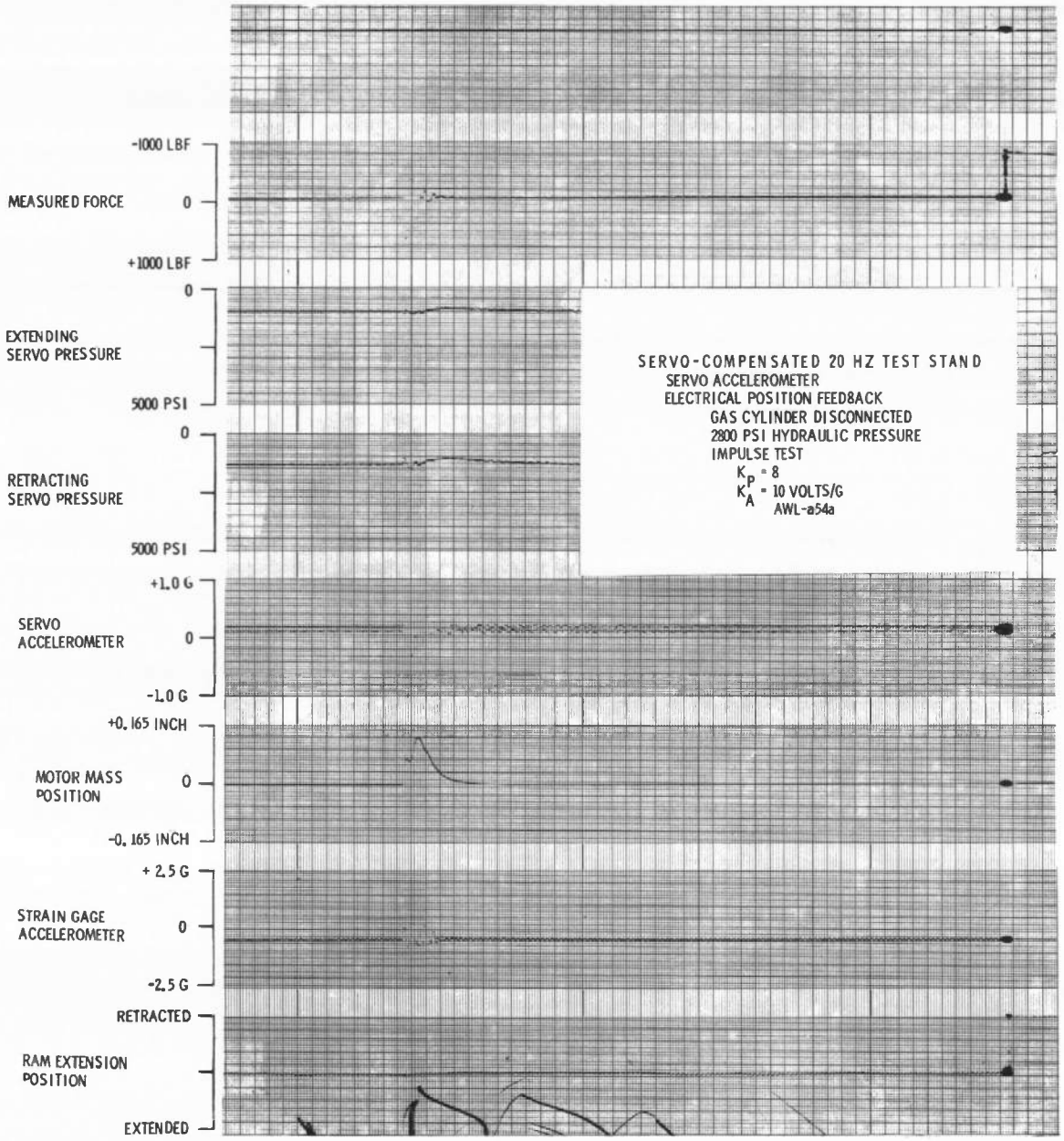

Fig. 53 Active Strut Response Data with Servo Accelerometer Feedback - 20 Hertz Test Stand with Gos Cylinder Disconnected

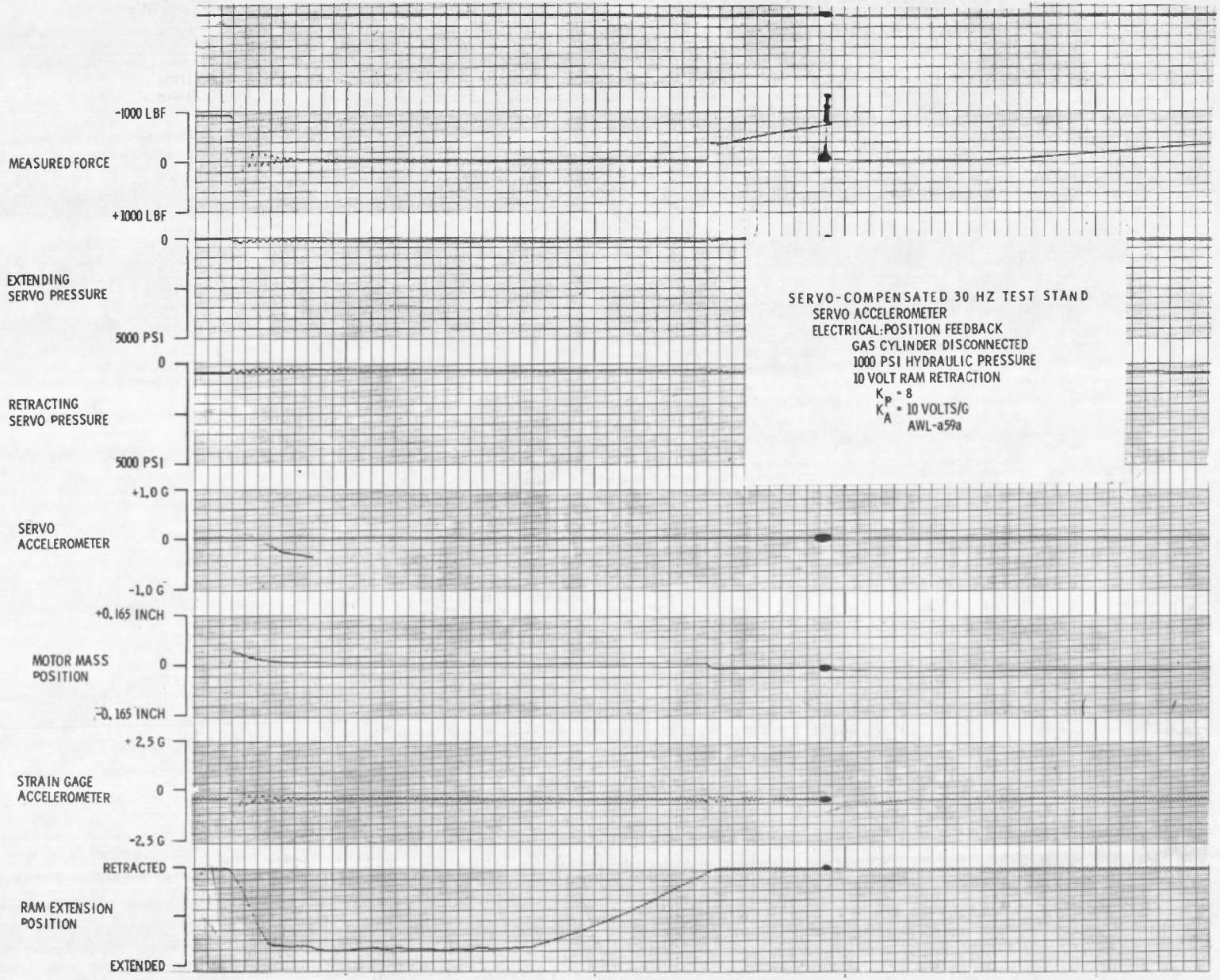

Fig. 54 Active Strut Response Data with Servo Accelerometer Feedback - 30 Hertz Test Stand with Gas Cylinder Disconnected

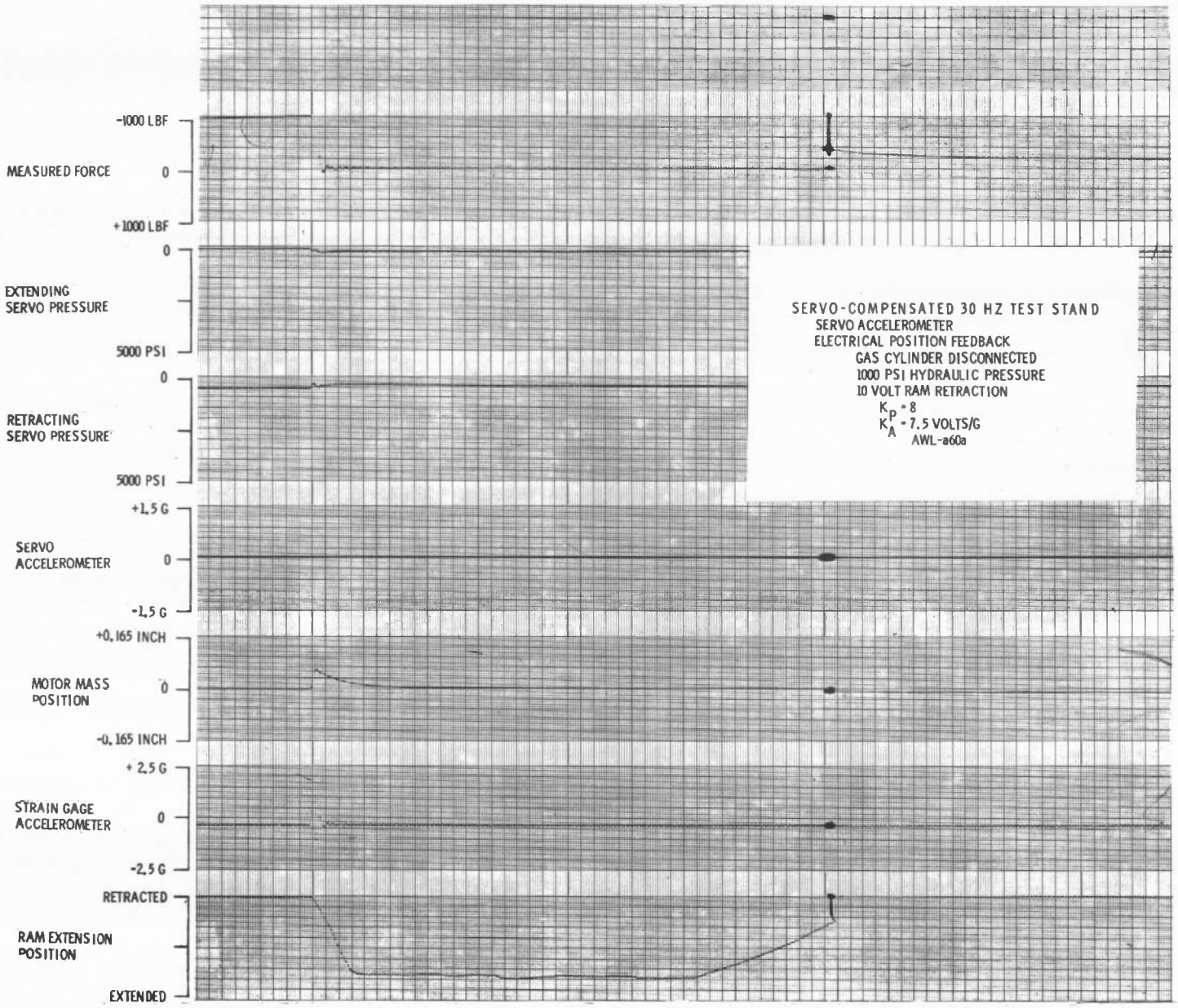

Fig. 55 Active Strut Response Data with Servo Accelerometer Feedback - 30 Hertz Test Stand with Gas Cylinder Disconnected

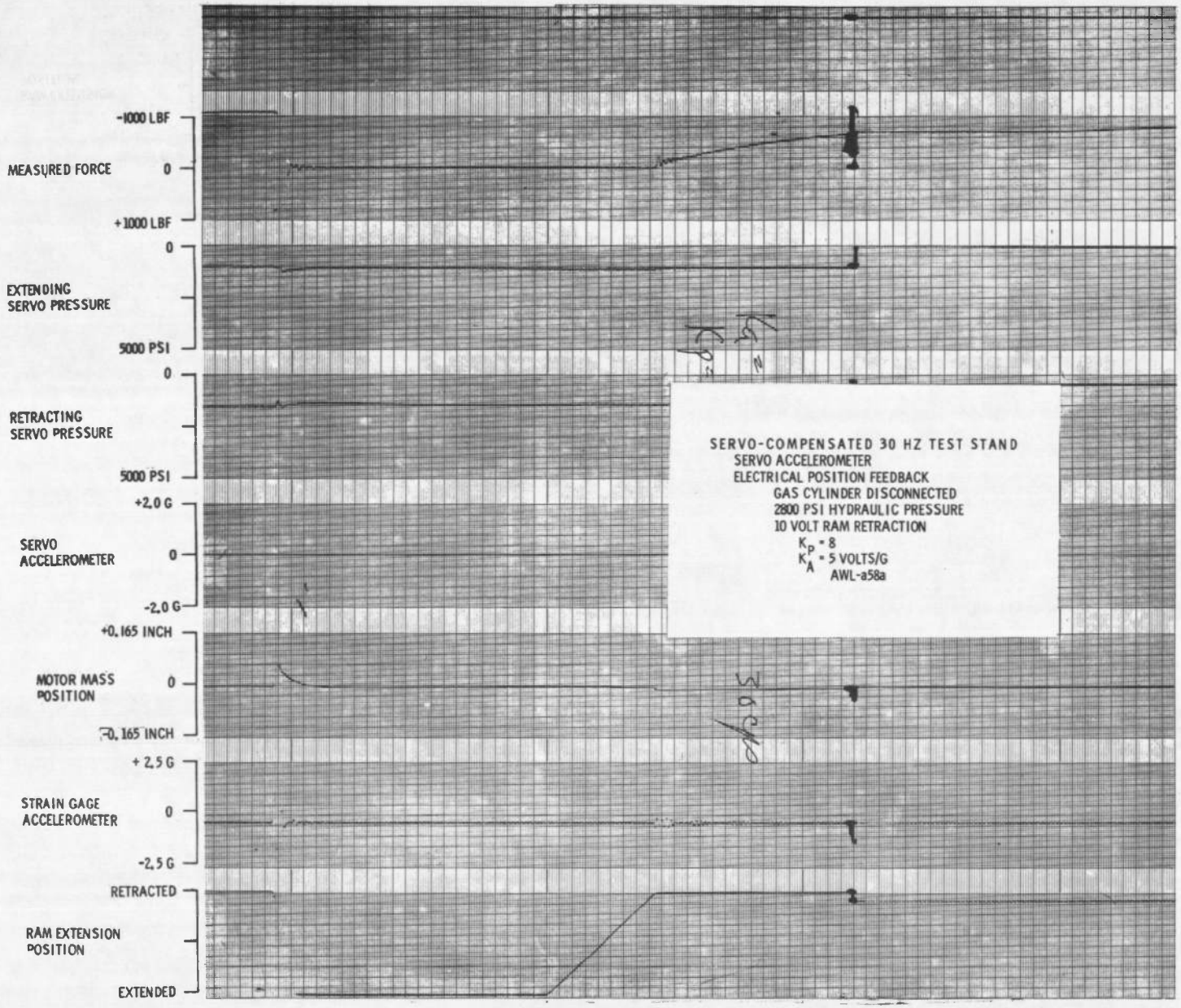

Fig. 56 Active Strut Response Data with Servo Accelerometer Feedback - 30 Hertz Test Stand with Gas Cylinder Disconnected

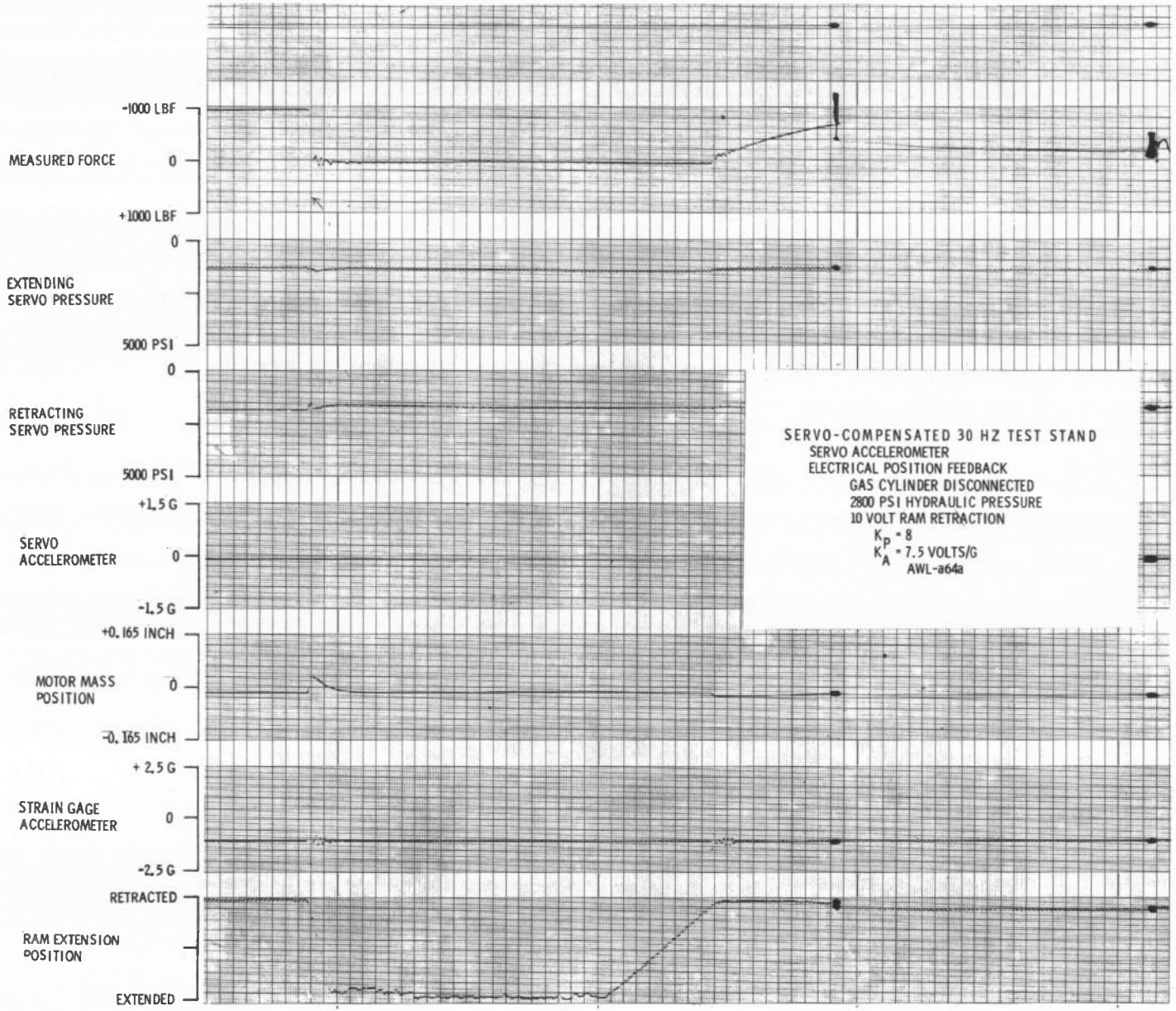

Fig. 57 Active Strut Response Data with Servo Accelerometer Feedback - 30 Hertz Test Stand with Gas Cylinder Disconnected

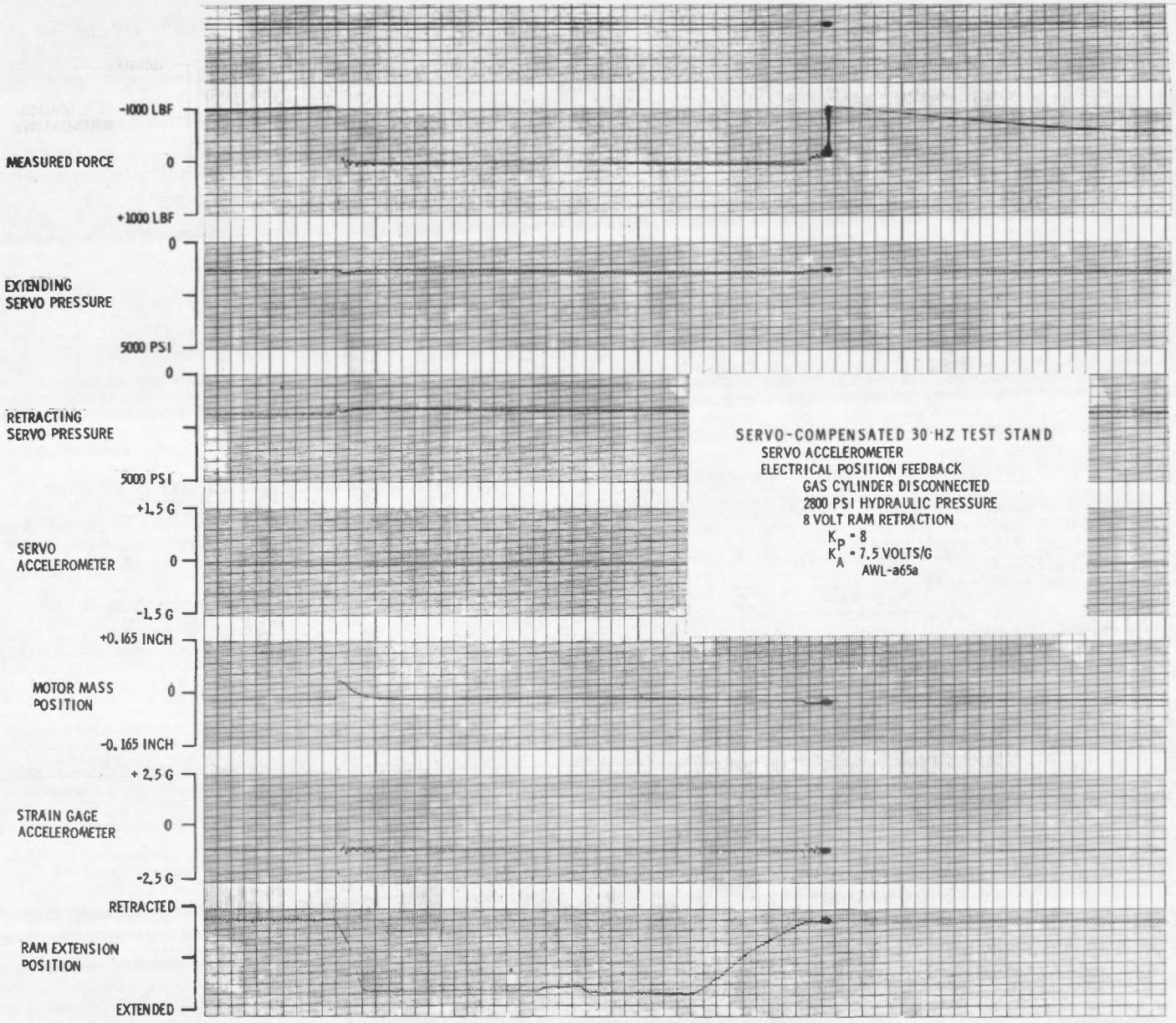

Fig. 58 Active Strut Response Data with Servo Accelerometer Feedback - 30 Hertz Test Stand with Gas Cylinder Disconnected

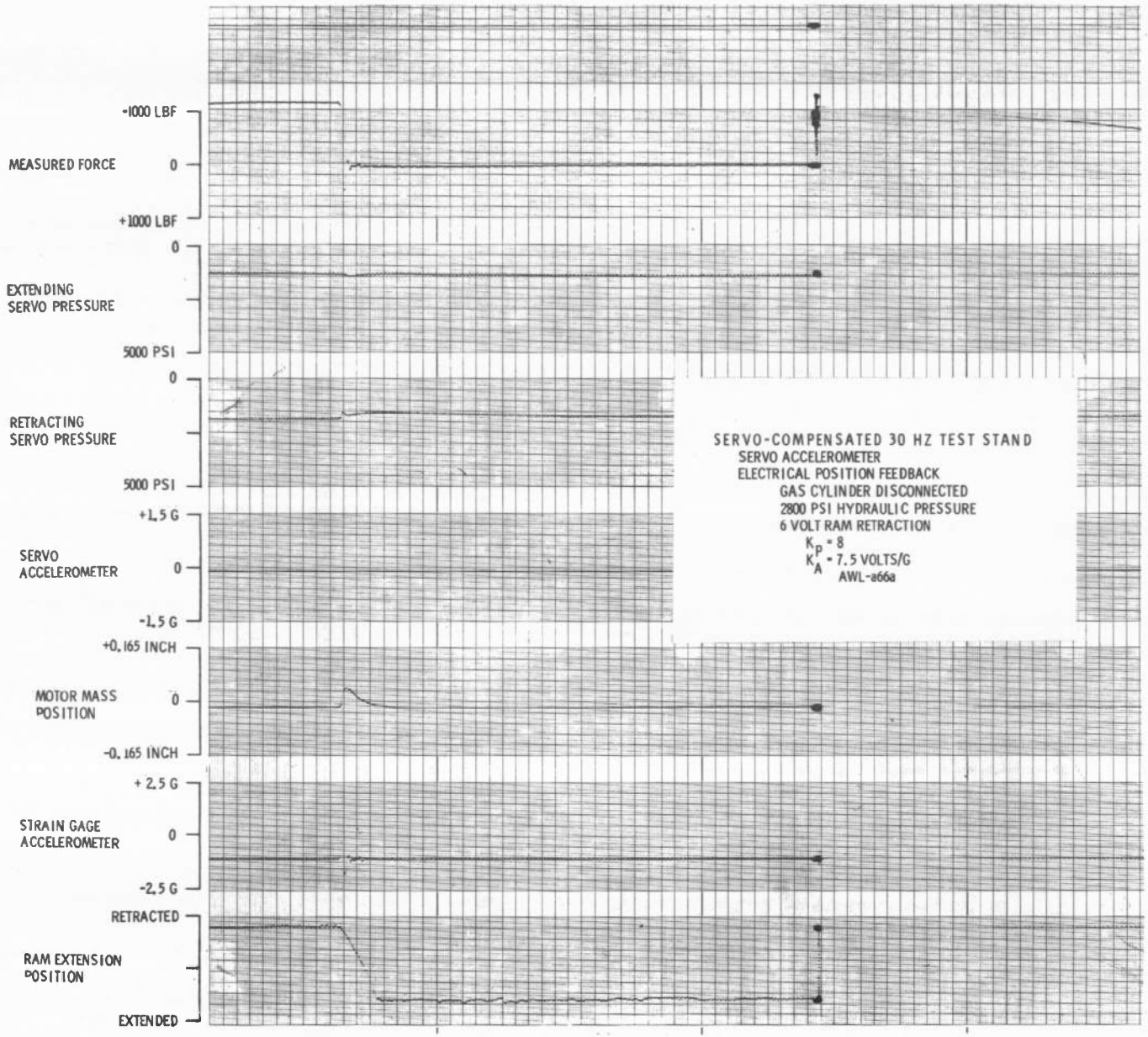

Fig. 59 Active Strut Response Data with Servo Accelerometer Feedback - 30 Hertz Test Stand with Gas Cylinder Disconnected

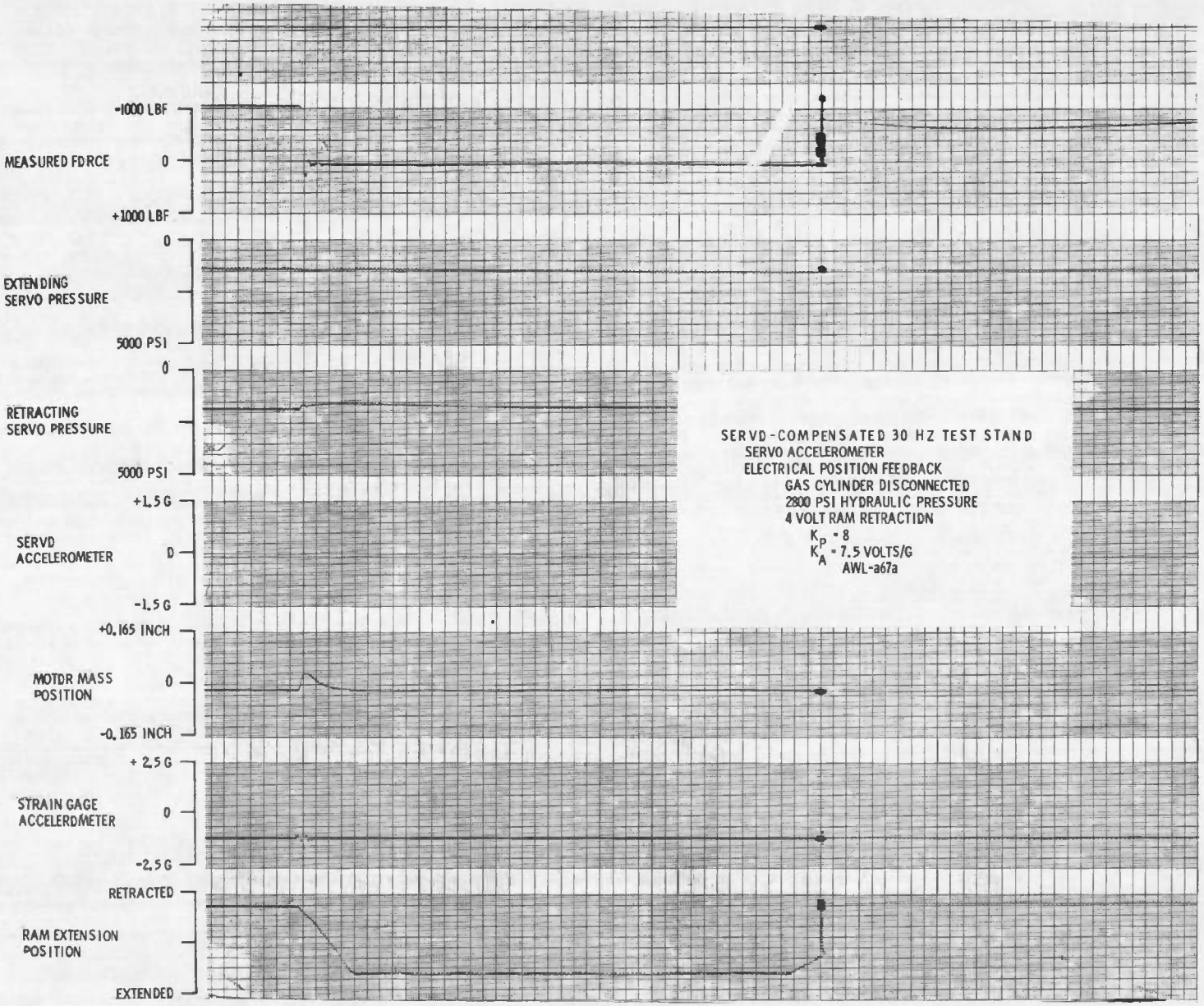

Fig. 60 Active Strut Response Data with Servo Accelerometer Feedback - 30 Hertz Test Stand with Gas Cylinder Disconnected

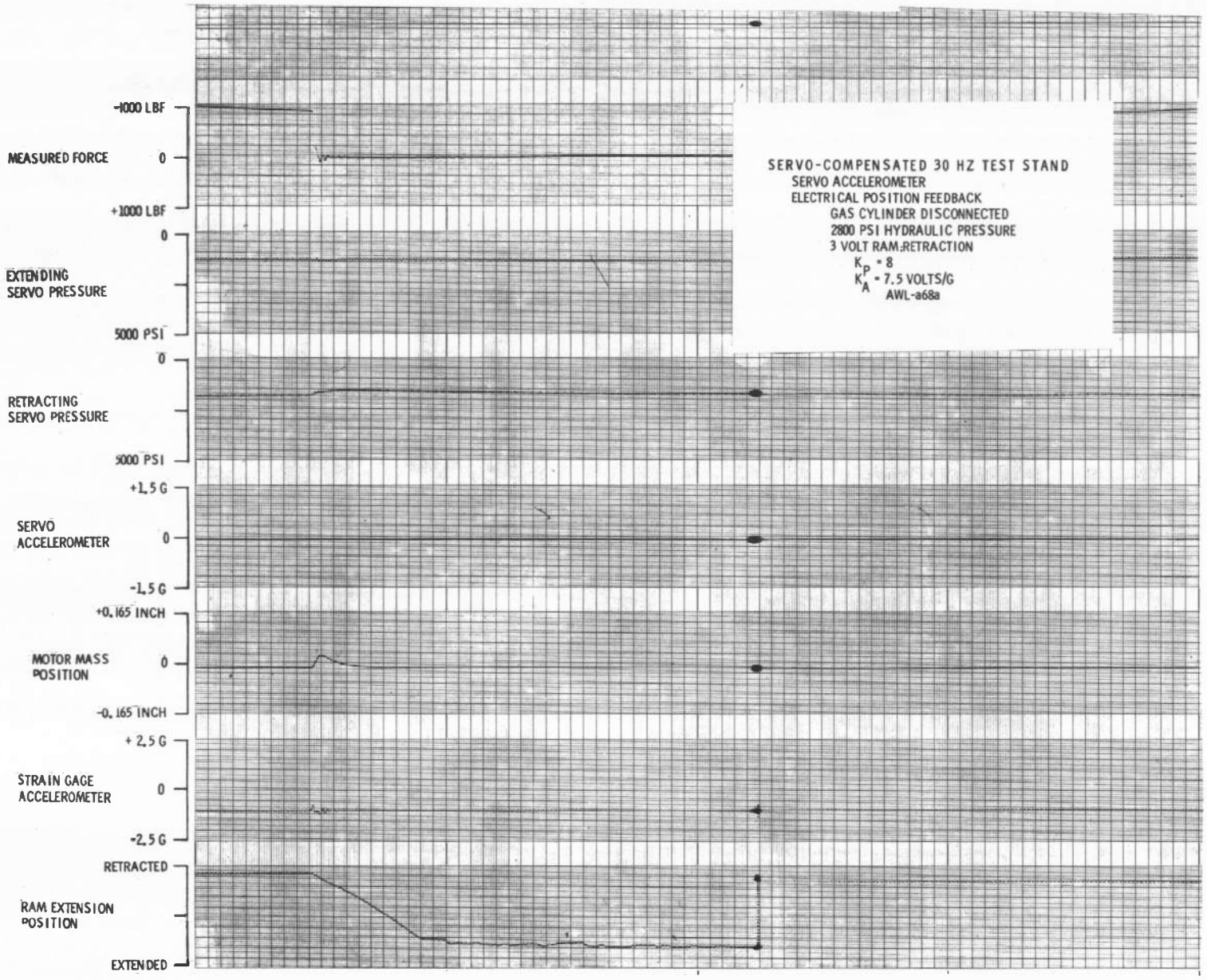

Fig. 61 Active Strut Response Data with Servo Accelerometer Feedback - 30 Hertz Test Stand with Gas Cylinder Disconnected

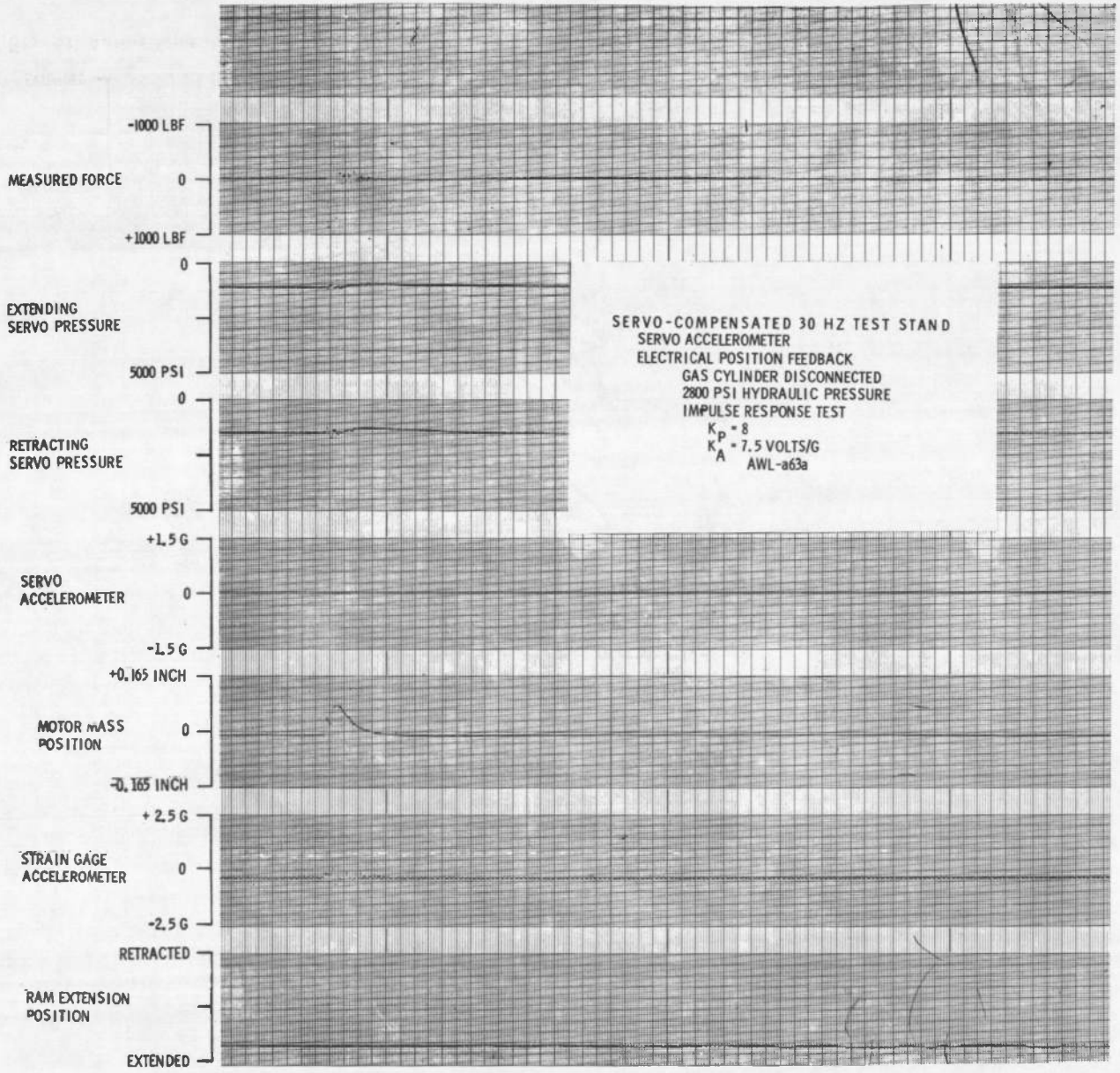

Fig. 62 Active Strut Response Data with Servo Accelerometer Feedback - 30 Hertz Test Stand with Gas Cylinder Disconnected

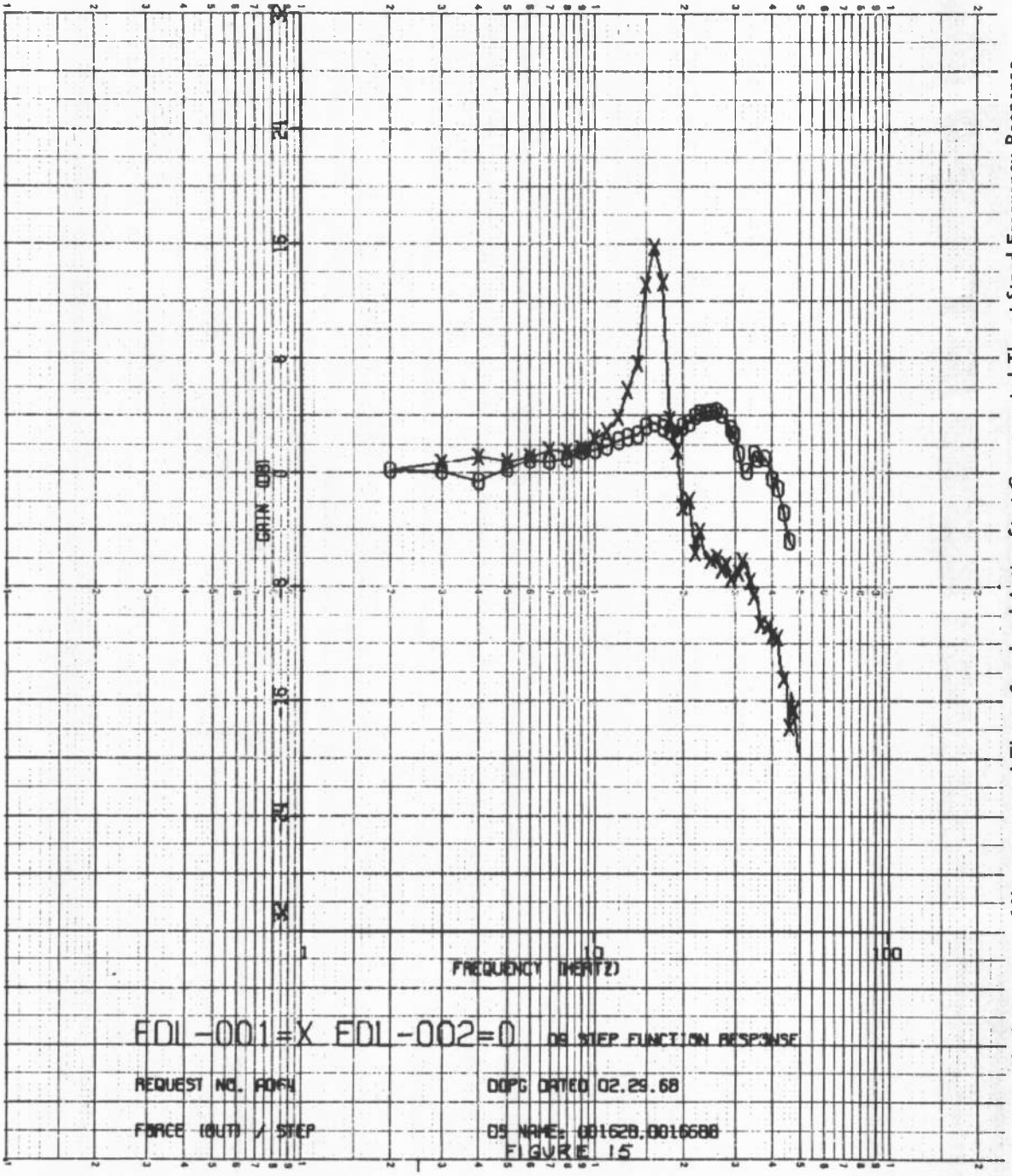

Fig. 63 Comparison of Uncompensated Thrust Stand and Active Strut Compensated Thrust Stand Frequency Response

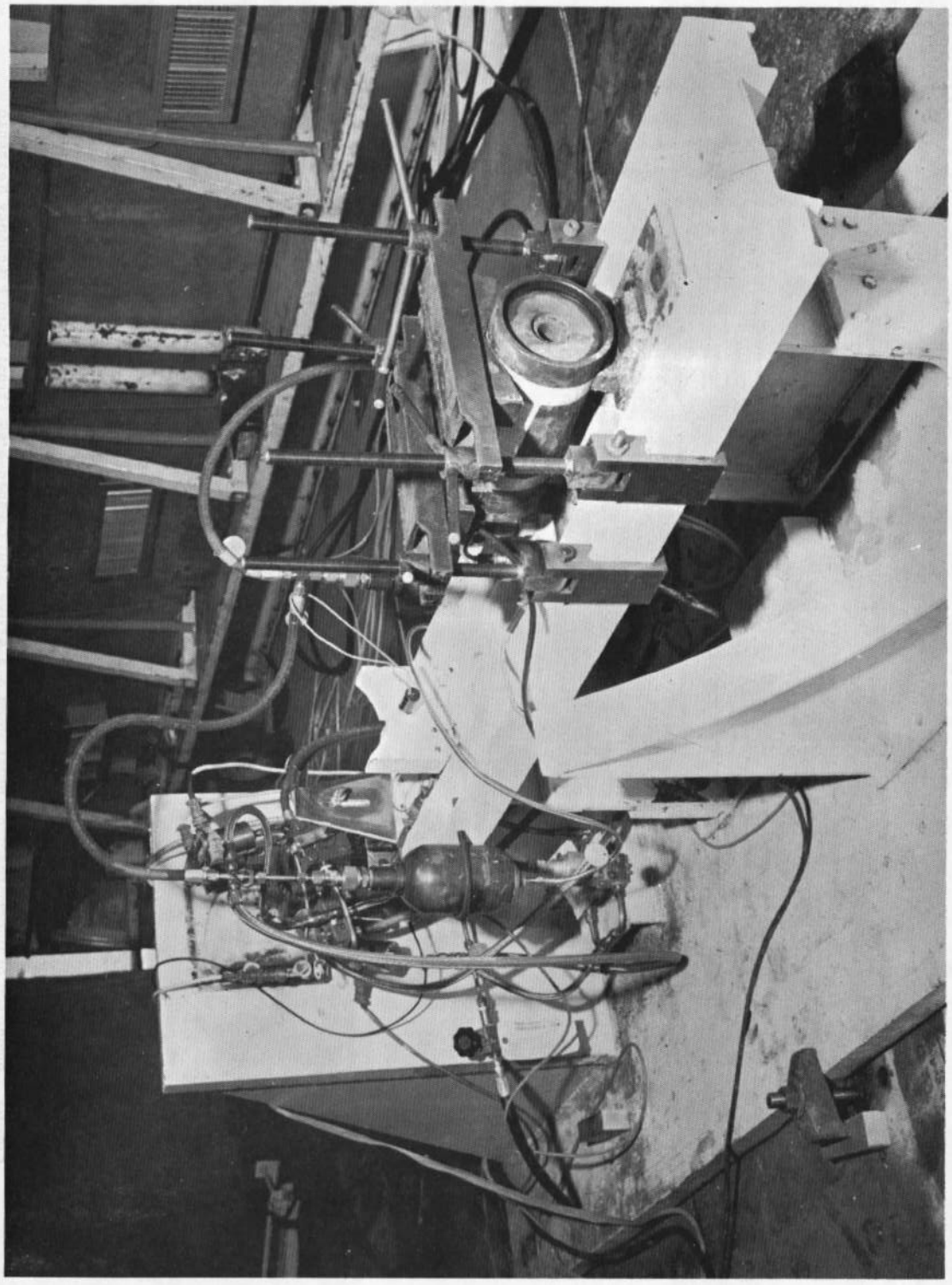

Fig. 64 Active Strut Assembled in Test Area

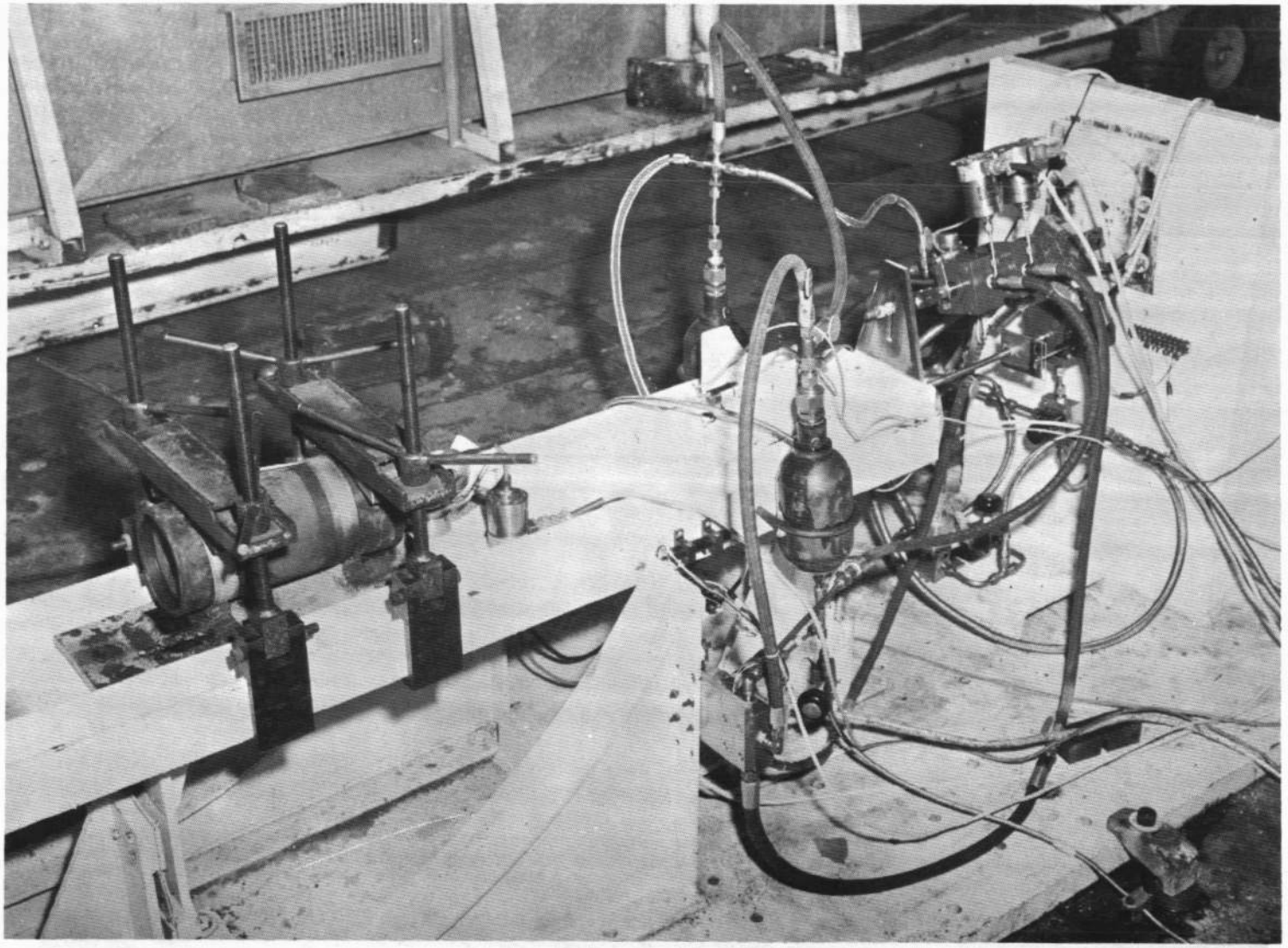

Fig. 65 Active Strut - Side View

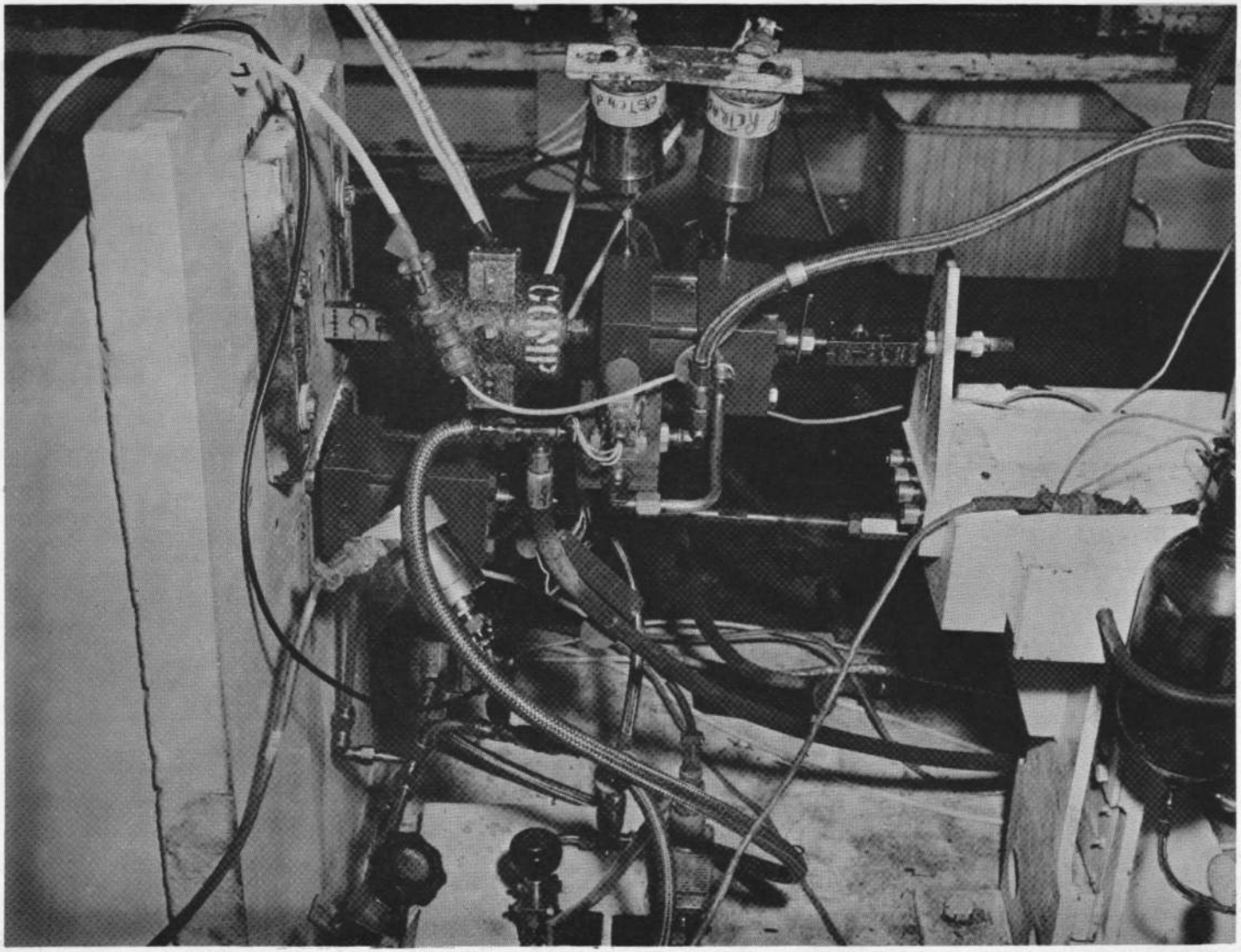

Fig. 66 Active Strut Compensator and Ram Retraction Force Generator

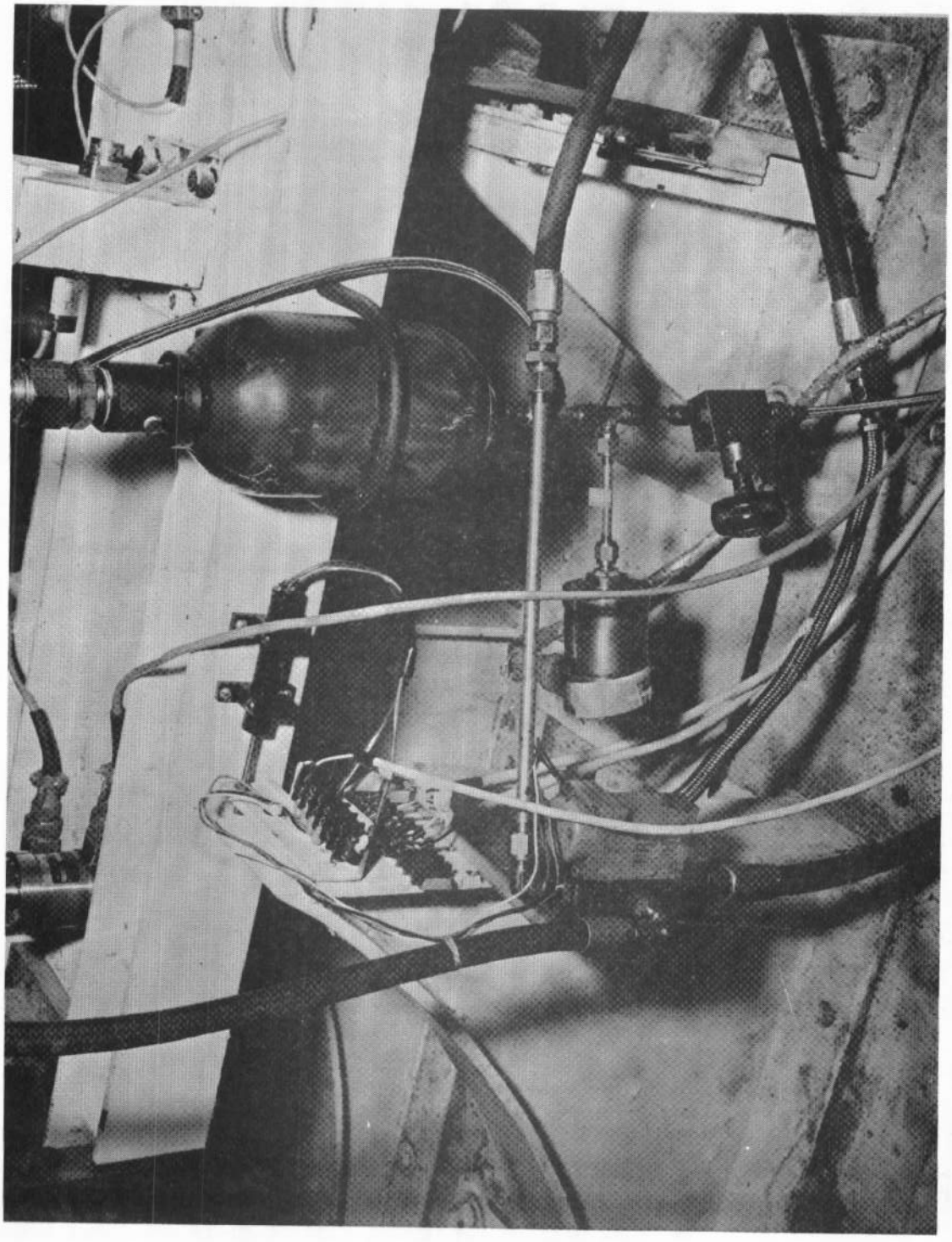

Fig. 67 Electrical Position Feedback System

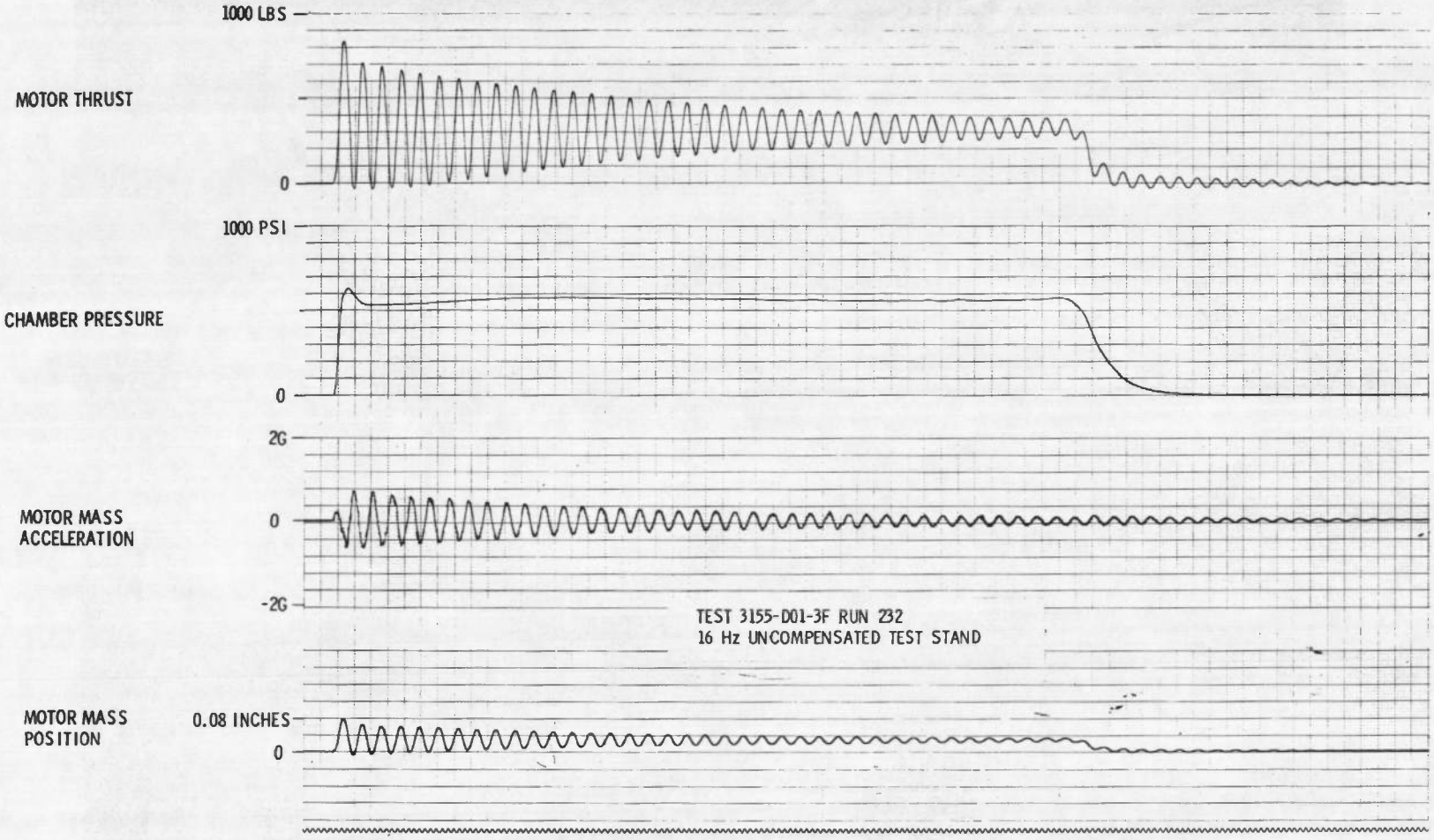

Fig. 68 Solid Rocket Motor Test Firing Data - Uncompensated Thrust Stand

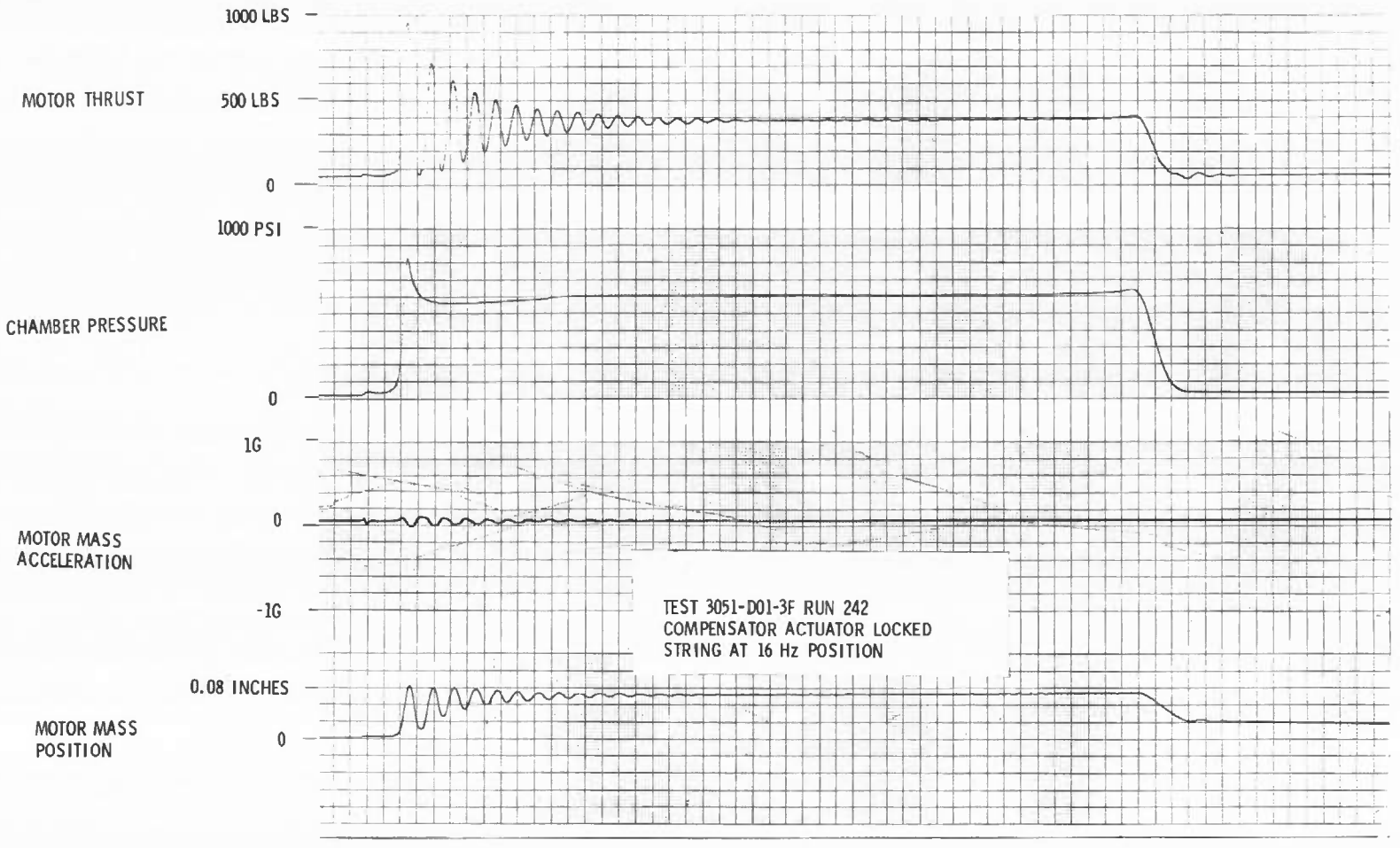

Fig. 69 Solid Rocket Motor Test Firing Data - Damped Thrust Stand

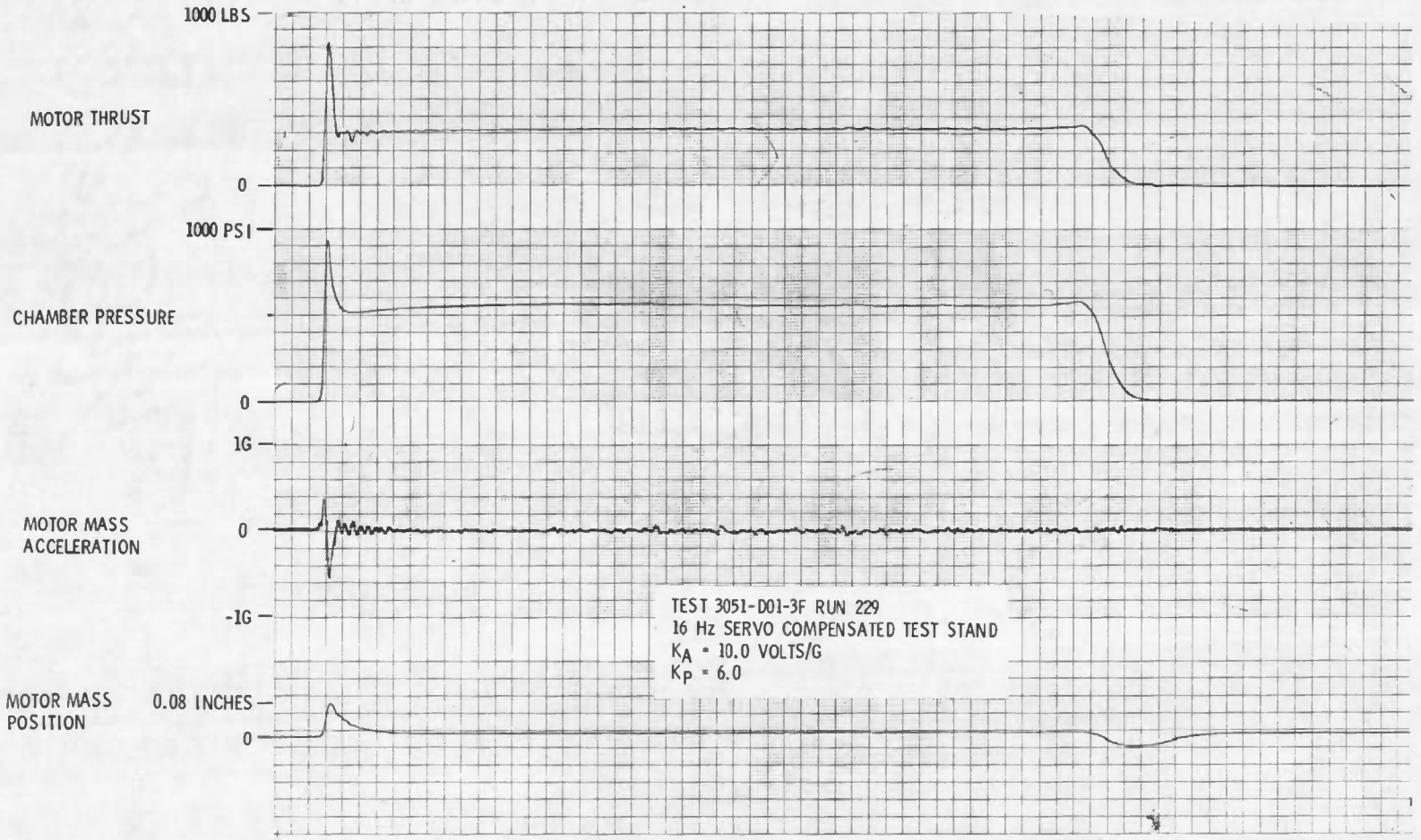

Fig. 70 Solid Rocket Motor Test Firing Data - Compensated Thrust Stan

APPENDIX II
EQUATIONS OF THE MATHEMATICAL MODEL

II-1. $$P_{ACC} - P_S = \frac{L}{ga} \ddot{w}_{IN} + \frac{c}{\rho} \dot{w}_{IN}^2$$

II-2. $$\dot{P}_S = \frac{\beta}{\rho V_{IN}} (\dot{w}_{IN} - \dot{w}_{SV})$$

$$\dot{w}_{SV} = \dot{w}_1 \ (a_e > 0) = -\dot{w}_2 \ (a_e < 0)$$

II-3. $$\dot{w}_1 = .66875 \ a_e \sqrt{\rho \ (P_S - P_{OP})} \quad (a_e > 0)$$

$$= -.66875 \ a_e \sqrt{\rho \ (P_{OP} - P_R)} \quad (a_e < 0)$$

II-4. $$\dot{w}_2 = .66875 \ a_e \sqrt{\rho \ (P_{CL} - P_R)} \quad (a_e > 0)$$

$$= -.66875 \ a_e \sqrt{\rho \ (P_S - P_{CL})} \quad (a_e < 0)$$

II-5. $$\dot{P}_{OP} = \frac{\beta}{\rho V_{FLEX}} (\dot{w}_1 - \dot{w}_{OP})$$

II-6. $$\dot{P}_{CL} = \frac{\beta}{\rho V_{FLEX}} (\dot{w}_{CL} - \dot{w}_2)$$

II-7. $$P_{OP} - P_1 = L/ga \ \ddot{w}_{OP} + \frac{c}{\rho} \dot{w}_{OP}^2$$

II-8. $$P_2 - P_{CL} = L/ga \ \ddot{w}_{CL} + \frac{c}{\rho} \dot{w}_{CL}^2$$

II-9. $$\dot{w}_{1_D} = .66875\ a_{DAMP}\ \sqrt{\rho\ (P_{ACC} - P_1)} \qquad (a_{DAMP} > 0)$$

$$= -.66875\ a_{DAMP}\ \sqrt{\rho\ (P_1 - P_a)} \qquad (a_{DAMP} < 0)$$

II-10. $$\dot{w}_{2_D} = .66875\ a_{DAMP}\ \sqrt{\rho\ (P_2 - P_a)} \qquad (a_{DAMP} > 0)$$

$$= -.66875\ a_{DAMP}\ \sqrt{\rho\ (P_{ACC} - P_2)} \qquad (a_{DAMP} < 0)$$

II-11. $$\dot{P}_R = \frac{\beta}{\rho V_{OUT}}\ (\dot{w}_R - \dot{w}_{OUT})$$

$$\dot{w}_R = \dot{w}_2\ (a_e > 0) = -\dot{w}_1\ (a_e < 0)$$

II-12. $$P_R - P_a = L/ga\ W_{OUT} + \frac{c}{\rho}\ \dot{w}_{OUT}^2$$

II-13. $$\dot{P}_1 = \frac{\beta}{\rho V_1}\ \dot{w}_{OP} - \frac{\beta}{\rho}\ \frac{W_1 \dot{V}_1}{V_2^2} + \frac{\beta}{\rho V_1}\ \dot{w}_{1_D}$$

II-14. $$W_1 = W_1(0) + \int_0^t (\dot{w}_{OP} + \dot{w}_{ID})\ dt \cong \text{constant}$$

II-15. $$\dot{V}_1 = \frac{a_{CP}}{1728}\ (\dot{x}_{CASE} - \dot{x}_{CP})$$

II-16. $$-\dot{P}_2 = \frac{\beta}{\rho V_2}\ \dot{w}_{CL} + \frac{\beta}{\rho}\ \frac{W_2 \dot{V}_2}{V_2^2} + \frac{\beta}{\rho V_1}\ \dot{w}_{2_D}$$

II-17. $$W_2 = W_2(0) - \int_0^t (\dot{w}_{CL} + \dot{w}_{2_D})\ dt \cong \text{constant}$$

II-18. $$\dot{V}_2 = \frac{a_{CP}-a_S}{1728} (\dot{x}_{CP} - \dot{x}_{CASE})$$

II-19. $$V_1 = \frac{a_{CP}}{1728} (x_{CASE} - x_{CP}) + V_1(0)$$

II-20. $$V_2 = \frac{a_{CP}-a_S}{1728} (x_{CP} - x_{CASE}) + V_2(0)$$

II-21. $$a_e = K_{x_M} x_M$$

II-22. $$a_{DAMP} = \frac{K_{\ddot{x}_M} \ddot{x}_M}{\tau S+1}$$

II-23. $$F_A - B_M \dot{x}_M - \frac{K_T}{2} (x_M - x_T) = M_M \ddot{x}_M$$

II-24. $$\frac{K_{LC}}{2} (x_M - x_T) - B_T \dot{x}_T - \frac{K_T}{2} (x_T - x_{CP}) = M_T \ddot{x}_T$$

II-25. $$\frac{K_T}{2} (x_T - x_{CP}) - P_1 a_{CP} + P_2 (a_{CP} - a_S) - B_{CP} \dot{x}_{CP} = M_{CP} \ddot{x}_{CP}$$

II-26. $$P_1 a_{CP} - P_2 (a_{CP} - a_S) - \frac{K_{LC}}{2} (x_{CASE} - x_{LC}) = M_{CASE} \ddot{x}_{CASE}$$

II-27. $$\frac{K_{LC}}{2} (x_{CASE} - x_{LC}) - B_{LC} \dot{x}_{LC} - \frac{K_{LC}+K_{Fx}}{2} (x_{LC} - x_{Fx}) = M_{LC} \ddot{x}_{LC}$$

II-28. $$\frac{K_{LC} + K_{Fx}}{2} (x_{LC} - x_{Fx}) - B_{Fx} \dot{x}_{Fx} - \frac{K_{Fx}}{2} (x_{Fx} - x_{HW}) = M_{Fx} \ddot{x}_{Fx}$$

II-29. $$\frac{K_{Fx}}{2} (x_{Fx} - x_{HW}) L - B_{HW} \dot{\theta}_{HW} - K_{HW} L x_{HW} = J_{HW} \ddot{\theta}_{HW}$$

II-30. $x_{HW} = L\theta_{HW}$

II-31. $F_C = (K_{LC} - \frac{K_{Fx}}{2}) \quad (x_{Fx} - x_{CASE})$

UNCLASSIFIED
Security Classification

DOCUMENT CONTROL DATA - R & D

(Security classification of title, body of abstract and indexing annotation must be entered when the overall report is classified)

1. ORIGINATING ACTIVITY *(Corporate author)*
Aerojet-General Corporation
Sacramento, California

2a. REPORT SECURITY CLASSIFICATION
UNCLASSIFIED

2b. GROUP
N/A

3. REPORT TITLE
THE FEASIBILITY OF A CLOSED LOOP MULTIPLE COMPONENT ROCKET THRUST STAND

4. DESCRIPTIVE NOTES *(Type of report and inclusive dates)*
Final Report June 1967 through May 1968

5. AUTHOR(S) *(First name, middle initial, last name)*
Aerojet-General Corporation, Test Systems Engineering Department

6 REPORT DATE	7a. TOTAL NO. OF PAGES	7b. NO. OF REFS
October 1968	132	0

8a. CONTRACT OR GRANT NO.
F40600-67-C-0015

b. PROJECT NO.
5730 (Task 573004) and 4344

c. Program Elements 6240518F and 6540215F

9a. ORIGINATOR'S REPORT NUMBER(S)
AEDC-TR-68-164

9b. OTHER REPORT NO(S) *(Any other numbers that may be assigned this report)*
N/A

10 DISTRIBUTION STATEMENT
This document has been approved for public release and sale; its distribution is unlimited.

11 SUPPLEMENTARY NOTES
Available in DDC.

12. SPONSORING MILITARY ACTIVITY
Arnold Engineering Development Center (AETS), Arnold Air Force Station, Tennessee 37389

13 ABSTRACT

This report considers the extension of rocket engine thrust stand and jet engine thrust stand dynamics by the use of an "active strut" hydraulic compensator unit installed as an integral member of the force measurement system. A mathematical model was constructed to approximate the dynamic characteristics of a typical rocket engine thrust stand and active strut servo system; the model was mechanized for analog computer simulation. Based upon results of the computer analysis, a physical test stand model was constructed in the Aerojet-General Corporation Sacramento Controls Laboratory. A hydraulic force generator was mechanized to introduce a step-like forcing function to the physical test model. After preliminary testing of the "uncompensated" thrust stand, the active strut compensator was inserted into the thrust stand force measurement system. Controls Laboratory developmental testing of this compensated system suggested that significant improvements could be achieved in the force measurement system dynamic response characteristics. Frequency response data indicated that the compensated force measurement system bandwidth could be increased by a factor of four with a significant increase in damping. The Controls Laboratory physical test model was reassembled in the Aerojet Sacramento Test Area. Three solid rocket motors were statically test fired on the uncompensated thrust stand to form a reference base.

DD FORM 1 NOV 65 1473

UNCLASSIFIED
Security Classification

14 KEY WORDS	LINK A		LINK B		LINK C	
	ROLE	WT	ROLE	WT	ROLE	WT
Test Equipment						
Rocket Engines						
Test Stands						
Thrust						
Static Tests						